Optimal shaping of lightweight structures

Benoît Descamps

A thesis submitted in fulfillment for the
degree of Doctor in Engineering Sciences in the

Building, Architecture & Town planning Department
Brussels School of Engineering
Université libre de Bruxelles

November 19, 2013

Supervisors

Prof. Rajan Filomeno Coelho (Université libre de Bruxelles)
Prof. Philippe Bouillard (Université libre de Bruxelles)

Members of the jury

Prof. Thierry J. Massart (Université libre de Bruxelles)
Prof. Michel Kinnaert (Université libre de Bruxelles)
Prof. Sigrid Adriaenssens (Princeton University – Vrije Universiteit Brussel)
Prof. Ruy Marcelo de Oliveira Pauletti (Universidade de São Paulo)
Prof. Pierre Villon (Université de technologie de Compiègne)

Front cover: the picture has been drawn using the Voronoi's diagram (see Section 5.5) of the Dutch Maritime Museum in Amsterdam, which was designed by Ney+Partners.

"Tout est musique, tout est rythme. Nul ne peut briser l'élan vital des rythmes libres. Et si d'aventure nous tentons de l'emprisonner, il nous échappe pour revenir là où nous ne l'attendons plus. La meilleure rythmique que je connaisse: la mer, le vent, aucun problème de tempo."

"There is something else in John Coltrane's music that goes beyond. If his music was only music, it might have made me weary. He certainly opened the door to a world we did not know. It's probably this unbridled spiritual quest that led him there."

– Christian Vander, founder of the music band Magma

Acknowledgements

Firstly I would like to thank Rajan Filomeno Coelho for his huge involvement in supervising me through this work. His contribution was not limited to helping and supporting me; he really created an atmosphere conducive to take unexplored paths. Besides, his contagious interest for innovative ideas combined with a strong sense of humor motivated me to always go further.

I gratefully thank my co-supervisor Philippe Bouillard. This work would not have been possible without him. I owe him a lot: at the very beginning of my master thesis, he aroused my interest for research and since, he is continuously guiding me in every steps of my works by making the best strategic decisions with his sharp eye.

I would like to show my gratitude to Ruy Pauletti for his welcome during my short stay abroad at the Universidade de São Paulo. I really enjoy the time spent there thanks to him, our inspiring and productive discussions, and his unwavering open-mindedness.

There are many other people I would like to thank for their input, namely Thierry J. Massart, Arnaud Deraemaeker, and Sigrid Adriaenssens for these insightful discussions, as well as Laurent Ney and his colleagues who greatly inspired my work through stimulating meetings. The members of the jury are also thanked for their fruitful comments.

The time spent working on this thesis was made much more pleasant thanks to all members of the BATir Department over the years, especially Peter Berke and Armande Hellebois, but also my office mates Jérémy Lebon, David Attas, Bernard Sonon, James Richardson, Valentine Everaert, Aurélie Progneaux, Gilles Tondreau, Maik Brehm, Sudhar Raman, and Guy Paulus with whom I almost spent the entire part of my time in the Department; without forgetting my dear colleague Philippe de Grasse.

More personally, I would like to thank my mother and my father, my parents-in-law, and my two lovely sisters Jessica and Virginie, as well as my whole family for supporting me through my time as a student. Obviously, I should also thank my sweetheart Aude for tolerating my excessive working-time and constantly providing me with the best possible diversions from any difficulty; your love and encouragement has made this thesis possible. Last but not least, thanks to all my faithful friends I know for so long.

Finally, thanks to the Fonds de la Recherche Scientifique (F.R.S.-FNRS) for the financial support of the Research Fellowship. This support is gratefully acknowledged.

Summary

Designing structures for lightness is an intelligent and responsible way for engineers and architects to conceive structural systems. Lightweight structures are able to bridge wide spans with a least amount of material. However, the quest for lightness remains an utopia without the driving constraints that give sense to contemporary structural design.

Previously proposed computational methods for designing lightweight structures focused either on finding an equilibrium shape, or are restricted to fairly small design applications. In this work, we aim to develop a general, robust, and easy-to-use method that can handle many design parameters efficiently. These considerations have led to truss layout optimization, whose goal is to find the best material distribution within a given design domain discretized by a grid of nodal points and connected by tentative bars.

This general approach is well established for topology optimization where structural component sizes and system connectivity are simultaneously optimized. The range of applications covers limit analysis and identification of failure mechanisms in soils and masonries. However, to fully realize the potential of truss layout optimization for the design of lightweight structures, the consideration of geometrical variables is necessary.

The resulting truss geometry and topology optimization problem raises several fundamental and computational challenges. Our strategy to address the problem combines mathematical programming and structural mechanics: the structural properties of the optimal solution are used for devising the novel formulation. To avoid singularities arising in optimal configurations, the present approach disaggregates the equilibrium equations and fully integrates their basic elements within the optimization formulation. The resulting tool incorporates elastic and plastic design, stress and displacements constraints, as well as self-weight and multiple loading.

Besides, the inherent slenderness of lightweight structures requires the study of stability issues. As a remedy, we develop a conceptually simple but efficient method to include local and nodal stability constraints in the formulation. Several numerical examples illustrate the impact of stability considerations on the optimal design.

Finally, the investigation on realistic design problems confirms the practical applicability of the proposed method. It is shown how we can generate a range of optimal designs by varying design settings. In that regard, the computational design method mostly requires the designer a good knowledge of structural design to provide the initial guess.

Contents

1 Introduction

This introductory chapter first describes lightweight structures in a historical context and points out current design issues. To tackle these challenges, Section 2.2 briefly discusses an empirical design process along with available methods for form finding and structural optimization. As a prelude to the novel method presented in this work, Section 2.3 introduces the conceptual framework of hanging models, plastic design, and layout optimization to end in the computational design problem. The main achievements of the thesis are finally given in Section 2.4.

1.1 About lightweight structures

Structural design is an inseparable discipline of the art of building, whose governing factors are of social, cultural, environmental, technical, and financial nature. Given the considerable impact of the construction sector in terms of resources, today's expectations are directed towards "meeting growing demand with limited resources"[1]. In this context, designing structures as light as possible may greatly contribute to more sustainability: by reducing the structural mass, we do not only reduce the quantity of raw material, but we also decrease the embodied energy used for its production, transport, assembly, maintenance, and demolition or re-use, as well as the impact on the ground and foundations [1].

Lightweight structures are best suited for covering wide spans with a limited amount of material. It is often argued that aesthetic values that make these structures visually appealing come from a functionally correct form, which mainly determines whether the system is able to withstand external loads without deteriorating serviceability, in addition to assessing the range of structural performance that can be attained. Mass and stiffness are the two fundamental criteria whose optimum is alike systems of minimum energy in nature. To achieve the lowest mass-to-stiffness ratio, lightweight structures must be conceived as a force-differentiated system where tension, compression, and shear are distributed on different components (cables, bars, membranes, etc.) [2]. If the structural form is inadequate, bending stiffness is required to compensate unbalanced forces but this additional resistance adversely affects structural performance.

The emergence of lightweight structures traces back to the second half of the 19^{th} century. This period saw the advent of new material technologies such as steel, reinforced concrete, resistant glass, and later fabric membrane. Together with advances in analysis and design tools, engineers and architects have been challenged to build increasingly lighter structures [3]. This has led to the development of the structural typologies depicted in Fig. 1.1. An early example is the Crystal Palace designed by Joseph Paxton for the Great Exhibition in 1851. The roof of 80kg/m^2 was a real progress at that time [4]. Another pioneering construction is the hyperboloid lattice tower of the Russian engineer Vladimir Shukhov in 1896. In the 1920s, Anton Tedesko first introduced reinforced concrete thin shells in the United States [5]. This expansion has been pursued worldwide by Félix Candela [6], Heinz Isler [7], or André Paduart in Belgium [8]. The limit of lightness have been reached with tensile structures constructed of pre-stressed cable nets and fabric membranes; the strength coming from

[1] This issue was the topic of IABSE-IASS Symposium entitled "Taller, Longer, Lighter", held in London in 2011, and jointly organized by the International Association for Bridge and Structural Engineering (IABSE) and the International Association for Shell and Spatial Structures (IASS).

the anticlastic curvature of the geometric surface. A famous example of cable net is the Olympic stadium's roof in Munich built in 1972, qualified as "architecture of the minimal" by its designer Frei Otto [9]. Pneumatic structures exhibit a close resemblance with tensile structures except that they are stabilized by the pressure of compressed air and pre-stressed cables. They also have an extremely low mass, as witnessed by the air-supported roof of 3kg/m^2 covering the US Pavillon at Expo'70.

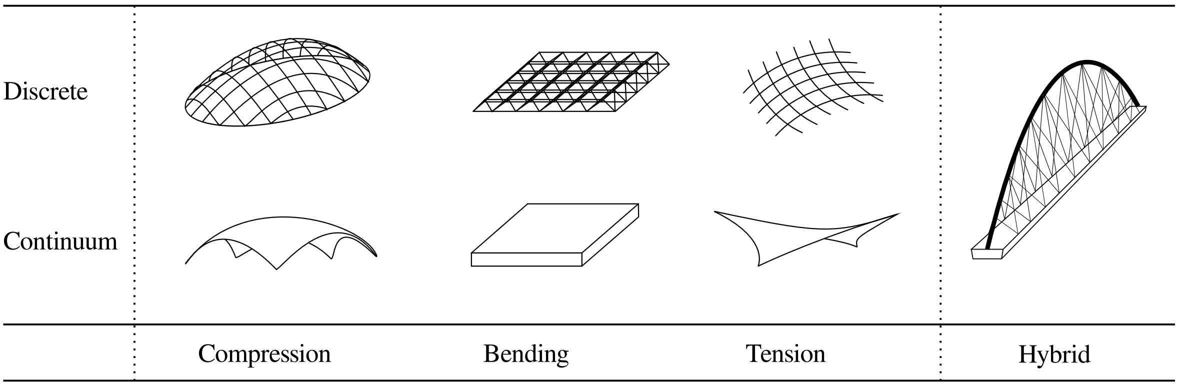

Figure 1.1: Classification of typologies of lightweight structures according to the actual stress state and the type of structural components

It should be mentioned that these historical examples have been constructed in a period where the labor was highly qualified and inexpensive, the requirements for safety and durability were more permissive, and where technical innovation gave meaning to the project. At the dawn of the 21$^{\text{st}}$ century, a question arises: "the lighter, the better?" [4]. Although lightness remains the leading design criterion, this sole achievement is largely insufficient to cope with the increasing complexity of contemporary architecture. Nowadays, lightweight structures should be designed as a whole by including the multitude of design constraints. This will result in hybrid systems lying at the boundary of different typologies.

1.2 Design methodologies

The shaping process of lightweight structures is traditionally based on empirical knowledge and designers' experience. An initial design is created, tested to failure, and updated in a series of structural analyses in order to achieve an optimal shape (Fig. 1.2(a)). However, each iteration requires engineers to manually generate the geometry of the analysis model. The task is time-consuming, error-prone, and cumbersome for the designer. Furthermore, no matter brilliant the designer is, it is often difficult to accurately predict and comprehend the effects of changing the geometry of lightweight structures without the risk of deteriorating the stiffness. This trial-and-error process can be advantageously pushed forward by computational design methods.

Still, two fundamental issues of lightweight structures must be thoroughly addressed for benefiting from those developments: *equilibrium* and *optimality* [10]. The search for equilibrium is the basic requirement for safety, but it may transform a satisfactory design to a masterpiece when it is properly considered. The search for optimality is the never-ending task of improving the design while satisfying project constraints. Over the last forty years, researchers have continuously devising innovative methods to address these issues.

Finding an equilibrium shape is the main purpose of structural form-finding methods. Given the boundary and external loading conditions, this *state-to-design* approach requires the designer to prescribe the internal forces to obtain the geometrical coordinates that solve the equilibrium equations (Fig. 1.2(b)). The literature covering structural form finding is briefly reviewed in Appendix A.1. Although structural efficiency may result as a welcome side-effect (no optimality criterion is used, in fact), there are frequent situations in which one wishes to impose geometrical constraints. In this

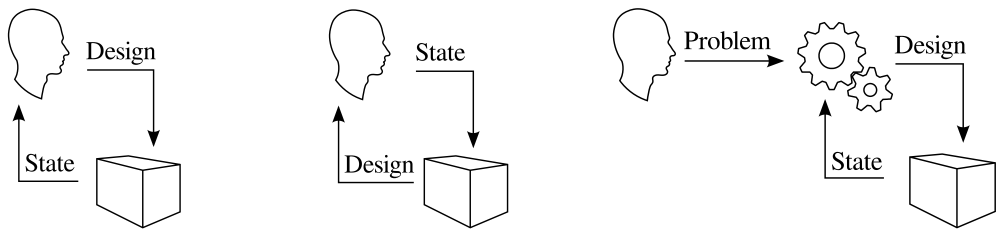

(a) Trial-and-error

(b) Form finding

(c) Optimization

Figure 1.2: Different kinds of design process with (a) the conventional trial-and-error process, (b) the structural form-finding process, (c) the structural optimization process

case, form-finding methods are inadequate since the shape is the output of the process. Furthermore, stability issues that may considerably affect the optimal shape cannot be considered. Some strategies have been proposed [11–15] but their scope is restricted to specific problems.

Finding an optimal shape is the ambitious task of structural optimization. The approach requires the designer to mathematically formulate the structural design problem as an optimization problem consisting in the minimization of an objective function subject to inequality and equality constraints. In the classical *design-to-state* (or nested) approach, the design variables are introduced in a dedicated structural analysis routine which computes the state variables. Based on these responses, an optimization algorithm iteratively updates the design towards the optimum (Fig. 1.2(c)). As a rule for selecting an optimization algorithm, the more intensive the local exploitation, the stronger the need for specialized information about the problem to be optimized: deterministic methods are problem-specific and best-suited for local search (these aspects will be discussed later in this dissertation), whereas metaheuristics (see the review in Appendix A.2) have broader search capabilities. Structural optimization problems are often very large (several thousands of variables and constraints) and the design space comprises many local optima. Hence, deterministic methods might produce small improvements if the problem is not properly stated, whereas metaheuristics might be inefficient if no variable selection has been applied a priori. Furthermore, the variable nature of the structural layout causes singularities during the optimization process [16, 17].

Although structural optimization methods held tremendous potential, one has to accept that the promise of these approaches is not easily realized. These persisting problems prevent their routine use by structural designers. Instead, the widespread use of computer-aided design tools has enabled the development of increasingly complex geometries in freeform architecture. In this long-awaited freedom of design, structural considerations were perceived as restraining the creativity of designers. As a consequence, structural engineers have been excluded from the preliminary shape design process and their role has been re-centred on sizing and checking arbitrarily-defined structures to meet standard code requirements. Against all odds, a handful of structural designers still pursue the line of thought for unity and coherence between form and force in architecture. Former theories on structural design can inspire the development of creative, yet rigorous, strategies to empower this momentum.

1.3 Back to the roots of structural design

The design of lightweight structures relies on the catenary, whose mathematical definition is a hyperbolic cosine curve idealizing a hanging chain under its own weight when supported at its ends. The development of hanging-chain models started at the end of the 17^{th} century [18]. In a Royal Society Meeting, Robert Hooke raised the issue of finding the ideal shape for an arch and its thrust for which buttresses must resist. As a pioneering idea, he proposed the today's well-established approach of inverting the hanging-chain model to determine the equilibrium shape of an arch [19]. Soon after, Gregory extends the Hooke's idea by saying, without formal proof, that any other arch whose thickness encompasses a catenary curve is also stable [20]. The first rigorous calculation of the thrust line based on funicular polygon of graphic statics is due to Moseley [21] and Méry [22].[2] This (static) "equilibrium approach" was sparsely used in Europe until the Antoni Gaudí's nature-inspired work applies the method for the chapel of Colònia Güell and the arches of Casa Milà [25].

During the 19th century, the equilibrium approach has been severely criticized by proponents of the elastic philosophy [26]. Classical elastic theory states that, in statically indeterminate structures made of linear-elastic material, among the infinity of statically admissible stress field, the actual state is obtained by enforcing the compatibility conditions between strains and displacements (continuity of elements, boundary conditions). However, experimental measures on masonry and steel frameworks[3] exhibited discrepancies with elasticity theory. As claimed by Wilson [27], "equilibrium is essential, compatibility is optional" because compatibility is often violated, for instance in masonry due to cracks. Thus, plastic theory was born by the inability of elastic design theory to predict the actual stress state in a built structure.

Gregory's statement about the stability of arches was in fact precursor of plastic theory (or limit analysis). Assume a ductile material in absence of elastic instability, *any* stress distribution enforcing static equilibrium equations without violating the yield condition is carried safely by the structure via plastic redistribution [28]. Together with the safe theorem, plastic theory replaces the problem of determining the actual stress distribution by a projected limit situation. The selection of an equilibrium state can be performed by adding the requirement that the solution should require the least amount of material (i.e. a lower-bound solution). Hence, plastic theory is naturally oriented towards design [29].

Michell stated in 1904 a fundamental design principle of plastic theory [30]: given a design domain (Fig. 1.3(a)), the lightest structure satisfying the yield condition consists in a continuum with mutually orthogonal fields of tension/compression members oriented along principal strains (Fig. 1.3(b)). The analytical method to determine these lines assumes a fully stressed design in all load-carrying members. The displacement field must remain continuous throughout the design domain and satisfy the kinematic restrictions imposed on the solution [31]. Although the scope is essentially theoretical, the method is still developed today [32–35] because (i) it provides the essential information about the limit of economy for a given structural frame, and (ii) it lays the basis of *layout optimization*.

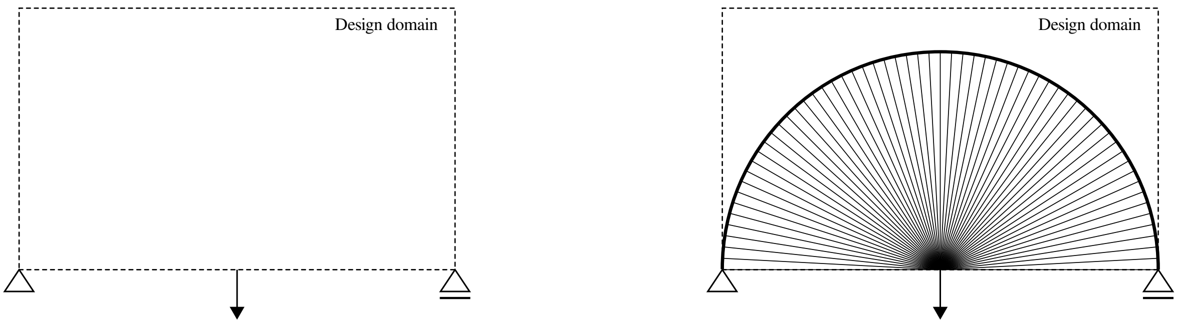

(a) Design domain (b) Michell's optimal solution

Figure 1.3: Michell's half-wheel. The design domain is subjected to a central load and supported at both extremities (a). The optimal solution is a semi-circular arch with tension spokes carrying the load (b).

Layout optimization is a computational method at the boundary between mathematical programming and structural mechanics. It deals with the simultaneous optimization of the sizing, the geometry, and the topology of discrete or continuum mechanical systems [36]. For discrete systems like trusses,

[2] Techniques based on graphic statics are still used today for their intuitive and visual features of equilibrium problems [23, 24].

[3] In 1920s, an experimental tests campaign on steel frames was carried out by the Committee for the Development of Steel Structures in UK [25].

the most investigated aspect is sizing and topology optimization[4] where structural component sizes and system connectivity are simultaneously optimized using continuous cross-sectional areas. The convexity of formulations in topology optimization allows for addressing very large structural designs by deterministic optimization algorithms. The range of current applications covers lower-bound analysis of masonry arch and vaulted structures, identification of critical failure mechanisms in soil mechanics, development of strut-and-tie models for reinforced concrete, and design optimization of truss frames. As topology optimization could also mimic geometry optimization by working with a dense grid, some attempts have been made to apply topology optimization to the preliminary shape design of lightweight structures [37], but it often results in impractical designs.

By introducing geometrical variables, the problem becomes inherently non-convex, thus prone to multiple local optima. This is not particularly troublesome as, in practice, the "perfect" structure is a theoretical delusion. Often for human's mind, a sub-optimal design makes more sense than the global optimum. Baker said: "Consider the Eiffel Tower: it is an extremely inefficient way of creating a restaurant, but Paris, and the world, would be much diminished by its absence" [38]. Any local optimum is potentially interesting for the designer. Hence, our approach will allow the designer to infuse an architectural intent to focus on meaningful regions of the infinite design space.

1.4 Achievements of the thesis

This thesis aims to give a unified optimization formulation for the preliminary shape design of lightweight structures. The choice of the truss element formulation for modeling such structures made of discrete components is vindicated at early design stages.

Most previous works in truss layout optimization focused on topology optimization. In the present work, we claim that incorporating geometry optimization gains the full potential of truss layout optimization. However, truss geometry and topology optimization arouses several fundamental design and mathematical challenges, which remain unsolved in the literature and will be thoroughly investigated to achieve our goal.

From a numerical point of view, the stumbling blocks are the non-convexity of the design space and the mathematical singularities. Since mathematical programming is based on the intrinsic properties of the problem to be optimized, the problem formulation should be simple and regular enough to allow for an efficient numerical treatment. Otherwise, any numerical deficiency or non-optimal solution will be detected by the optimization algorithm and sanctioned by misconvergence.

The key ingredient for the success of the present approach combines mathematical programming and structural mechanic theories: the structural properties of optimal shapes are used to devise suitable formulations. The proposed method will be general enough to tackle the following issues (Fig. 1.4):

- lightness and stiffness as design targets;
- cross-section, system connectivity, and nodal position as design variables;
- consideration of multiple loading to closely resemble real-world engineering design problems;
- self-weight of structural members especially impacting long-span lightweight structures;
- fundamental restrictions in structural design such as allowable stresses and displacements;
- a conceptually simple way to ensure stability of structural frameworks;
- an open box for incorporating structural, geometrical, and technological constraints.

The remainder of this dissertation is organized as follows. Chapter 2 lays the basis of truss layout optimization. The basic problem statement of topology optimization is introduced and extended to

[4]In the literature, sizing and topology optimization is often called topology optimization for short.

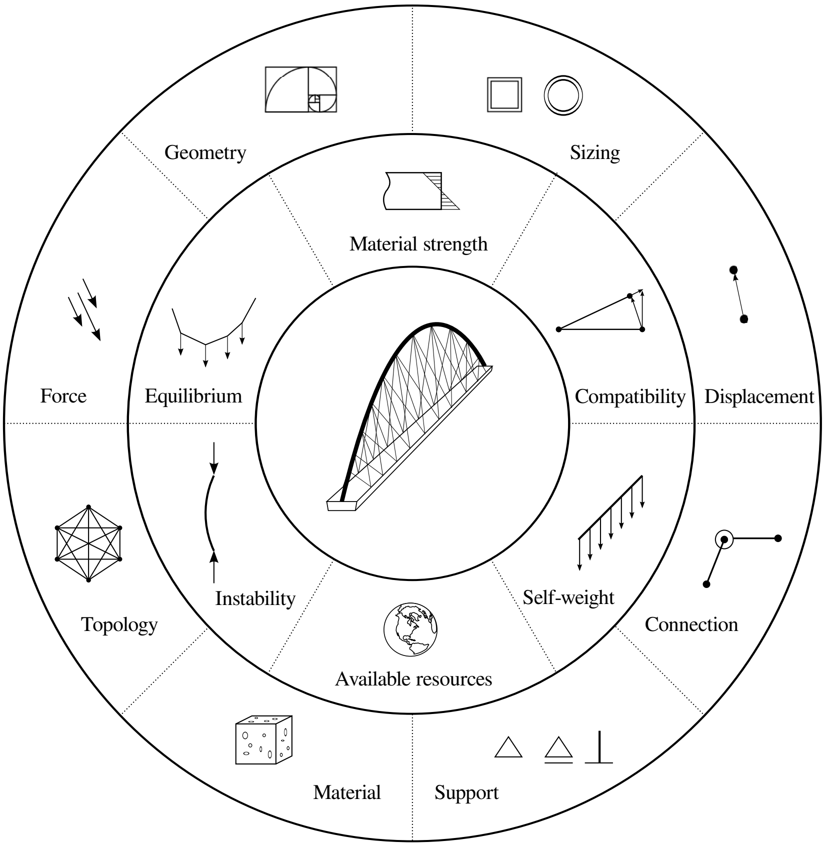

Figure 1.4: Symbolic representation of the design features incorporated in the present method. The outer ring contains design parameters and the inner ring contains design requirements.

cover different design settings and geometry optimization. At each step, the numerical difficulties are clearly identified and illustrated on simple examples.

Chapter 3 proposes a novel formulation for truss geometry and topology which constitutes the first main contribution of this thesis. The formulation is derived for both volume and compliance optimization including multiple loading and self-weight. The selection of the most appropriate algorithm to solve the problem is also investigated. Finally, two numerical experiments highlight the impact of design settings on the solution.

In Chapter 4, the stability of lightweight structures is considered in the context of truss layout optimization. After a description of current approaches in topology optimization, the proposed method introduces nominal loading cases together with Euler buckling criterion to ensure local and nodal stability. The method is efficient and readily applied to several numerical examples.

Finally, Chapter 5 demonstrates the effectiveness and the versatility of the proposed method to tackle structural design applications from engineering design practice, including system stabilizations, reticulated domes, and bridge designs.

2 Truss layout optimization

This chapter presents the general problem of truss layout optimization. After a brief introduction to standard theory of mathematical programming in Section 2.1, Section 2.2 derives the governing equations of truss structures. Then, Section 2.3 states the basic problem of topology optimization. The equivalence between volume and compliance minimization problems is also studied by means of necessary conditions of optimality. On this basis, Section 2.4 progressively builds up a general formulation by adding different design settings. At each step, the numerical difficulties associated with these building blocks are explained. Finally, the optimization of nodal positions is considered in Section 2.5, leading to the general design problem of truss geometry and topology optimization, which remains unsolved in the literature.

2.1 Standard theory of mathematical programming

Consider a general nonlinear optimization problem consisting in the minimization of an objective function subject to inequality and equality constraints [39]:

$$\min_{\mathbf{z}\in\mathbb{R}^{N_z}} \; f(\mathbf{z}) \tag{2.1a}$$

$$\text{s.t.: } g_i(\mathbf{z}) \leq 0, \;\; \forall i = 1, \dots, N_g, \tag{2.1b}$$

$$h_j(\mathbf{z}) = 0, \;\; \forall j = 1, \dots, N_h, \tag{2.1c}$$

where $f : \mathbb{R}^{N_z} \to \mathbb{R}$, $\mathbf{g} : \mathbb{R}^{N_z} \to \mathbb{R}^{N_g}$, $\mathbf{h} : \mathbb{R}^{N_z} \to \mathbb{R}^{N_h}$ are smooth functions and $\mathbf{z} \in \mathbb{R}^{N_z}$ is a vector of continuous variables. Smoothness of the objective function and the constraints is important to allow for a good prediction of the search direction by optimization algorithms. The feasible set of the optimization problem (2.1) is defined as

$$Z := \left\{ \mathbf{z} \in \mathbb{R}^{N_z} \;\middle|\; g_i(\mathbf{z}) \leq 0, \; h_j(\mathbf{z}) = 0, \; \forall i = 1, \dots, N_g, \; \forall j = 1, \dots, N_h \right\}. \tag{2.2}$$

In the feasible region, the inequality constraint $g_i(\mathbf{z}) \leq 0$ is said to be *active* if $g_i(\mathbf{z}) = 0$ and *inactive* if $g_i(\mathbf{z}) < 0$. To solve problem (2.1), we first transform it into an unconstrained optimization problem by introducing Lagrange multipliers $\boldsymbol{\lambda}_g \in \mathbb{R}_+^{N_g}$ and $\boldsymbol{\lambda}_h \in \mathbb{R}^{N_h}$ such that

$$\mathcal{L}(\mathbf{z}, \boldsymbol{\lambda}_g, \boldsymbol{\lambda}_h) := f(\mathbf{z}) + \sum_{i=1}^{N_g} \lambda_{g,i} g_i(\mathbf{z}) + \sum_{j=1}^{N_h} \lambda_{h,j} h_j(\mathbf{z}). \tag{2.3}$$

Thus, solving problem (2.1) amounts now to finding a stationary point to (2.3). If $g_i(\mathbf{z})$ is active, we ensure that the search direction points towards the feasible region by enforcing the dual feasibility $\lambda_{g,i} \geq 0$. If g_i is inactive, one can remove the constraint by setting the complementary slackness $\lambda_{g,i} g_i(\mathbf{z}) = 0$. These additional constraints are parts of the Karush-Kuhn-Tucker (KKT) optimality conditions [39]. Let $\mathbf{z}^*$ be a local minimizer of problem (2.1). Provided that some regularity conditions hold, then there exists $\lambda_{g,i}$ and $\lambda_{h,j}$ such that the first-order necessary conditions of optimality, or

KKT conditions, are satisfied

$$\nabla f\left(\mathbf{z}^{*}\right)+\sum_{i=1}^{N_g} \lambda_{g,i} \nabla g_i\left(\mathbf{z}^{*}\right)+\sum_{j=1}^{N_h} \lambda_{h,j} \nabla h_j\left(\mathbf{z}^{*}\right)=0, \tag{2.4a}$$

$$h_j\left(\mathbf{z}^{*}\right)=0,\ \forall j=1, \ldots, N_h, \tag{2.4b}$$

$$\lambda_{g,i} \geq 0,\ g_i\left(\mathbf{z}^{*}\right) \leq 0, \lambda_{g,i} g_i\left(\mathbf{z}^{*}\right)=0,\ \forall i=1, \ldots, N_g. \tag{2.4c}$$

The *regularity conditions* or *constraint qualifications* of problem (2.1) are necessary conditions that enable a numerical treatment by standard algorithms of mathematical programming. There are many constraints qualifications in the literature (see [40] for a comprehensive survey). Hereafter, three prominent conditions are listed:

- the *linear constraint qualification* implies that if g_i and h_j are affine functions, then all subsequent constraints qualifications are satisfied;
- the *linear-independence constraint qualification* holds if the gradients of active inequality constraints $\nabla g_i\left(\mathbf{z}^{*}\right)$ and equality constraints $\nabla h_j\left(\mathbf{z}^{*}\right)$ are linearly independent at $\mathbf{z}^{*}$;
- the *Mangasarian-Fromovitz constraint qualification* holds if the gradients of active inequality constraints $\nabla g_i\left(\mathbf{z}^{*}\right)$ and equality constraints $\nabla h_j\left(\mathbf{z}^{*}\right)$ are positive-linearly independent at $\mathbf{z}^{*}$.

For the remainder, the special case of *linear programming* should be mentioned. Such an optimization problem minimizes a linear objective function subject to linear equality and inequality constraints with non-negative variables. The convexity of the problem implies that a local optimum is also a global optimum and authorizes an efficient treatment by optimization algorithms [41]. We will see in Section 2.3 that, very often, it is possible to reformulate topology optimization problems so that linear programming applies.

2.2 Governing equations of truss structures

Before stating the structural optimization problem, let us start with some basic notations for a linear elastic truss structure as depicted in Fig. 2.1. Using standard finite element concepts, we consider a pin-jointed structure composed of N_n nodes interconnected by truss elements $e \in \{1, \ldots, N_b\}$. With $d \in \{2,3\}$ being the spatial dimension and N_s the number of support reactions, the number of degrees of freedom is $N_d = d.N_n - N_s$. The vector of nodal coordinates is denoted by $\mathbf{x} \in \mathbb{R}^{d.N_n}$, the vector of nodal displacements by $\mathbf{u} \in \mathbb{R}^{N_d}$, and the vector of external forces by $\mathbf{f} \in \mathbb{R}^{N_d}$ (excluding support reactions). The member force is $t_e \in \mathbb{R}$. The design parameters associated to every truss element are the length $l_e \in \mathbb{R}_+$ and the cross-sectional area $a_e \in \mathbb{R}_+$ which, together, give the member volume $v_e = a_e l_e \in \mathbb{R}_+$. Using these notations, the static equilibrium equations between the internal forces

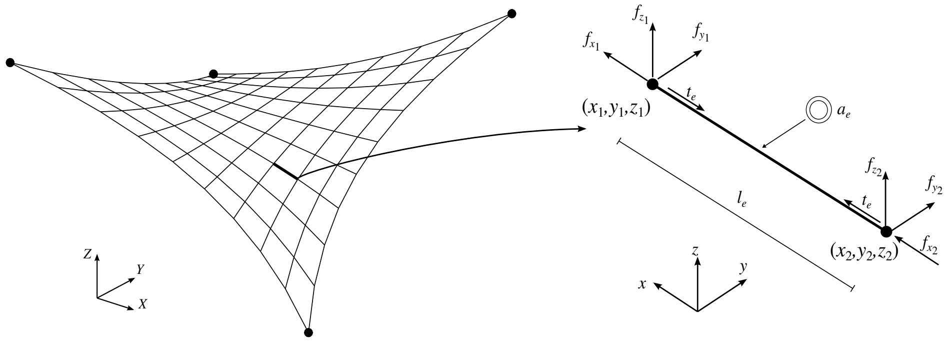

Figure 2.1: Notation for a truss element belonging, for instance, to a pre-stressed cable-net structure

and the external loading are written into an expanded form as [42]

$$\sum_{e=1}^{N_b} t_e \boldsymbol{\gamma}_e = \mathbf{f}, \tag{2.5}$$

or more compactly

$$\mathbf{B}\mathbf{t} = \mathbf{f}. \tag{2.6}$$

where, for all member $e = 1, \ldots, N_b$, the symbol $\boldsymbol{\gamma}_e \in \mathbb{R}^{N_d}$ represents the vector collecting the direction cosines, and $\mathbf{B} \in \mathbb{R}^{N_d \times N_b}$ is the so-called equilbrium matrix concatenating the vector of directions cosines, i.e. $\mathbf{B} = \begin{bmatrix} \boldsymbol{\gamma}_1 & \ldots & \boldsymbol{\gamma}_e & \ldots & \boldsymbol{\gamma}_{N_b} \end{bmatrix}$. Assuming small deformations, the linear compatibility condition between the nodal displacements $\mathbf{u} \in \mathbb{R}^{N_d}$ and the element elongation $\boldsymbol{\epsilon} \in \mathbb{R}^{N_b}$ is [42]

$$\boldsymbol{\gamma}_e^\top \mathbf{u} = \epsilon_e, \ \forall e = 1, \ldots, N_b, \tag{2.7}$$

or using the compact notation of the equilibrium matrix

$$\mathbf{B}^\top \mathbf{u} = \boldsymbol{\epsilon}. \tag{2.8}$$

Then, for an elastic material of Young's modulus $E_e \in \mathbb{R}_+$, the Hooke's law stating the relation between the axial stress $\sigma_e := t_e/a_e \in \mathbb{R}$ and strains $\varepsilon_e \in \mathbb{R}$ of the e-th element is simply

$$\frac{t_e}{a_e} = E_e \varepsilon_e, \ \forall e = 1, \ldots, N_b, \tag{2.9}$$

where the axial strain is given by the ratio of the elongation ϵ_e on the length, i.e.

$$\varepsilon_e = \frac{\epsilon_e}{l_e}, \ \forall e = 1, \ldots, N_b. \tag{2.10}$$

The solution to Eqs. (2.5), (2.7), and (2.9) requires a thorough study of the statical and kinematical determinacies of the structural system. Pellegrino [43, 44] identified four classes of truss structural assembly, as reported in Table 2.1. It is important to note that lightweight structures may belongs to any of those classes. This will have serious consequences on the structural optimization process.

Frequently, the equilibrium equations for classical truss structures are formulated in terms of displacements by combining Eqs. (2.5)-(2.9), leading to the following equality

$$\mathbf{K}\mathbf{u} = \mathbf{f}, \tag{2.11}$$

where, by definition of the reduced stiffness matrix,

$$\mathbf{K} := \sum_{e=1}^{N_b} \frac{E_e a_e}{l_e} \boldsymbol{\gamma}_e \boldsymbol{\gamma}_e^\top \in \mathbb{R}^{N_d \times N_d}. \tag{2.12}$$

In absence of mechanisms in the structural assembly (i.e. for assembly classes I and III), the stiffness matrix is symmetric positive definite and there exists a unique solution $\mathbf{u}$ to linear system (2.11). In Section 2.3, we will see that the treatment of equilibrium equations is a central issue in structural optimization and depends on whether the optimal structure might contain indeterminacy.

Class	Properties	Existence of solution	Example
I	$N_{ss} = 0$ $N_m = 0$	(2.5) has a unique solution for any loads. (2.7) has a unique solution for any elongations.	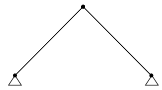
II	$N_{ss} = 0$ $N_m > 0$	(2.5) has a unique solution for compatible loads. (2.7) has an infinity of solutions for any elongations.	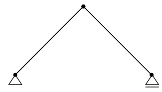
III	$N_{ss} > 0$ $N_m = 0$	(2.5) has an infinity of solutions for any loads. (2.7) has a unique solution for compatible elongations.	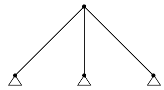
IV	$N_{ss} > 0$ $N_m > 0$	(2.5) has an infinity of solutions for compatible loads. (2.7) has an infinity of solutions for compatible elongations.	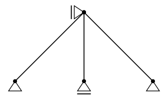

Table 2.1: Classification of truss structural systems according to Pellegrino [44]. N_{ss} denotes the number of independent states of self-stress, or degree of hyperstaticity, and N_m denotes the number of independent zero-energy deformation modes, or mechanisms. The structure is said to be statically and kinematically determinate when $N_{ss} = 0$ and $N_m = 0$, respectively.

2.3 Layout and topology optimization

2.3.1 Basic problem statement

Layout optimization is among one of the most general approach for structural design. Given a design domain subjected to boundary and loading conditions, layout optimization aims to find the best material distribution according to the problem definition. The stress-constrained minimum volume problem has been studied more than a century ago with the classical Michell's theorem [30], which gives the limit of economy for a structural frame. As said in Section 1.3, the scope is essentially theoretical but it provides an essential information on how far a structure can be further optimized by relaxing constraints (in the general sense).

The exact optimal layout given by Michell's theory can be numerically approached via truss layout optimization. Based on a discretized model, the method follows the ground structure approach [46] where the design domain (Fig. 2.2(a)) is divided into a grid of nodal points interconnected by tentative bars (Fig. 2.2(b)). The most investigated strategy to solve the problem is topology optimization where both structural component sizes and system connectivity are simultaneously optimized. Cross-sectional areas $\mathbf{a} \in \mathbb{R}^{N_b}$ are generally defined as continuous design variables. As such, topology optimization can be viewed as a sizing optimization problem with side constraints:

$$a_1, \ldots, a_e, \ldots, a_{N_b} \geq 0. \tag{2.13}$$

The accuracy of truss topology optimization with respect to the exact analytical solution depends on the density of the grid, but also on the system connectivity: it can be limited to neighboring nodes (Figs. 2.2(c) and 2.2(d)), to a given order of vicinity, or expanded to all nodes (Figs. 2.2(e) and 2.2(f)). Obviously, the latter case leads to better results, but at the expense of a considerable computational cost along with the presence of long and slender elements that are seemed inefficient to resist local buckling.

Regarding the problem definition, most of the developments in the literature are concentrated on compliance despite the fact that stress is among the most important consideration (see the monograph [47] for a comprehensive overview). Two main reasons explains this choice. Firstly, compliance optimization problems are generally convex and thus easier to solve by mathematical programming [48]. Secondly, for single loading, compliance optimization is equivalent to the stress-constrained

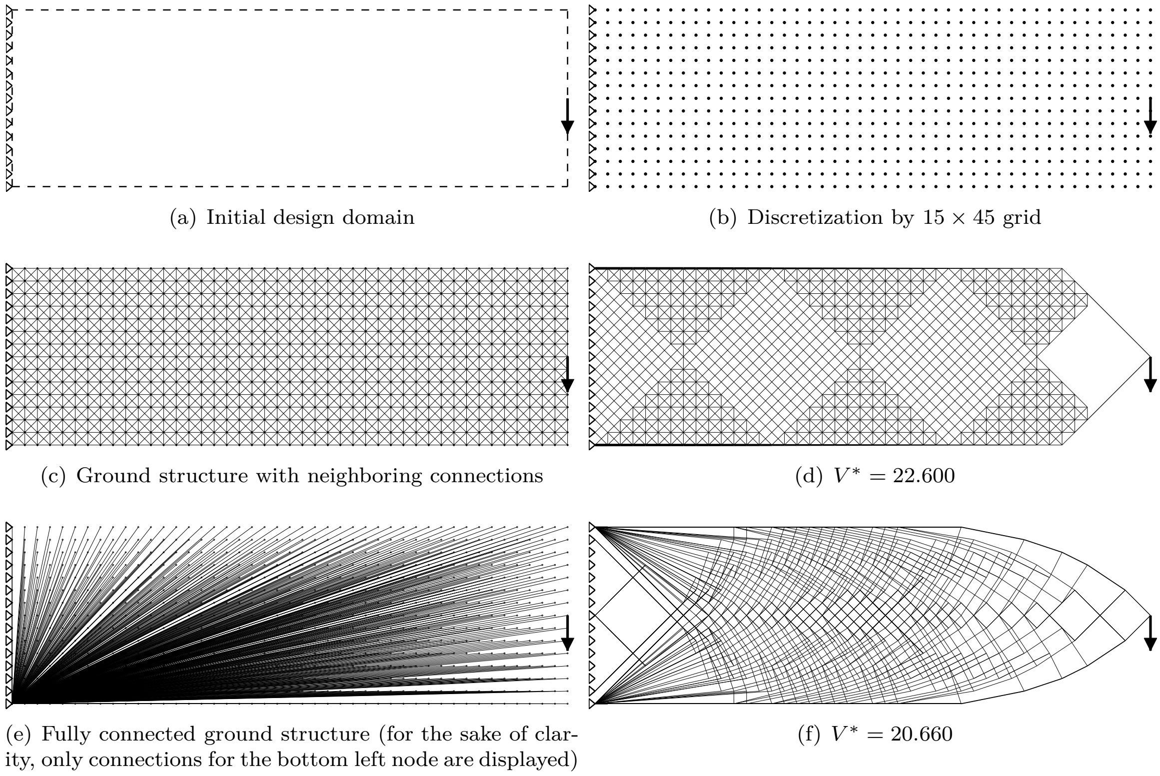

(a) Initial design domain

(b) Discretization by 15 × 45 grid

(c) Ground structure with neighboring connections

(d) $V^* = 22.600$

(e) Fully connected ground structure (for the sake of clarity, only connections for the bottom left node are displayed)

(f) $V^* = 20.660$

Figure 2.2: A cantilever truss. The design domain is a rectangular panel of ratio 3:1. The supports are applied on leftmost nodes. A downward unit load is applied on the rightmost middle node. The exact analytical solution of 19.036 was calculated in [45]. The design domain and the initial ground structure are given in (a) and (b), respectively. For a ground structure with adjacently connected nodes (c), the optimal layout is depicted in (d). For a fully connected ground structure (e), the optimal layout is depicted in (f).

minimum volume problem [49] (see also Section 2.3.2).

The goal of compliance optimization is to distribute a given amount of material to obtain a structure with maximum stiffness (i.e. of minimum compliance). Typically, the external work of applied loads is minimized subject to a global constraint on the allowable volume $\overline{V} \in \mathbb{R}_+$:

$$\min_{\mathbf{a}\in\mathbb{R}^{N_b},\mathbf{u}\in\mathbb{R}^{N_d}} \quad \mathbf{f}^T\mathbf{u} \tag{2.14a}$$

$$\text{s.t.: } \mathbf{K}\left(\mathbf{a}\right)\mathbf{u} = \mathbf{f}, \tag{2.14b}$$

$$\sum_{e=1}^{N_b} v_e\left(\mathbf{a}\right) = \overline{V},\ a_e \geq 0,\ \forall e = 1,\ldots,N_b. \tag{2.14c}$$

The enforcement of strict zero lower-bounds on cross-sectional areas permits the removal of structural members. The resulting problem may converge to optimal structures with mechanisms: the system under unstable equilibrium is optimized for the applied loads but any perturbation of loads might lead to the structural collapse. Stability issues will be investigated in Chapter 4.

Equivalently, compliance optimization can be solved by minimizing the complementary (strain) energy. This switch is permitted because the total potential energy principle states that the external work and the complementary energy are equal at equilibrium:

$$\mathbf{f}^\top\mathbf{u} = \sum_{e=1}^{N_b} \frac{t_e^2 l_e}{E_e a_e}. \tag{2.15}$$

Using this objective function, the implementation benefits from the minimum complementary energy principle. In linear elasticity theory, among all stress components satisfying the static equilibrium equations, the actual stress distribution that enforces the compatibility condition is obtained by minimizing the complementary energy [50]. Hence, compatibility equations can be removed from the problem formulation and the problem is stated with static equilibrium equations (2.5). Once again, a non-negative lower-bound must be enforced to avoid infinite values of the complementary energy (2.15). With these considerations, we end up with the following problem [48]:

$$\min_{\mathbf{a}\in\mathbb{R}^{N_b},\mathbf{t}\in\mathbb{R}^{N_b}} \sum_{e=1}^{N_b} \frac{t_e^2 l_e}{E_e a_e} \tag{2.16a}$$

$$\text{s.t.:} \sum_{e=1}^{N_b} t_e \boldsymbol{\gamma}_e = \mathbf{f}, \tag{2.16b}$$

$$\sum_{e=1}^{N_b} v_e(\mathbf{a}) = \overline{V},\ a_e \geq \overline{a}^{\,-},\ \forall e = 1,\ldots,N_b. \tag{2.16c}$$

Finally, we consider a tractable form of the classical problem which consists in reducing as much as possible the volume of material while enforcing that member stresses remain below the maximal allowable value $\overline{\sigma} \in \mathbb{R}_+$. Early work formulates this stress-constrained minimum volume problem in plastic design by neglecting the compatibility condition [46, 51–53]:

$$\min_{\mathbf{a}\in\mathbb{R}^{N_b},\ \mathbf{t}\in\mathbb{R}^{N_b}} \sum_{e=1}^{N_b} a_e l_e \tag{2.17a}$$

$$\text{s.t.:} \sum_{e=1}^{N_b} t_e \boldsymbol{\gamma}_e = \mathbf{f}, \tag{2.17b}$$

$$-a_e\overline{\sigma} \leq t_e \leq a_e\overline{\sigma},\ a_e \geq 0,\ \forall e = 1,\ldots,N_b, \tag{2.17c}$$

where stress constraints (2.17c) are multiplied by cross-sectional areas in order to avoid that $\sigma_e \to \pm\infty$ when $a_e \to 0$ for some vanishing members $e \in \{1,\ldots,N_b\}$ [48].

For solving problems (2.14), (2.16), and (2.17), it is important to observe that they are all are equivalent in a certain sense. This property can be used to reformulate them as a linear programming problem, as shown in Section 2.3.2.

2.3.2 Problem equivalence and numerical solution

The present section shows that compliance and volume optimization under single loading lead to the same optimal truss and that a unique formulation in linear programming can be used for solving them. The study of optimality conditions is thus necessary for devising an efficient optimization process. In this aim, the relationship between compliance and volume optimization is first studied via the single-bar truss example of Fig. 2.3.

For compliance optimization, we intuitively understand that the process tends to increase a while enforcing the limit on the allowable volume of material $al = \overline{V}$, whereas volume optimization tends to decrease a while enforcing the limit on the allowable stress $\sigma < \overline{\sigma}$. It turns out that both problems converge to the same optimum in the design space (up to a factor which depends on the ratio between $\overline{V}$ and $\overline{\sigma}$). This can be demonstrated if there is a unique solution satisfying the KKT conditions for the three following formulations: the minimum compliance (2.14) identified by I, the minimum

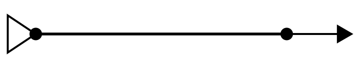

Figure 2.3: The one-bar truss example. For convenience, the length is set at $l = 1$, the pulling force at $f = 1$, the Young's modulus at $E = 1$, the direction cosine at $\gamma = 1$, the allowable volume at $\overline{V} = 1$, and the limiting stresses at $\overline{\sigma} = 1$.

complementary energy (2.16) identified by II, and the minimum volume (2.17) identified by III. For the single-bar truss, these problems are given by

$$\min_{a^{\mathrm{I}}\in\mathbb{R},u^{\mathrm{I}}\in\mathbb{R}} \left\{ f^{\mathrm{I}}u^{\mathrm{I}} \;\middle|\; \frac{Ea^{\mathrm{I}}}{l}\gamma^2 u^{\mathrm{I}} = f^{\mathrm{I}},\ a^{\mathrm{I}}l = \overline{V},\ a^{\mathrm{I}} \geq 0 \right\}, \tag{2.18}$$

$$\min_{a^{\mathrm{II}}\in\mathbb{R},t^{\mathrm{II}}\in\mathbb{R}} \left\{ \frac{t^{\mathrm{II},2}l}{Ea^{\mathrm{II}}} \;\middle|\; t^{\mathrm{II}}\gamma = f^{\mathrm{II}},\ a^{\mathrm{II}}l = \overline{V},\ a^{\mathrm{II}} \geq \overline{a}^{\ -} \right\}, \tag{2.19}$$

$$\min_{a^{\mathrm{III}}\in\mathbb{R},t^{\mathrm{III}}\in\mathbb{R}} \left\{ a^{\mathrm{III}}l \;\middle|\; t^{\mathrm{III}}\gamma = f^{\mathrm{III}},\ -a^{\mathrm{III}}\overline{\sigma} \leq t^{\mathrm{III}} \leq a^{\mathrm{III}}\overline{\sigma},\ a^{\mathrm{III}} \leq 0 \right\}. \tag{2.20}$$

The Lagrangian of these problems are respectively

$$\mathcal{L}^{\mathrm{I}} = f^{\mathrm{I}}u^{\mathrm{I}} + \lambda_1^{\mathrm{I}}\left(\frac{Ea^{\mathrm{I}}}{l}\gamma^2 u^{\mathrm{I}} - f^{\mathrm{I}}\right) + \lambda_2^{\mathrm{I}}\left(a^{\mathrm{I}}l - \overline{V}\right) + \lambda_3^{\mathrm{I}}\left(-a^{\mathrm{I}}\right), \tag{2.21}$$

$$\mathcal{L}^{\mathrm{II}} = \frac{t^{\mathrm{II},2}l}{Ea^{\mathrm{II}}} + \lambda_1\left(t^{\mathrm{II}}\gamma - f^{\mathrm{II}}\right) + \lambda_2^{\mathrm{II}}\left(a^{\mathrm{II}}l - \overline{V}\right) + \lambda_3^{\mathrm{II}}\left(\overline{a}^{\ -} - a^{\mathrm{II}}\right), \tag{2.22}$$

$$\mathcal{L}^{\mathrm{III}} = a^{\mathrm{III}}l + \lambda_1^{\mathrm{III}}\left(t^{\mathrm{III}}\gamma - f^{\mathrm{III}}\right) + \lambda_2^{\mathrm{III}}\left(t^{\mathrm{III}} - a^{\mathrm{III}}\overline{\sigma}\right) + \lambda_3^{\mathrm{III}}\left(-t^{\mathrm{III}} - a^{\mathrm{III}}\overline{\sigma}\right) + \lambda_4^{\mathrm{III}}\left(-a^{\mathrm{III}}\right). \tag{2.23}$$

By differentiation we obtain the KKT conditions for (2.21) by

$$\lambda_1^{\mathrm{I}}\frac{E}{l}\gamma^2 u^{\mathrm{I}} + \lambda_2^{\mathrm{I}}l - \lambda_3^{\mathrm{I}} = 0,\ f^{\mathrm{I}} + \lambda_1^{\mathrm{I}}\frac{Ea^{\mathrm{I}}}{l}\gamma^2 = 0, \tag{2.24a}$$

$$\frac{Ea^{\mathrm{I}}}{l}\gamma^2 u^{\mathrm{I}} = f^{\mathrm{I}},\ al^{\mathrm{I}} = \overline{V},\ -a^{\mathrm{I}} \leq 0,\ \lambda_3^{\mathrm{I}} \geq 0,\ \lambda_3^{\mathrm{I}}a^{\mathrm{I}} = 0, \tag{2.24b}$$

for (2.22) by

$$-\frac{t^{\mathrm{II},2}l}{Ea^{\mathrm{II},2}} + \lambda_2^{\mathrm{II}}l - \lambda_3^{\mathrm{II}} = 0,\ \frac{2t^{\mathrm{II}}l}{Ea^{\mathrm{II}}} + \lambda_1^{\mathrm{II}}\gamma = 0, \tag{2.25a}$$

$$t^{\mathrm{II}}\gamma = f^{\mathrm{II}},\ a^{\mathrm{II}}l = \overline{V},\ a^{\mathrm{II}} \geq \overline{a}^{\ -},\ \lambda_3^{\mathrm{II}} \geq 0,\ \lambda_3^{\mathrm{II}}\left(\overline{a}^{\ -} - a^{\mathrm{II}}\right) = 0, \tag{2.25b}$$

and for (2.23) by

$$l - \lambda_2^{\mathrm{III}}\overline{\sigma} - \lambda_3^{\mathrm{III}}\overline{\sigma} - \lambda_4^{\mathrm{III}} = 0,\ \lambda_1^{\mathrm{III}}\gamma + \lambda_2^{\mathrm{III}} - \lambda_3^{\mathrm{III}} = 0, \tag{2.26a}$$

$$t^{\mathrm{III}}\gamma = f^{\mathrm{III}},\ t^{\mathrm{III}} \leq a^{\mathrm{III}}\overline{\sigma},\ -t^{\mathrm{III}} \leq a^{\mathrm{III}}\overline{\sigma},\ -a^{\mathrm{III}} \leq 0, \tag{2.26b}$$

$$\lambda_2^{\mathrm{III}}, \lambda_3^{\mathrm{III}}, \lambda_4^{\mathrm{III}} \geq 0, \tag{2.26c}$$

$$\lambda_2^{\mathrm{III}}\left(t^{\mathrm{III}} - a^{\mathrm{III}}\overline{\sigma}\right) = 0,\ \lambda_3^{\mathrm{III}}\left(-t^{\mathrm{III}} - a^{\mathrm{III}}\overline{\sigma}\right) = 0,\ \lambda_4^{\mathrm{III}}a^{\mathrm{III}} = 0. \tag{2.26d}$$

For the same optimal design $a^{\mathrm{I}} = a^{\mathrm{II}} = a^{\mathrm{III}} = 1$ with state variables $u^{\mathrm{I}} = u^{\mathrm{II}} = u^{\mathrm{III}} = 1$, $t^{\mathrm{I}} = t^{\mathrm{II}} = t^{\mathrm{III}} = 1$, and $\sigma^{\mathrm{I}} = \sigma^{\mathrm{II}} = \sigma^{\mathrm{III}} = 1$, one can find Lagrange multipliers satisfying the optimality conditions (2.24)-(2.26). We also verify that the compatibility condition (2.7) is satisfied at the optimum, i.e. $\sigma^* = (E/l)\,\gamma u^*$. Hence, the following assertions hold for the single loading case:

- the optimal compliance problems using the external work or complementary energy are identical,
- the compliance and volume optimization problems converge to an equivalent solution,
- this equivalent solution is a fully stressed design with the same strain energy density σ^2/E in each bar,
- such a solution obtained in plastic design automatically enforces the compatibility condition.

The assertions are still valid when the optimal structure is statically indeterminate [49] and for different yield stresses in tension and compression [53]. These properties allows to reformulate the problem by linear programming algorithms.

To do so, the vector of internal forces can be expressed by non-negative tension force $\mathbf{t}^+ \in \mathbb{R}_+^{N_b}$ and compression force $\mathbf{t}^- \in \mathbb{R}_+^{N_b}$ such that $\mathbf{t} = \mathbf{t}^+ - \mathbf{t}^-$. The fully stressed design assumption allows to define the cross-sectional area in terms of internal forces:

$$a_e\left(t_e^+, t_e^-\right) := \frac{1}{\overline{\sigma}}\left(t_e^+ + t_e^-\right),\ \forall e = 1, \ldots, N_b. \tag{2.27}$$

Introducing these variable changes in the minimum volume problem results in the linear programming formulation:

$$\min_{\mathbf{t}^+ \in \mathbb{R}^{N_b}, \mathbf{t}^- \in \mathbb{R}^{N_b}} \sum_{e=1}^{N_b} \frac{l_e}{\overline{\sigma}}\left(t_e^+ + t_e^-\right) \tag{2.28a}$$

$$\text{s.t.:} \sum_{e=1}^{N_b}\left(t_e^+ - t_e^-\right)\boldsymbol{\gamma}_e = \mathbf{f}, \tag{2.28b}$$

$$t_e^+ \geq 0, t_e^- \geq 0,\ \forall e = 1, \ldots, N_b. \tag{2.28c}$$

The problem structure implies that either t_e^+ or t_e^- will be non-zero at the optimum. The use of specific linear programming algorithm will efficiently find the global optimum for very large design space [54].

Using this formulation, much effort is currently devoted to developing adding member procedures for high-density ground structures [54–56]. This loosely constrained problem in topology optimization with many nodes will converge to continuous-like Michell's truss. However, the practical applicability is not obvious. For this reason, the formulation must be extended to consider more realistic designs.

2.4 Generalization

2.4.1 Self-weight and multiple loading

Truss topology optimization can be generalized in various ways to include additional design settings. A first aspect, often neglected in the literature, is self-weight of structural members and assemblies, which may have a considerable impact on the design of long-span lightweight structures. In this work, we assume that self-weight is equally carried by truss end-nodes while bending is neglected. Self-weight loads are considered as external forces that depends on the structural volume subject to gravity effects [47]. Let $\mathbf{g}_e \in \mathbb{R}^{N_d}$ be the vector of nodal gravitational forces for each member, the vector of external forces $\mathbf{f}$ becomes a design-dependent loading:

$$\mathbf{f} \xrightarrow{\text{self-weight}} \mathbf{f} + \sum_{e=1}^{N_b} v_e\left(\mathbf{a}\right)\mathbf{g}_e. \tag{2.29}$$

This seemingly minor extension significantly influences the design problem as well as the numerical procedure. The external force vector is no longer constant but varies with respect to the design variables. This might lead to trivial situations where self-weight loads exactly balance the external loading, thus resulting in unstressed structures. In the remainder, we will formally exclude such situations [47]:

$$\left\{\mathbf{a} \in \mathbb{R}_+^{N_b} \;\middle|\; \sum_{e=1}^{N_b} v_e\left(\mathbf{a}\right) = \overline{V},\ \mathbf{f} + \sum_{e=1}^{N_b} v_e\left(\mathbf{a}\right)\mathbf{g}_e = \mathbf{0}\right\} = \emptyset. \tag{2.30}$$

Another important consideration is multiple loading [57]. In practical applications, the structure is often subject to significant load changes. The designer must identify the envelope of most critical loading cases for which the structure is designed accordingly. Let $\mathbf{f}_k \in \mathbb{R}^{N_d}$ be the vector of external forces, at each loading condition $k = 1, \dots, N_c$ corresponds an equilibrium state. Hence, the system of equilibrium equations is expanded N_c times. Besides, the consideration of multiple loading conditions has consequences on the formulations and the design issues.

2.4.2 Compliance optimization

The extension of compliance optimization to include multiple loadings is not straightforward since there is one specific compliance measure by loading case:

$$c_k(\mathbf{a}, \mathbf{u}_k) = \left[\mathbf{f}_k + \sum_{e=1}^{N_b} v_e(\mathbf{a})\,\mathbf{g}_e\right]^\top \mathbf{u}_k,\ \forall k = 1, \dots, N_c. \tag{2.31}$$

Ideally, a structure minimizing simultaneously all specific compliances would be the optimal solution. However, such a solution does not exist in general, and a trade-off can be found by multicriteria optimization [58]. To combine these specific compliances in a single global measure, commonly accepted formulations are either the weighted-average or the worst-case compliance. In the former case, non-negative weights $w_k \in [0, 1]$ with $\sum_{k=1}^{N_c} w_k = 1$ are assigned to every specific compliance. Then, the weighted sum of specific compliances is minimized subject to a global constraint on the allowable volume of material $\overline{V}$:

$$\min_{\substack{\mathbf{a} \in \mathbb{R}^{N_b} \\ \mathbf{u}_k \in \mathbb{R}^{N_d}}} \quad \sum_{k=1}^{N_c} w_k c_k(\mathbf{a}, \mathbf{u}_k) \tag{2.32a}$$

$$\text{s.t.: } \mathbf{K}(\mathbf{a})\,\mathbf{u}_k = \mathbf{f}_k + \sum_{e=1}^{N_b} v_e(\mathbf{a})\,\mathbf{g}_e,\ \forall k = 1, \dots, N_c \tag{2.32b}$$

$$\sum_{e=1}^{N_b} v_e(\mathbf{a}) = \overline{V},\ a_e \geq 0,\ \forall e = 1, \dots, N_b. \tag{2.32c}$$

The latter case is a min-max optimization problem where the worst compliance over all loading cases is minimized:

$$\min_{\substack{\mathbf{a} \in \mathbb{R}^{N_b} \\ \mathbf{u}_k \in \mathbb{R}^{N_d}}} \quad \max_{k=1,\dots,N_c} c_k(\mathbf{a}, \mathbf{u}_k) \tag{2.33a}$$

$$\text{s.t.: } \mathbf{K}(\mathbf{a})\,\mathbf{u}_k = \mathbf{f}_k + \sum_{e=1}^{N_b} v_e(\mathbf{a})\,\mathbf{g}_e,\ \forall k = 1, \dots, N_c, \tag{2.33b}$$

$$\sum_{e=1}^{N_b} v_e(\mathbf{a}) = \overline{V},\ a_e \geq 0,\ \forall e = 1, \dots, N_b. \tag{2.33c}$$

Problems (2.32) and (2.33) can be reformulated as convex problems and solved by several techniques, for instance semi-definite programming [59] or second-order cone programming [60].

2.4.3 Volume optimization

The most useful formulation to explore different design settings remains the minimum volume problem. There are scenarios in which one wishes to impose different stress constraints corresponding to different load cases, and possibly on different regions of the structure [61]. For instance, stress constraints for permanent loads would be related the material's yield limit whereas stress constraints for repetitive loads would be related to the material's endurance limit. In steel structure, stress constraints may also depend on the region of the structure when different steel strength classes or element types are used (strut, cable, etc.). Similarly, limiting stresses in tension and compression can be different.

Other examples for displacements can be mentioned: tight displacement constraints can be enforced for permanent loads while accidental loading are not restricted. Moreover, displacement constraints can be different following the directions. For all these reasons, stress and displacement bounds must have the possibility to take different values with respect to each loading case $k = 1, \ldots, N_c$, spatial direction $i = 1, \ldots, N_d$, and structural member $e = 1, \ldots, N_b$.

Unlike some particular cases (e.g. [62]), the minimum volume problem with self-weight and multiple loading is generally not equivalent to compliance optimization [58]. Furthermore, the compatibility condition is required to obtain the actual stress field. To ensure meaningful solutions, limiting stresses in tension $\overline{\sigma}_{e,k}^{\,+} \in \mathbb{R}_+$ and compression $\overline{\sigma}_{e,k}^{\,-} \in \mathbb{R}_+$ are imposed for every structural loading cases and truss members. Moreover, nodal displacements can be restricted by different extrema denoted $\overline{u}_{i,k}^{\,-} \in \mathbb{R}_+$ and $\overline{u}_{i,k}^{\,+} \in \mathbb{R}_+$. Finally, compressive members are also sized to remains below the Euler critical buckling load $\overline{\sigma}_e^{\,\mathrm{cr}}$. Setting $\mathbf{u}_k$ as optimization variable, stresses are computed by combining compatibility equations (2.7) with Hooke's law (2.9) [63] and the minimum volume problem subject to stress, local buckling [64], and displacement constraints [65] takes the form [66]

$$\min_{\substack{\mathbf{a} \in \mathbb{R}^{N_b} \\ \mathbf{u}_k \in \mathbb{R}^{N_d}}} \quad \sum_{e=1}^{N_b} v_e\left(\mathbf{a}\right) \tag{2.34a}$$

$$\text{s.t.: } \mathbf{K}\left(\mathbf{a}\right)\mathbf{u}_k = \mathbf{f}_k + \sum_{e=1}^{N_b} v_e\left(\mathbf{a}\right)\mathbf{g}_e,\ \forall k = 1, \ldots, N_c, \tag{2.34b}$$

$$-\,\overline{\sigma}_{e,k}^{\,-} \leq \frac{E_e}{l_e}\boldsymbol{\gamma}^\top \mathbf{u}_k \leq \overline{\sigma}_{e,k}^{\,+},\ \forall e = 1, \ldots, N_b,\ \forall k = 1, \ldots, N_c, \tag{2.34c}$$

$$-\,\frac{E_e}{l_e}\boldsymbol{\gamma}_e^\top \mathbf{u}_k \leq \overline{\sigma}_e^{\,\mathrm{cr}}\left(\mathbf{a}\right),\ \forall e = 1, \ldots, N_b,\ \forall k = 1, \ldots, N_c, \tag{2.34d}$$

$$-\,\overline{u}_{i,k}^{\,-} \leq u_{i,k} \leq \overline{u}_{i,k}^{\,+},\ \forall i = 1, \ldots, N_d,\ \forall k = 1, \ldots, N_c, \tag{2.34e}$$

$$a_e \geq 0,\ \forall e = 1, \ldots, N_b. \tag{2.34f}$$

Problem (2.34) is inherently non-convex and does not have a specific mathematical structure (e.g. linear or quadratic programming). A formulation of the form (2.34) is called *simultaneous analysis and design* in the literature [67]. In those formulations both design and state variables are treated as optimization variables and the equilibrium equations set as equality constraints, which are solved by general-purpose nonlinear programming algorithms. Because we will follow the lines of this approach in our method, more details are given in Chapter 3.

Still, the most widespread approach to solve stress-constrained optimization problem (especially for the design of continuum structures) is *nested analysis and design* [67]: displacement variables are removed from (2.14) by performing a structural analysis via the displacement model (2.11). However, truss topology optimization is an unusual structural optimization problem because the stiffness matrix may become singular when members vanish (see Section 2.2). The intent of positive lower-bounds $\overline{a}^{\,-} \in \mathbb{R}_+$ on cross-sectional areas is to ensure that the stiffness matrix remains non-singular. These lower bounds are assumed small enough to be structurally insignificant. The resulting problem is stated as

$$\min_{\mathbf{a}\in\mathbb{R}^{N_b}} \sum_{e=1}^{N_b} v_e(\mathbf{a}) \tag{2.35a}$$

$$\text{s.t.:} \; -\overline{\sigma}_{e,k}^{\,-} \leq \frac{E_e}{l_e}\boldsymbol{\gamma}^\top \mathbf{u}_k(\mathbf{a}) \leq \overline{\sigma}_{e,k}^{\,+}, \;\forall e=1,\ldots,N_b,\; \forall k=1,\ldots,N_c, \tag{2.35b}$$

$$-\frac{E_e}{l_e}\boldsymbol{\gamma}_e^\top \mathbf{u}_k(\mathbf{a}) \leq \overline{\sigma}_e^{\,\mathrm{cr}}(\mathbf{a}), \;\forall e=1,\ldots,N_b,\; \forall k=1,\ldots,N_c, \tag{2.35c}$$

$$-\overline{u}_{i,k}^{\,-} \leq u_{i,k}(\mathbf{a}) \leq \overline{u}_{i,k}^{\,+}, \;\forall i=1,\ldots,N_d,\; \forall k=1,\ldots,N_c, \tag{2.35d}$$

$$a_e \geq \overline{a}^{\,-}, \;\forall e=1,\ldots,N_b. \tag{2.35e}$$

where the displacement variables are computed via a dedicated linear algebra routine

$$\mathbf{u}_k(\mathbf{a}) = \mathbf{K}(\mathbf{a})^{-1}\left(\mathbf{f}_k + \sum_{e=1}^{N_b} v_e(\mathbf{a})\,\mathbf{g}_e\right), \;\forall k=1,\ldots,N_c, \tag{2.36}$$

The solution process might converge to sub-optimal solutions because some members are not completely eliminated from the ground structure [68,69]. For more accuracy, Bruns [70] employs singular value decomposition but the analysis operation is also more expensive.

However, both problems (2.34) and (2.35) are very difficult to solve because the numerical process is prone to numerical difficulties due to the presence of stress and local buckling constraints, as discussed in the following.

2.4.4 Stress singularity

Topology optimization with stress constraints is difficult to solve because the optimum might correspond to a singular point in the design space. This phenomenon is called *stress singularity* or *singular topology* in the literature. Sved and Ginos [71] first pointed out singular topologies. The first representation of the corresponding feasible region is due to Hajela [72]. Kirsch also showed several properties of optimal topologies [73,74].

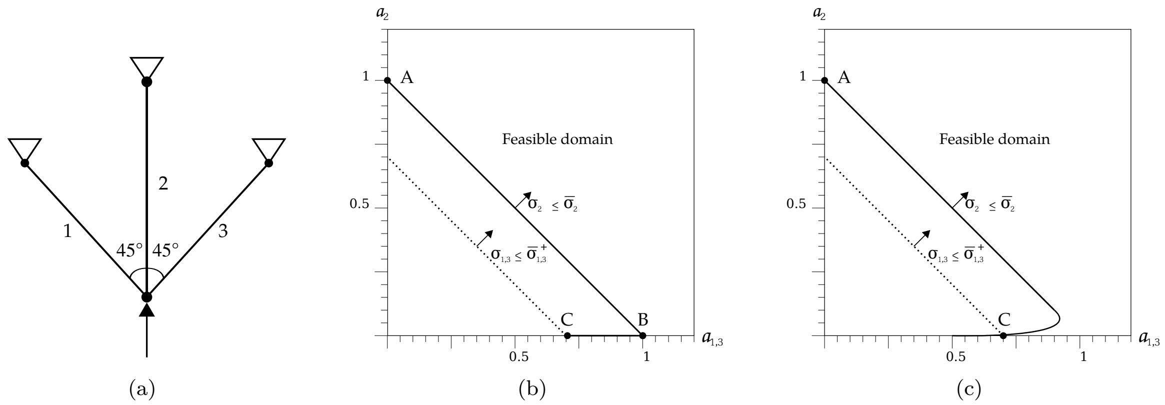

Figure 2.4: The three-bar truss example with stress singularity. The representation of the initial ground structure is given in (a). The system is subject to an upward unit load. Young's moduli are taken as $E_e = 1$, the length $l_e = 1$, and the limiting stresses are $\overline{\sigma}_e^{\,-} = 1$ and $\overline{\sigma}_e^{\,+} = 1$ for all $e = 1, 2, 3$. The corresponding design space with respect to a_1 and $a_{2,3}$ for the case with singular optimum (b) and using relaxed constraints (c).

For illustrative purpose, consider a variant of the three-bar truss example proposed by Kirsch [75]. The structure and the design settings are depicted in Fig. 2.4(a). To investigate various possibilities of optimal topologies, we introduce a non-negative parameter $\beta \in \mathbb{R}_+$ varying the cost of the second bar in the total volume function. Thus, the minimum volume problem subject to stress constraints is

$$\min_{\mathbf{a}\in\mathbb{R}^3_+,\mathbf{u}\in\mathbb{R}^2} \left\{ a_1 l_1 + \beta a_2 l_2 + a_3 l_3 \;\middle|\; \mathbf{K}(\mathbf{a})\,\mathbf{u} = \mathbf{f},\ -\overline{\sigma}_e^{\,-} \leq \frac{E_e}{l_e}\boldsymbol{\gamma}_e^\top \mathbf{u} \leq \overline{\sigma}_e^{\,+},\ \forall e = 1,2,3 \right\}. \tag{2.37}$$

Figure 2.4(b) depicts the corresponding design space. Using standard algorithms of mathematical programming, the solution process will converge to either point A or point B:

$$\text{Point A:} \qquad a_1 = 0, \qquad a_2 = 1, \qquad a_3 = 0, \qquad \text{if } \beta \leq 2, \tag{2.38a}$$

$$\text{Point B:} \qquad a_1 = 1, \qquad a_2 = 0, \qquad a_3 = 1, \qquad \text{if } \beta \geq 2. \tag{2.38b}$$

The optimal volume of point B is $V^* = 2$. However, the true optimum for this problem is

$$\text{Point A:} \qquad a_1 = 0, \qquad a_2 = 1, \qquad a_3 = 0, \qquad \text{if } \beta \leq \frac{1}{\sqrt{2}}, \tag{2.39a}$$

$$\text{Point C:} \qquad a_1 = \frac{1}{\sqrt{2}}, \qquad a_2 = 0, \qquad a_3 = \frac{1}{\sqrt{2}}, \qquad \text{if } \beta \geq \frac{1}{\sqrt{2}}. \tag{2.39b}$$

The value $V^* = \sqrt{2}$ of point C is below the optimal volume of point B. This demonstrates that optimization algorithms are unable to properly eliminate the redundant member 2. To figure that out, we expand the system $\mathbf{Ku} = \mathbf{f}$ into the following two equilibrium and three compatibility equations:

$$\frac{\sqrt{2}}{2}a_1\sigma_1 - \frac{\sqrt{2}}{2}a_3\sigma_3 = 0, \tag{2.40a}$$

$$-\frac{\sqrt{2}}{2}a_1\sigma_1 - a_2\sigma_2 - \frac{\sqrt{2}}{2}a_3\sigma_3 = 1, \tag{2.40b}$$

$$\frac{\sqrt{2}}{2}u_x - \frac{\sqrt{2}}{2}u_y = \frac{\sigma_1}{E_1}l_1, \tag{2.40c}$$

$$-u_y = \frac{\sigma_2}{E_2}l_2, \tag{2.40d}$$

$$-\frac{\sqrt{2}}{2}u_x - \frac{\sqrt{2}}{2}u_y = \frac{\sigma_3}{E_3}l_3. \tag{2.40e}$$

Stresses and displacements constitute the five unknowns of the linear system. We easily verify that solutions of Eqs. (2.40) for points A and B also satisfy stress constraints. By contrast, at point C, the compatibility condition (2.40d) of member 2 enforces $\sigma_2 = -2/\sqrt{2}$. This value is inconsistent with stress constraints because the allowable stress $-\overline{\sigma}_2^{\,-} = -1$ is exceeded. Hence, both stress and compatibility constraints for member 2 cannot be satisfied simultaneously and point C is discarded by the optimization algorithm. The situation is paradoxical since member 2 does not exist at point C but the optimization algorithm still handles those physically meaningless constraints.

Such a problem was recently identified as a *mathematical program with vanishing constraints* [76]. The major difficulty is that some regularity conditions of vanishing constraints – which are required to reach the true optimum – are violated. For instance, the dependence between compatibility condition and stress constraint of member 2 violates the *linear-independence constraint qualification*, and thus all subsequent regularity conditions. Obviously, assuming a plastic design (by neglecting compatibility equations) would prevent this conflict but the true optimum could be found only if the optimal topology is statically determinate [63, 68, 75]. A general relaxation method was developed in the framework of mathematical programming [77, 78].

Alternatively, the optimization problem can be stated in terms of cross-sectional areas by solving the equilibrium equations separately. Thus, the stress-constrained minimum volume takes the form

$$\min_{\mathbf{a}\in\mathbb{R}^3_+} \left\{ a_1 l_1 + \beta a_2 l_2 + a_3 l_3 \;\middle|\; -\overline{\sigma}_e^{\,-} \leq \frac{E_e}{l_e}\boldsymbol{\gamma}_e^\top \left(\mathbf{K}(\mathbf{a})^{-1}\mathbf{f}\right) \leq \overline{\sigma}_e^{\,+},\ \forall e = 1,2,3 \right\}. \tag{2.41}$$

To avoid that $\sigma_e(\mathbf{a}) \to \pm\infty$ when $a_e \to 0$, some authors [72, 79] proposed a variant but equivalent expression to make stress constraints feasible:

$$\left(\sigma_e(\mathbf{a}) - \overline{\sigma}_e^{+}\right) a_e \leq 0, \ \forall e = 1, \ldots, N_b, \tag{2.42a}$$

$$\left(\overline{\sigma}_e^{-} - \sigma_e(\mathbf{a})\right) a_e \leq 0, \ \forall e = 1, \ldots, N_b. \tag{2.42b}$$

Despite the fact that the stress constraints of non-existing members seemingly vanish, the design space represented in Fig. 2.4(b) shows that point C belongs to the strip BC. The difference of dimension between this degenerate subspace and the main feasible space is precisely the number of vanishing members. Standard algorithms of nonlinear programming cannot deal with these infinitesimally narrow strips. However, Cheng and Guo [79] pointed out that they are always connected to the main feasible design space.

This assertion has conducted several authors to develop techniques to relax stress constraints by expanding the region BC, as shown in Fig. 2.4(c). Among others, Rozvany [80] employed the Kreisselmeier-Steinhauser smooth envelope function, but the most popular and widely studied technique for truss topology optimization remains the ϵ-relaxation method [81]. The basic idea is to introduce a relaxation parameter $\epsilon \geq 0$ which continuously decreases $\epsilon \to 0$ so that the original problem is recovered at the optimum [42]. For this, the parameter ϵ is introduced into the stress constraints as follows

$$\left(\sigma_e(\mathbf{a}) - \overline{\sigma}_e^{+}\right) a_e \leq \epsilon, \ \forall e = 1, \ldots, N_b, \tag{2.43a}$$

$$\left(\overline{\sigma}_e^{-} - \sigma_e(\mathbf{a})\right) a_e \leq \epsilon, \ \forall e = 1, \ldots, N_b, \tag{2.43b}$$

$$a_e \geq \epsilon^2, \ \forall e = 1, \ldots, N_b. \tag{2.43c}$$

Nevertheless, Stolpe and Svanberg [82] proved that the trajectory of the ϵ-relaxation method may be nonsmooth and even discontinuous. Even worse, its application to moderate-size structures introduces additional local optima [83].

2.4.5 Local buckling singularity

The consideration of local buckling constraints exhibits similar issues with stress constraints. The problem was first identified by Guo et al. [84]. To illustrate the problem, consider again the three-bar truss (Fig. 2.5(a)). The minimum volume problem with local buckling constraints is

$$\min_{\mathbf{a}\in\mathbb{R}^3_+, \mathbf{u}\in\mathbb{R}^2} \left\{ a_1 l_1 + \beta a_2 l_2 + a_3 l_3 \;\middle|\; \mathbf{K}(\mathbf{a})\,\mathbf{u} = \mathbf{f}, \ -\frac{E_e}{l_e}\boldsymbol{\gamma}_e^{\top}\mathbf{u} \leq \overline{\sigma}_e^{\mathrm{cr}}(\mathbf{a}), \ \forall e = 1, 2, 3 \right\}, \tag{2.44}$$

where $\overline{\sigma}_e^{\mathrm{cr}}(\mathbf{a})$ represents the Euler critical buckling load written in terms of cross-sectional areas (see Section 4.4 for more details). Fig. 2.5(b) depicts the corresponding design space. The true optimum is given by the following points:

$$\text{Point A:} \quad a_1 = 0, \quad a_2 = 1, \quad a_3 = 0, \quad \text{if } \beta \leq \frac{1}{\sqrt{2}}, \tag{2.45a}$$

$$\text{Point B:} \quad a_1 = \frac{1}{\sqrt{2}}, \quad a_2 = 0, \quad a_3 = \frac{1}{\sqrt{2}}, \quad \text{if } \beta \geq \frac{1}{\sqrt{2}}. \tag{2.45b}$$

The optimal volume is $V^* = 1$ at point A and $V^* = \sqrt{2}$ at point B. However, standard algorithms are unable to reach neither point A, nor point B. The cause is the inconsistency between local buckling and compatibility constraints of vanishing members. On the one hand, we easily verify with Eqs. (2.40) that compatibility equations enforce non-zero stresses. On the other hand, zero stresses are required to ensure feasibility of local buckling constraints when $a_e \to 0$. Hence, both constraint types cannot be satisfied simultaneously.

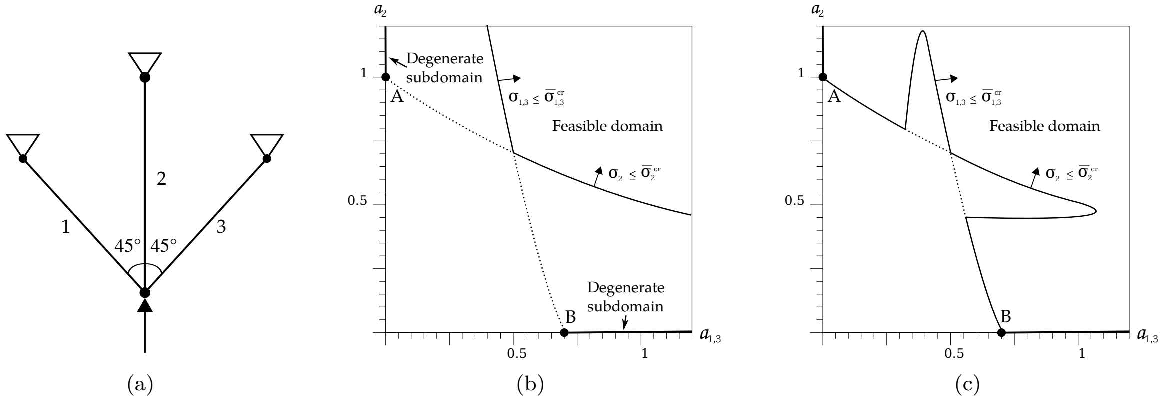

Figure 2.5: The three-bar truss example with local buckling singularity. The representation of the ground structure is given in (a). The system is subjected to a upward unit load. Young's moduli are taken as $E_e = 1$, and the length $l_e = 1$ for all $e = 1, 2, 3$. The design space is given in (b) for the case with singular optimum and (c) using relaxed constraints.

As for stress constraints, the singularity also arises when the problem is stated in terms of cross-sectional areas only:

$$\min_{\mathbf{a}\in\mathbb{R}^3_+} \left\{ a_1 l_1 + \beta a_2 l_2 + a_3 l_3 \;\middle|\; -\frac{E_e}{l_e}\boldsymbol{\gamma}_e^\top \left(\mathbf{K}\left(\mathbf{a}\right)^{-1}\mathbf{f}\right) \leq \overline{\sigma}_e^{\,\mathrm{cr}}\left(\mathbf{a}\right),\ \forall e = 1, 2, 3 \right\}. \tag{2.46}$$

The design space of Fig. 2.5(b) shows that the optimal points belongs to degenerate subspaces. Compared to stress constraints, the problem is even more critical because the feasible design domain is disjoint. Guo et al. [84] proposed a variant of the ϵ-relaxation method to reconnect the different parts by modifying the local buckling constraints as follows

$$-\sigma_e\left(\mathbf{a}\right) - \overline{\sigma}_e^{\,\mathrm{cr}}\left(\mathbf{a}\right) \leq \epsilon,\ \forall e = 1, \ldots, N_b, \tag{2.47}$$

The reconnected design space is depicted in Fig. 2.5(c). Despite this modification, the feasible design domain is highly non-convex and the problem remains difficult to solve by optimization algorithms. Hence, the proposal was enhanced via a second-order smooth approximation of relaxed constraints. Applications are yet limited to structures of moderate size.

2.5 Truss geometry and topology optimization

2.5.1 Optimization of nodal positions

In the quest for more practical design methods, some recent works in topology optimization focused on incorporating technological considerations to prevent short, thin, and overlapping bars or to restrict the number of joints [37, 85]. Yet, truss layout optimization might also comprise the search for the optimal nodal locations; a natural way of dealing with these constraints. This feature is especially relevant in view of designing lightweight structures. In that case, the overall problem is called truss geometry and topology optimization. Kirsch [86] pointed out that good results can be obtained with sparse ground structures by optimizing the structural geometry.

For this highly nonlinear problem, an important issue is how to define the geometrical variables. Computer-aided geometrical design parametrization [87] and sensitivity filtering techniques [88, 89] for freeform surfaces are unsuitable because they discard potentially interesting regions of the design space. Contrariwise, the variable giving a maximal control on the geometry is the position of nodes $\mathbf{x} \in \mathbb{R}^{d.N_n}$. This vector is defined on the set of permissible positions $X \subset \mathbb{R}^{d.N_d}$ which, in its general form, reads

$$X := \left\{ \mathbf{x} \in \mathbb{R}^{d.N_n} \mid g_i(\mathbf{x}) \leq \mathbf{0}, h_j(\mathbf{x}) = \mathbf{0},\ i = 1, \ldots, N_g,\ j = 1, \ldots, N_h \right\}. \tag{2.48}$$

The set X can be more or less difficult to enforce, depending on the vector functions of geometrical constraints $g_i(\mathbf{x}) : X \to \mathbb{R}^{N_g}$ and $h_j(\mathbf{x}) : X \to \mathbb{R}^{N_h}$. To mention a simple one, all nodes could lie within a bounding box apart from those coordinates where support conditions are prescribed:

$$X := \{\mathbf{x} \in \mathbb{R}^{d.N_n} \mid \overline{x}_i^{\,-} \leq x_i \leq \overline{x}_i^{\,+},\ \forall i = 1, \ldots, N_d, \tag{2.49a}$$

$$x_i = \overline{x}_i,\ \forall i = N_d + 1, \ldots, d.N_n\}. \tag{2.49b}$$

Here, $\overline{x}_i^{\,-} \in \mathbb{R}$ and $\overline{x}_i^{\,+} \in \mathbb{R}$ are respectively the lower and upper bounds of the i-th nodal coordinate whereas $\overline{x}_i \in \mathbb{R}$ stands for the support reactions.

The impact of varying nodal coordinates has consequences on the member length l_e and the vector of direction cosines $\boldsymbol{\gamma}_e$. For these functions, the following formula hold (see [90] for the proof):

$$l_e : X \to \mathbb{R}_+,\ \mathbf{x} \mapsto l_e(\mathbf{x}) := \frac{1}{\sqrt{2}} \|\mathbf{C}_e \mathbf{x}\|_2,\ \forall e = 1, \ldots, N_b, \tag{2.50}$$

$$l_e^2 : X \to \mathbb{R}_+,\ \mathbf{x} \mapsto l_e^2(\mathbf{x}) := \mathbf{x}^\top \mathbf{C}_e \mathbf{x},\ \forall e = 1, \ldots, N_b, \tag{2.51}$$

$$\boldsymbol{\gamma}_e : \mathcal{X} \to \mathbb{R}^{N_d}, \mathbf{x} \mapsto \boldsymbol{\gamma}_e(\mathbf{x}) := \frac{1}{l_e(\mathbf{x})} \mathbf{P} \mathbf{C}_e \mathbf{x},\ \forall e = 1, \ldots, N_b, \tag{2.52}$$

where $\|.\|_2$ denotes the Euclidean norm, $\mathbf{C}_e \in \mathbb{R}^{d.N_n \times d.N_n}$ is a symmetric, positive-semidefinite assembly matrix containing exactly d^3 non-zero entries of ± 1, and $\mathbf{P} \in \mathbb{R}^{N_d \times d.N_n}$ relates the system in non-reduced coordinates to the system in reduced coordinates. Note that l_e and $\boldsymbol{\gamma}_e$ are present almost everywhere in volume and compliance problem formulations. Especially, the global stiffness matrix in reduced coordinates can be formally defined as the following matrix-valued function with respect to the design variables

$$\mathbf{K} : \mathbb{R}_+^{N_b} \times X \to \mathbb{R}^{N_d \times N_d},\ (\mathbf{a}, \mathbf{x}) \mapsto \mathbf{K}(\mathbf{a}, \mathbf{x}) := \sum_{e=1}^{N_b} \frac{E_e a_e}{l_e(\mathbf{x})} \boldsymbol{\gamma}_e(\mathbf{x}) \boldsymbol{\gamma}_e^\top(\mathbf{x}). \tag{2.53}$$

Besides the nonlinear behavior, the variation of nodal positions poses some numerical difficulties when dealing with mathematical programming. The issue is investigated in Section 2.5.2.

2.5.2 Melting node effect

In optimal geometries, the *melting node effect* is referred to vanishing members due to the melting of truss end nodes. The phenomenon was first identified by Achtziger [91]. To give an illustrative example, consider the five-bar truss depicted in Fig. 2.6(a). For this example, the position of nodes 2 and 3 are optimized along the vertical direction without restriction. With the design variables $(\mathbf{a}, \mathbf{x})$, the minimum volume problem subject to stress constraints is

$$\min_{\substack{\mathbf{a} \in \mathbb{R}_+^5 \\ \mathbf{u} \in \mathbb{R}^4 \\ \mathbf{x} \in X}} \left\{ \sum_{e=1}^{5} a_e l_e(\mathbf{x}) \;\middle|\; \mathbf{K}(\mathbf{a}, \mathbf{x}) \mathbf{u} = \mathbf{f},\ -\overline{\sigma}_e^{\,-} \leq \frac{E_e}{l_e(\mathbf{x})} \gamma_e(\mathbf{x}) \mathbf{u} \leq \overline{\sigma}_e^{\,+},\ \forall e = 1, \ldots, 5 \right\}. \tag{2.54}$$

The true optimum of $V^* = 2.5$ includes melting nodes 2 and 3 (Fig. 2.6(c)). However, standard algorithms of mathematical programming are unable to reach the solution because the presence of melting nodes causes serious convergence difficulties: the solution process will move close to the optimum (Fig. 2.6(b)) without being able to find a KKT point. At the vicinity of the solution, the algorithm suddenly exhibits an erratic behavior with zigzags between two non-optimal points.

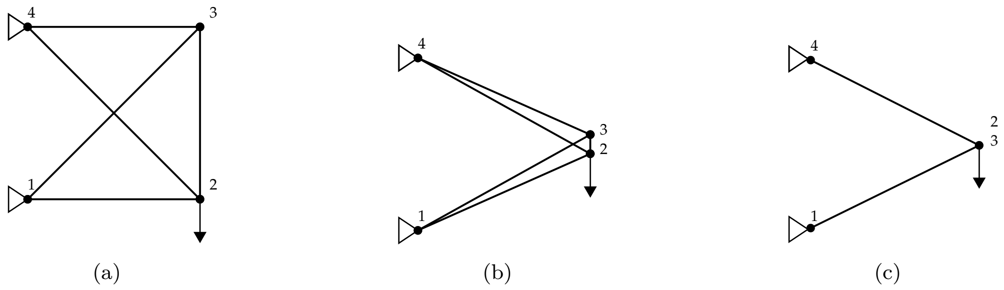

Figure 2.6: The three-bar truss example. The representation of the initial ground structure is based on a square of unit side and given in (a). A downward unit load is applied on node 2. Young's moduli are taken as $E_e = 1$ and limiting stresses are $\overline{\sigma}_e^{-} = 1$ and $\overline{\sigma}_e^{+} = 1$ for all $e = 1, \ldots, 5$. The solution close to the optimum is given in (b) and the actual optimum in (c).

The length function is the bottleneck for the admission of melting nodes in optimal structures. At melting nodes, the length vanishes, i.e. $\|\mathbf{C}_e\mathbf{x}\|_2 = 0$ for some $e \in \{1, \ldots, N_b\}$. The consequence for the solution process is twofold. Firstly, consider the derivative of the length function (2.50) with respect to the nodal coordinates:

$$\nabla l_e(\mathbf{x}) = \frac{\mathbf{C}_e\mathbf{x}}{\|\mathbf{C}_e\mathbf{x}\|_2}, \ \forall e = 1, \ldots, N_b. \tag{2.55}$$

A close inspection reveals that the derivative is undefined for melting nodes since the length appears in the denominator. This prevents the determination of a KKT point.

Secondly, the optimization problem involves some functions (e.g. the stiffness (2.53) and the direction cosine (2.52)) which are undefined for melting nodes since, once again, the length appears in the denominator. A common approach to avoid it is to define the set of permissible positions X_0 so that the melting node effect cannot occur [92]:

$$X_0 := \{\mathbf{x} \in X \mid l_e(\mathbf{x}) \neq 0, \ \forall e = 1, \ldots, N_b\}. \tag{2.56}$$

However, this approach is cumbersome and possibly intractable for complex applications. Actually, optimal geometries with melting nodes are even desirable to the extent that such solutions may achieve more effective results [48, 93, 94].

2.6 Concluding remarks

In this chapter, we described truss layout optimization in a mathematical programming context. First, topology optimization for minimum volume and compliance problems under single loading is stated along with the equivalence between both problems. Then, the formulation is progressively extended to obtain the general problem of truss geometry and topology optimization including member self-weight and multiple loading, as well as stress, displacement, and local buckling constraints. For these extensions, the singularities that arise in optimum solutions are identified.

In the literature, truss geometry and topology optimization remains unsolved. Thus, the purpose of Chapter 3 is to develop a novel formulation to treat the problem by mathematical programming.

3 Unified formulation

This chapter presents a novel formulation for efficiently solving geometry and topology optimization of large-scale truss structures. In Section 3.1, previously proposed methods are reviewed and the critical issues are pointed out. The major obstacles are the singularities of the optimal solution with respect to the design parameters. These difficulties especially arise when nesting displacement formulations with nonlinear programming. By contrast, the formulation presented in Section 3.2 differs in several respects by the use of a simultaneous analysis and design approach, which is successfully applied to volume and compliance minimization problems including self-weight and multiple loading. The minimum volume formulation is developed in Section 3.3 for the general case of elastic design and specialized to plastic design for computational efficiency. In Section 3.4, the minimum compliance problem is in turn formulated for the weighted-average and the worst-case compliance using the principle of minimum complementary energy. For the single loading case, both types of problem reduce to a compact formulation in Section 3.5. Furthermore, Section 3.6 studies the properties of these formulations and compares several methods of nonlinear programming to solve them. The effects of different design settings on the optimal solution are also investigated in Section 3.7.

3.1 Literature review

Truss geometry and topology optimization is a challenging task due to the non-convex and non-smooth nature of the design space. This non-convexity is the fundamental difference with topology optimization. Because of these inherent difficulties, there exists a rich and diversified literature covering the topic. The present work is particularly concerned by formulations and methods tailored for mathematical programming. Indeed, nonlinear programming algorithms can efficiently solve large problems with multiple constraint types. Although the basic problem has been stated a long time ago, a stable and robust formulation is still missing.

Early works in structural optimization addressed sizing and geometry optimization. Using continuous variables, this problem shares common issues with geometry and topology optimization. Among pioneering contributions in the field, Dobbs and Felton [95] proposed an alternating approach: for a fixed geometry, the cross-sectional areas are sequentially optimized and vice-versa. This alternating approach has been revisited several times until recently [92, 96, 97]. However, it has been shown that such a procedure may get stuck in non-optimal points, even for very simple problems [90]. Alternatively, Pedersen [98] investigated an approach where the statical determinacy of the optimal solution is used. The same author proposed a sequential linear programming method for dealing with multiple loading [99] and 3D structures [100]. Similarly, other optimization algorithms were specifically developed for the case of truss sizing and geometry optimization [101, 102]. See also review [103].

When cross-sectional areas are allowed to vanish, the problem is referred as geometry and topology optimization. Due to stress and local buckling singularities, the approaches considered either compliance formulations, simplified approaches, or heuristic procedures (i.e. without mathematical evidence). For instance, the well-known heuristic procedure based on fully stress design assumption was combined with geometry optimization in [104]. Lev [105] first wrote the KKT conditions for a truss structure under two loading cases. The use of KKT conditions can also be found in [106]. Kirsch [68] studied the relationship between optimal topologies and geometries, and derived a number of methods whose take certain optimality properties into account. Other more general approaches stated geometry and topology optimization by bilevel programming [48, 90, 93, 107]: for any variation of the outer problem of geometry optimization, the inner problem of topology optimization in linear programming is solved. However, bilevel programming problems are non-differentiable and their design space comprises disjoint feasible regions. Hence, non-smooth techniques are required, but the lack of gradient information restricts their scope to applications of moderate size [108, 109].

Recently, an approach where geometry and topology are optimized simultaneously was forwarded for compliance optimization under single loading [90, 91]. An important contribution of this work is the rigorous identification of issues related to the melting node effect and the development of several formulations to solve the problem. In opposition to the ground structure approach, some authors [110, 111] employed a growing ground structure method where members are progressively added. The procedure is efficient but the applicability is restricted to loosely constrained Michell's problems. Bojczuk et al. [112] proposed a method based on the virtual bar concept where a number of equivalent optimal topologies are generated and then optimized with regard to geometrical parameters.

The methods mentioned above all contribute to the field of geometry and topology. However, they suffer from either a lack of rigour in covering numerical singularities, they fail at properly converging to local optima, or are meant to be applied on specific design problems of moderate size. In this work, a general approach for lightweight structures, able to handle various structural, geometrical, and technological constraints, is proposed. Ideally, the method could also tackle very large problems with limited computational effort. Given the fact that the simultaneous geometry and topology optimization can be treated by mathematical programming, this approach is primarily investigated in Section 3.2.

3.2 Disaggregation of equilibrium equations

Classical methods to address truss geometry and topology optimization by mathematical programming relies on nested analysis and design formulations where state variables are obtained by solving equilibrium equations via a dedicated linear algebra routine. An example of nested formulation for topology optimization is formulation (2.35). By contrast, our strategy [113] relies on simultaneous analysis and design, whose basic concepts has been introduced in Section 2.4.3. Schmit and Fox's pioneering works [114, 115] on simultaneous analysis and design have been successfully applied in different fields of engineering including topology optimization [116]. In those formulations both design and state variables are treated as optimization variables and the equilibrium equations set as equality constraints [67]. Consequently, the equilibrium equations are explicit and do not need to be solved at every iteration, allowing the treatment of any classes of truss assembly (from I to IV, cf. Section 2.2). Moreover, the constraint Jacobian and the Hessian of the Lagrangian function are readily calculated and their inherent sparsity can be advantageously exploited to save memory. However, as for any optimization problem subject to equality constraints, an important challenge lies in the numerical treatment of the equilibrium constraints.

Formulations based on displacement analysis models are inappropriate because $\mathbf{K}(\mathbf{a}, \mathbf{x})$ is highly nonlinear with respect to the geometrical parameters. In this section, we will derive a variant but equivalent formulation by disaggregating (2.11) into static equilibrium (2.5), elastic compatibility (2.7), and constitutive law (2.9). Any point enforcing these equalities is automatically a solution of

(2.11). Hence, we do have an equivalent model:

$$\mathbf{K}(\mathbf{a},\mathbf{x})\,\mathbf{u}_k = \mathbf{f}_k + \sum_{e=1}^{N_b} a_e l_e(\mathbf{x})\,\mathbf{g}_e \Longleftrightarrow \left\{ \begin{array}{l} \displaystyle\sum_{e=1}^{N_b} t_{e,k}\boldsymbol{\gamma}_e(\mathbf{x}) = \mathbf{f}_k + \sum_{e=1}^{N_b} a_e l_e(\mathbf{x})\,\mathbf{g}_e, \\ \boldsymbol{\gamma}_e^\top(\mathbf{x})\,\mathbf{u}_k = \epsilon_{e,k}, \\ \displaystyle\frac{t_{e,k}}{a_e} = E_e\frac{\epsilon_{e,k}}{l_e(\mathbf{x})}. \end{array} \right| _{\substack{\forall e=1,\ldots,N_b \\ \forall k=1,\ldots,N_c}} \tag{3.1}$$

With these governing equations, the challenge ahead is to find the simplest possible mathematical structure which covers the melting node effect (and the stress singularity if any) without regularization techniques. For this purpose, we start by putting the constitutive law into the compatibility condition to remove the member elongation term $\epsilon_{e,k}$. Then, introducing the explicit function of direction cosines (2.52) gives, after a few algebra, the following equations for the static equilibrium and the compatibility condition:

$$\sum_{e=1}^{N_b} \frac{t_{e,k}}{l_e(\mathbf{x})}\mathbf{P}\mathbf{C}_e\mathbf{x} = \mathbf{f}_k + \sum_{e=1}^{N_b} a_e l_e(\mathbf{x})\,\mathbf{g}_e,\ \forall k=1,\ldots,N_c, \tag{3.2}$$

$$\frac{a_e}{l_e(\mathbf{x})}E_e\mathbf{x}^\top\mathbf{C}_e\mathbf{P}^\top\mathbf{u}_k = t_{e,k}l_e(\mathbf{x}),\ \forall e=1,\ldots,N_b,\ \forall k=1,\ldots,N_c. \tag{3.3}$$

In this form, Eqs. (3.2)-(3.3) are not yet differentiable with respect to $\mathbf{x}$. In the following, we will see how it is possible to formulate the minimum volume and compliance problems including self-weight and multiple loading via a unique set of parameters.

3.3 Minimum volume problem

Consider the minimum volume problem subject to stress and displacement constraints. In elastic design, both static equilibrium and compatibility condition must be enforced for the k-th loading cases. Since the length function is non-differentiable, our basic idea relies on variable changes either to avoid the explicit calculation or to use the differentiable expression $l_e^2(\mathbf{x})$ given by (2.51). This can be achieved by encompassing the quantities of interest for each member in the following variables:

$$q_{a,e} := \frac{a_e}{l_e} \in \mathbb{R}_+,\ \forall e=1,\ldots,N_b, \tag{3.4}$$

$$q_{t,e,k} := \frac{t_{e,k}}{l_e} \in \mathbb{R}_+,\ \forall e=1,\ldots,N_b,\ \forall k=1,\ldots,N_c. \tag{3.5}$$

By analogy with the force density method used in form finding [117], these variables are respectively called section density and force density. The substitution does not alter the nature of the topological problem since the cross-sectional area is solely scaled by the length. Introducing these variables into the static equilibrium and compatibility equations leads to the expression

$$\sum_{e=1}^{N_b} q_{t,e,k}\mathbf{P}\mathbf{C}_e\mathbf{x} = \mathbf{f}_k + \sum_{e=1}^{N_b} v_e(\mathbf{q}_a,\mathbf{x})\ \mathbf{g}_e,\ \forall k=1,\ldots,N_c, \tag{3.6}$$

$$q_{a,e}E_e\mathbf{x}^\top\mathbf{C}_e\mathbf{P}^\top\mathbf{u}_k = q_{t,e,k}\mathbf{x}^\top\mathbf{C}_e\mathbf{x},\ \forall e=1,\ldots,N_b,\ \forall k=1,\ldots,N_c, \tag{3.7}$$

with the volume function given by

$$v_e(\mathbf{q}_a,\mathbf{x}) = q_{a,e}\mathbf{x}^\top\mathbf{C}_e\mathbf{x},\ \forall e=1,\ldots,N_b. \tag{3.8}$$

By setting $\{\mathbf{q}_a, \mathbf{q}_{t,k}, \mathbf{u}_k, \mathbf{x}\}$ as optimization variables, these equalities become differentiable everywhere. With Eqs. (3.6), (3.7), and (3.8), the general formulation in elastic design for the minimum volume problem including self-weight and multiple loading takes the form

$$\min_{\substack{\mathbf{q}_a \in \mathbb{R}^{N_b} \\ \mathbf{q}_{t,k} \in \mathbb{R}^{N_b} \\ \mathbf{u}_k \in \mathbb{R}^{N_d} \\ \mathbf{x} \in \mathbb{R}^{d.N_n}}} \quad \sum_{e=1}^{N_b} v_e\left(\mathbf{q}_a, \mathbf{x}\right) \tag{3.9a}$$

$$\text{s.t.:} \quad \sum_{e=1}^{N_b} q_{t,e,k} \mathbf{P} \mathbf{C}_e \mathbf{x} = \mathbf{f}_k + \sum_{e=1}^{N_b} v_e\left(\mathbf{q}_a, \mathbf{x}\right) \mathbf{g}_e, \qquad \forall k = 1, \ldots, N_c, \tag{3.9b}$$

$$E_e q_{a,e} \mathbf{x}^\top \mathbf{C}_e \mathbf{P}^\top \mathbf{u}_k = q_{t,e,k} \mathbf{x}^\top \mathbf{C}_e \mathbf{x}, \qquad \forall e = 1, \ldots, N_b,\ \forall k = 1, \ldots, N_c, \tag{3.9c}$$

$$- q_{a,e} \overline{\sigma}_{e,k}^{-} \leq q_{t,e,k} \leq q_{a,e} \overline{\sigma}_{e,k}^{+}, \qquad \forall e = 1, \ldots, N_b,\ \forall k = 1, \ldots, N_c, \tag{3.9d}$$

$$- \overline{u}_{i,k}^{-} \leq u_{i,k} \leq \overline{u}_{i,k}^{+}, \qquad \forall i = 1, \ldots, N_d,\ \forall k = 1, \ldots, N_c, \tag{3.9e}$$

$$q_{a,e} \geq 0, \mathbf{x} \in X, \qquad \forall e = 1, \ldots, N_b. \tag{3.9f}$$

This formulation exhibits attractive outcomes. Firstly, the formulation is able to converge to optimal geometries including melting nodes. Secondly, compatibility and stress constraints vanish in a smooth way when $q_{a,e} \to 0$, and thus the stress singularity phenomenon is properly covered. Thirdly, linear stress and displacement constraints are handled without extra effort by the optimization algorithm. Fourthly, keeping geometrical variables fixed leads directly to a pure topology optimization problem within the same formulation. Finally, the gradient of the objective function and the constraint Jacobian are readily calculated thanks to this simple problem structure.

For computational efficiency, we can also work in plastic design by neglecting the compatibility condition. Such formulations are particularly well suited for simultaneous analysis and design. At the expense of a small error on stress constraints in redundant structures (typically a few per cent [68,75]), the removal of elastic compatibility equations eliminates many local optima. The resulting solution is a lower-bound of the stress-constrained minimum volume. Through the present approach, the plastic design formulation is obtained by simply removing the information on kinematics:

$$\min_{\substack{\mathbf{q}_a \in \mathbb{R}^{N_b} \\ \mathbf{q}_{t,k} \in \mathbb{R}^{N_b} \\ \mathbf{x} \in \mathbb{R}^{d.N_n}}} \quad \sum_{e=1}^{N_b} v_e\left(\mathbf{q}_a, \mathbf{x}\right) \tag{3.10a}$$

$$\text{s.t.:} \quad \sum_{e=1}^{N_b} q_{t,e,k} \mathbf{P} \mathbf{C}_e \mathbf{x} = \mathbf{f}_k + \sum_{e=1}^{N_b} v_e\left(\mathbf{q}_a, \mathbf{x}\right) \mathbf{g}_e,\ \forall k = 1, \ldots, N_c, \tag{3.10b}$$

$$- q_{a,e} \overline{\sigma}_{e,k}^{-} \leq q_{t,e,k} \leq q_{a,e} \overline{\sigma}_{e,k}^{+},\ \forall e = 1, \ldots, N_b,\ \forall k = 1, \ldots, N_c, \tag{3.10c}$$

$$q_{a,e} \geq 0, \mathbf{x} \in X,\ \forall e = 1, \ldots, N_b. \tag{3.10d}$$

An example of implementation of this formulation and its derivatives is given in Appendix A.3. Formulation (3.10) is an extension of the lower-bound plastic design formulation previously proposed by the author [118,119] to the inclusion of self-weight loads. It should be mentioned that, for a fixed geometry, the problem is convex and takes the form of a linear programming problem.

3.4 Minimum compliance problem

Truss geometry and topology optimization is in turn stated for the minimum compliance problem. To define consistent parameters, we first consider the objective function as a combination of the following specific compliances (2.31):

$$c_k\left(\mathbf{q}_a,\mathbf{u}_k,\mathbf{x}\right)=\left[\mathbf{f}_k+\sum_{e=1}^{N_b}v_e\left(\mathbf{q}_a,\mathbf{x}\right)\mathbf{g}_e\right]^\top\mathbf{u}_k,\ \forall k=1,\ldots,N_c. \tag{3.11}$$

Apparently, Eq. (3.11) is appropriate for computational use but numerical experiments show that this definition for simultaneous analysis and design adversely affects the results. More precisely, the first iteration points diverge from the feasible region towards areas of negative energies and the optimization algorithm has difficulty in restoring the feasibility of next iterates. To balance the misbehavior between the minimization of the objective function and the satisfaction of equality constraints, we consider an alternative expression by first changing the parametrization as follows:

$$\{\mathbf{q}_a,\mathbf{q}_{t,k},\mathbf{u}_k,\mathbf{x}\}\xrightarrow{q_{t,e,k}:=q_{a,e}\sigma_{e,k}}\{\mathbf{q}_a,\boldsymbol{\sigma}_k,\mathbf{u}_k,\mathbf{x}\} \tag{3.12}$$

Expressing Eqs. (3.6)-(3.7) with respect to $\{\mathbf{q}_a,\boldsymbol{\sigma}_k,\mathbf{u}_k,\mathbf{x}\}$ yields the alternative form of equilibrium and compatibility equations, respectively:

$$\sum_{e=1}^{N_b}q_{a,e}\sigma_{e,k}\mathbf{P}\mathbf{C}_e\mathbf{x}=\mathbf{f}_k+\sum_{e=1}^{N_b}q_{a,e}\mathbf{x}^\top\mathbf{C}_e\mathbf{x}\ \mathbf{g}_e,\ \forall k=1,\ldots,N_c, \tag{3.13}$$

$$E_e\mathbf{x}^\top\mathbf{C}_e\mathbf{P}^\top\mathbf{u}_k=\sigma_{e,k}\mathbf{x}^\top\mathbf{C}_e\mathbf{x},\ \forall e=1,\ldots,N_b,\ \forall k=1,\ldots,N_c. \tag{3.14}$$

On this basis, certain optimality properties are used. By assuming that static equilibrium constraints (3.13) are satisfied at the solution, the external forces (including self-weight) $\mathbf{f}_k+\sum_{e=1}^{N_b}v_e\left(\mathbf{q}_a,\mathbf{x}\right)\ \mathbf{g}_e$ in the specific compliance function can be replaced by its internal counterpart $\sum_{e=1}^{N_b}q_{a,e}\sigma_{e,k}\mathbf{P}\mathbf{C}_e\mathbf{x}$. After some algebra, we get

$$c_k\left(\mathbf{q}_a,\boldsymbol{\sigma}_k,\mathbf{u}_k,\mathbf{x}\right)=\sum_{e=1}^{N_b}q_{a,e}\sigma_{e,k}\mathbf{x}^\top\mathbf{C}_e\mathbf{P}^\top\mathbf{u}_k,\ \forall k=1,\ldots,N_c. \tag{3.15}$$

This function can be further modified. Multiplying both sides of the compatibility equations (3.14) by E_e^{-1} brings out the left-hand term $\mathbf{x}^\top\mathbf{C}_e\mathbf{P}^\top\mathbf{u}_k$, which appears in the compliance function (3.15). The satisfaction of compatibility equations at the optimum allows its replacement by the right-hand term $(\sigma_{e,k}/E_e)\mathbf{x}^\top\mathbf{C}_e\mathbf{x}$. The resulting function turns out to be the complementary energy:

$$c_k\left(\mathbf{q}_a,\boldsymbol{\sigma}_k,\mathbf{x}\right)=\sum_{e=1}^{N_b}\frac{\sigma_{e,k}^2}{E_e}q_{a,e}\mathbf{x}^\top\mathbf{C}_e\mathbf{x},\ \forall k=1,\ldots,N_c. \tag{3.16}$$

According to the principle of minimum complementary energy (see Section 2.1), compatibility equations are automatically satisfied and thus can be removed from the problem formulation to enhance the implementation. It follows two formulations for the minimum compliance problem which both cover the melting node effect in a correct way. Firstly, introducing Eqs. (3.8), (3.13), and (3.16) into the weighted-average compliance problem yields

$$\min_{\substack{\mathbf{q}_a \in \mathbb{R}^{N_b} \\ \boldsymbol{\sigma}_k \in \mathbb{R}^{N_b} \\ \mathbf{x} \in \mathbb{R}^{d.N_n}}} \quad \sum_{k=1}^{N_c} w_k c_k \left(\mathbf{q}_a, \boldsymbol{\sigma}_k, \mathbf{x}\right) \tag{3.17a}$$

$$\text{s.t.: } \sum_{e=1}^{N_b} q_{a,e}\sigma_{e,k}\mathbf{P}\mathbf{C}_e\mathbf{x} = \mathbf{f}_k + \sum_{e=1}^{N_b} v_e\left(\mathbf{q}_a, \mathbf{x}\right)\mathbf{g}_e,\ \forall k = 1, \ldots, N_c, \tag{3.17b}$$

$$\sum_{e=1}^{N_b} v_e\left(\mathbf{q}_a, \mathbf{x}\right) = \overline{V},\ q_{a,e} \geq 0,\ \mathbf{x} \in X,\ \forall e = 1, \ldots, N_b. \tag{3.17c}$$

Secondly, this principle can also be applied to the worst-case compliance. However, the objective function is not differentiable due to the presence of the max operator over discrete variables $k = 1, \ldots, N_c$. To use standard algorithms of nonlinear programming, the min-max problem must be reformulated. In this aim, the worst compliance can be represented by a variable $\tau \in \mathbb{R}_+$ such as

$$\tau = \max_{k=1,\ldots,N_c} c_k\left(\mathbf{q}_a, \boldsymbol{\sigma}_k, \mathbf{x}\right), \tag{3.18}$$

or equivalently by k inequality constraints

$$\tau \geq c_k\left(\mathbf{q}_a, \boldsymbol{\sigma}_k, \mathbf{x}\right),\ k = 1, \ldots, N_c. \tag{3.19}$$

Introducing this variable in the worst-case compliance problem leads to the equivalent formulation:

$$\min_{\substack{\mathbf{q}_a \in \mathbb{R}^{N_b} \\ \boldsymbol{\sigma}_k \in \mathbb{R}^{N_b} \\ \mathbf{x} \in \mathbb{R}^{d.N_n} \\ \tau \in \mathbb{R}}} \quad \tau \tag{3.20a}$$

$$\text{s.t.: } \sum_{e=1}^{N_b} q_{a,e}\sigma_{e,k}\mathbf{P}\mathbf{C}_e\mathbf{x} = \mathbf{f}_k + \sum_{e=1}^{N_b} v_e\left(\mathbf{q}_a, \mathbf{x}\right)\mathbf{g}_e,\ \forall k = 1, \ldots, N_c, \tag{3.20b}$$

$$\sum_{e=1}^{N_b} v_e\left(\mathbf{q}_a, \mathbf{x}\right) = \overline{V},\ \tau \geq c_k\left(\mathbf{q}_a, \boldsymbol{\sigma}_k, \mathbf{x}\right),\ \forall k = 1, \ldots, N_c, \tag{3.20c}$$

$$q_{a,e} \geq 0,\ \mathbf{x} \in X,\ \forall e = 1, \ldots, N_b. \tag{3.20d}$$

In (3.20), only the complementary energy for the loading case corresponding to the worst compliance is minimized. It means that the other stress components would not correspond to their respective loading, although they do not influence the design problem [60].

3.5 Reduced formulation for single loading

Unlike the multiple loading case with self-weight, the equivalence between volume and compliance minimization problems is clearly established for topology optimization under single loading (cf. Section 2.2). On the one hand, the minimum volume problem converges to a fully stressed design, i.e. the stress in all existing bars reaches the strength limit. On the other hand, the minimum compliance is actually its dual problem for which the optimal members all possess an equal strain energy density. One can derive from necessary conditions of optimality that both problems converge to an equivalent solution and the compatibility condition is automatically satisfied [49]. The equivalence is still valid for different limiting stresses in tension and compression [53]. Furthermore, the statement also holds for simultaneous geometry and topology optimization since the optimal geometry could be part of the

ground structure [90].
These properties can be advantageously employed to reduce the problem size. The vector of force densities can be expressed by non-negative tension $\mathbf{q}_t^+ \in \mathbb{R}_+^{N_b}$ and compression $\mathbf{q}_t^- \in \mathbb{R}_+^{N_b}$ parts such that $\mathbf{q}_t = \mathbf{q}_t^+ - \mathbf{q}_t^-$. Furthermore, the fully stressed design assumption allows to define

$$q_{a,e} := \frac{q_{t,e}^+}{\overline{\sigma}_e^{\,+}} + \frac{q_{t,e}^-}{\overline{\sigma}_e^{\,-}} \in \mathbb{R}_+, \ \forall e = 1, \dots, N_b. \tag{3.21}$$

By this means, we recover the compact formulation for truss geometry and topology optimization under single loading given in [90, 120]:

$$\boxed{\begin{aligned}
&\min_{\substack{\mathbf{q}_t^+ \in \mathbb{R}^{N_b} \\ \mathbf{q}_t^- \in \mathbb{R}^{N_b} \\ \mathbf{x} \in \mathbb{R}^{d.N_n}}} && \sum_{e=1}^{N_b} \left(\frac{q_{t,e}^+}{\overline{\sigma}_e^{\,+}} + \frac{q_{t,e}^-}{\overline{\sigma}_e^{\,-}} \right) \mathbf{x}^\top \mathbf{C}_e \mathbf{x} && \text{(3.22a)} \\
&\text{s.t.:} && \sum_{e=1}^{N_b} \left(q_{t,e}^+ - q_{t,e}^- \right) \mathbf{P}\mathbf{C}_e \mathbf{x} = \mathbf{f}, && \text{(3.22b)} \\
& && q_{t,e}^+ \geq 0, \ q_{t,e}^- \geq 0, \ \mathbf{x} \in X, \ \forall e = 1, \dots, N_b. && \text{(3.22c)}
\end{aligned}}$$

The simple problem structure is evident: the objective function is a third-order polynomial (linear in force densities and quadratic in nodal coordinates), and the equilibrium constraints are sign-constrained bilinear vector functions. A consequence of minimizing (3.22a) is that either tension $q_{t,e}^+$ or compression $q_{t,e}^-$ will be non-zero at the optimum for every non-vanishing bar. This formulation can be also derived from the compliance formulation based on the complementary energy by posing the strain energy $E_e = \left(\overline{\sigma}_e^{\,+,-}\right)^2$. Note that for a fixed geometry, (3.22) takes the form of a linear programming problem.
The minimum volume problems in elastic design (3.9) and plastic design (3.10), the minimum compliance problems in the weighted-average (3.17) and the worst-case sense (3.20), and the reduced formulation for single loading (3.22) are all well-posed optimization problems. Hence, they can be efficiently solved by standard algorithms of nonlinear programming. If the problem is feasible, the optimization process will generally converge to a KKT optimal point.

3.6 Nonlinear programming

In this section, we investigate how to solve volume and compliance optimization by nonlinear programming algorithms. Simultaneous analysis and design formulations are difficult to solve but they exhibit excellent performances when the whole problem is well posed. Hence, identifying the best strategy is crucial. In particular, the sparsity of the first and second derivatives can be advantageously exploited as nonzero components usually represents less than 1% of filling density. This makes the present formulations especially relevant for large problems involving several thousands of variables and constraints.
However, only few instances of nonlinear programming algorithms are capable of addressing such highly constrained optimization problems. Among potential candidates, sparse interior-point and sequential quadratic programming are widespread classes of optimization algorithms [121]. There exist, nevertheless, strong algorithmic differences. Especially, the strategy for updating the iterate is sensitive to the accuracy by which partial derivatives are provided [122]. Most approaches for solving simultaneous analysis and design formulations combine line search iteration with BFGS Hessian approximations [66, 90, 123–125]. Hereafter, we will see that trust region emerges as a sound and efficient alternative for focusing on feasibility.

3.6.1 Barrier problem

The present method is based on the interior-point method for dealing with large inequality constraints [126]. The basic idea of interior-point methods is to force iteration points to remain inside the feasible design space by following an interior path. To do so, inequality constraints are first transformed into equality constraints by introducing a vector of slack variable $\mathbf{s} \in \mathbb{R}_+^{N_g}$ as follows

$$g_i(\mathbf{z}) \leq 0 \longrightarrow g_i(\mathbf{z}) + s_i = 0, \ \forall i = 1, \ldots, N_g. \tag{3.23}$$

Then, the optimization problem is formulated as a barrier problem by adding a logarithmic barrier (or penalty) function in the objective function:

$$\min_{\mathbf{z} \in Z, \mathbf{s} \in \mathbb{R}_+^{N_g}} \ f(\mathbf{z}) - \mu \sum_{i=1}^{N_g} \ln s_i \tag{3.24a}$$

$$\text{s.t.: } g_i(\mathbf{z}) + s_i = 0, \ \forall i = 1, \ldots, N_g, \tag{3.24b}$$

$$h_j(\mathbf{z}) = 0, \ \forall j = 1, \ldots, N_h, \tag{3.24c}$$

where $\mu > 0$ is the barrier parameter. This constrained optimization problem can be represented by the Lagrangian function:

$$\mathcal{L}(\mathbf{z}, \mathbf{s}, \lambda_g, \lambda_h) := f(\mathbf{z}) - \mu \sum_{i=1}^{N_g} \ln s_i + \sum_{i=1}^{N_g} \lambda_{g,i} (g_i(\mathbf{z}) + s_i) + \sum_{j=1}^{N_h} \lambda_{h,j} h_j(\mathbf{z}). \tag{3.25}$$

The first-order necessary condition for the barrier problem (3.24) is written as

$$\nabla f(\mathbf{z}^*) + \sum_{i=1}^{N_g} \lambda_{g,i} \nabla g_i(\mathbf{z}^*) + \sum_{j=1}^{N_h} \lambda_{h,j} \nabla h_j(\mathbf{z}^*) = 0, \tag{3.26a}$$

$$h_j(\mathbf{z}^*) = 0, \qquad \forall j = 1, \ldots, N_h, \tag{3.26b}$$

$$s_i \lambda_{g,i} - \mu = 0, \qquad \forall i = 1, \ldots, N_g, \tag{3.26c}$$

$$s_i \geq 0, \ \lambda_{g,i} \geq 0, \ g_i(\mathbf{z}^*) \leq 0, \qquad \forall i = 1, \ldots, N_g. \tag{3.26d}$$

The classical approach to find a local minimizer $\mathbf{z}^*$ is to apply Newton's iteration method on (3.26). At each iteration $p \geq 0$, the resulting primal-dual linear system provides the search direction $\mathbf{d}_z$ and $\mathbf{d}_s$ for the next point $\mathbf{z}_{p+1} = \mathbf{z}_p + \alpha_{z,p} \mathbf{d}_z$ and $\mathbf{s}_{p+1} = \mathbf{s}_p + \alpha_{s,p} \mathbf{d}_s$. A line search procedure will determine the best position $\alpha_{z,p}$ and $\alpha_{s,p}$ along the direction vectors $\mathbf{d}_z$ and $\mathbf{d}_s$ so that a merit function is decreased. This remarkably simple and fairly inexpensive approach requires, nevertheless, strong assumptions to ensure a quadratic convergence [127]:

- the functions f, g_i and h_j have to be twice differentiable and Lipschitz continuous;
- the Jacobian of constraints $\nabla \mathbf{h}$ and $\nabla \mathbf{g}$ must have full rank;
- the Hessian of the Lagrangian function $\nabla^2_{\mathbf{zz}} \mathcal{L}$ has to be positive-definite on the tangent space of constraints.

However, the design space for our problems is non-convex, the Jacobian is rank deficient, and the Hessian is indefinite. Byrd [128] showed that, because of these deficiencies, Newton's method may converge to non-stationary points and must be adapted accordingly.

To overcome these difficulties, different alternatives are available (see [127] for a comprehensive overview). Some algorithms replace the Hessian $\nabla^2_{\mathbf{zz}} \mathcal{L}$ by a positive-definite BFGS approximation [129]. However, the approximation may be coarse for equality constrained optimization, and the inaccuracy is exacerbated by the leading presence of negative curvatures. In order to work with exact second derivatives, alternative strategies act directly on $\nabla^2_{\mathbf{zz}}\mathcal{L}$ during the process of matrix factorization [130,131]. Again, the procedure introduces distortions in the model which require several additional factorization steps. In order to reap all benefits from the availability of second derivative, an alternative strategy must be considered.

3.6.2 Sequential quadratic programming with trust regions

An appropriate method for solving the barrier problem (3.24) relies on combining sequential quadratic programming [132, 133] with trust region [126, 134]. The basic idea of sequential quadratic programming is to solve a sequence of approximated subproblems. Let $(\mathbf{z}_p, \mathbf{s}_p, \boldsymbol{\lambda}_{g,p}, \boldsymbol{\lambda}_{h,p})$ being now an estimate of the local minimizer $\left(\mathbf{z}^*, \mathbf{s}^*, \boldsymbol{\lambda}_g^*, \boldsymbol{\lambda}_h^*\right)$ at iteration $p \geq 0$. At each step, a search direction is computed by minimizing the quadratic model of a certain Lagrangian function subject to linearized constraints [132, 133] (with $\mathcal{L}(\mathbf{z}_p, \mathbf{s}_p, \boldsymbol{\lambda}_{g,p}, \boldsymbol{\lambda}_{h,p})$ denoted $\mathcal{L}_p$ for short):

$$\min_{\mathbf{d}_z \in \mathbb{R}^{N_z}, \mathbf{d}_s \in \mathbb{R}^{N_g}} \quad \nabla f(\mathbf{z}_p)^T \mathbf{d}_z + \frac{1}{2}\mathbf{d}_z^\top \nabla^2_{\mathbf{zz}}\mathcal{L}_p \mathbf{d}_z - \operatorname{diag}\left(\mu s_{i,p}^{-1}\right)\mathbf{d}_s + \frac{1}{2}\mathbf{d}_s^\top \nabla^2_{\mathbf{zz}}\mathcal{L}_p \mathbf{d}_s \tag{3.27a}$$

$$\text{s.t.:} \quad \mathbf{h}(\mathbf{z}_p) + \nabla\mathbf{h}(\mathbf{z}_p)^T \mathbf{d}_z = \mathbf{0}, \tag{3.27b}$$

$$\mathbf{g}(\mathbf{z}_p) + \mathbf{s}_p + \nabla\mathbf{g}(\mathbf{z}_p)^T \mathbf{d}_z + \mathbf{d}_s = \mathbf{0}. \tag{3.27c}$$

The rule for updating the step is of prominent issue. In order to achieve robustness for negative and zero curvatures in the design space, one may resort to trust regions. Despite their higher computational cost, the major advantage compared to line search methods is their ability to handle indefinite Hessian without factorization [126, 135].

The underlying principle behind trust region is to estimate a region where a local approximation – here, the quadratic model – can be trusted to reasonably represent the problem. At each iteration, the method serves to restrict trial steps $\mathbf{d}_{z,p}$ and $\mathbf{d}_{s,p}$ within a certain radius defined by the set T_p. A step improving the solution is always accepted. Otherwise, the radius is reduced and another attempt is carried out. This can be achieved by the following formulation:

$$\min_{\mathbf{d}_z \in \mathbb{R}^{N_z}, \mathbf{d}_s \in \mathbb{R}^{N_g}} \quad \nabla f(\mathbf{z}_p)^T \mathbf{d}_z + \frac{1}{2}\mathbf{d}_z^\top \nabla^2_{\mathbf{zz}}\mathcal{L}_p \mathbf{d}_z - \operatorname{diag}\left(\mu s_{i,p}^{-1}\right)\mathbf{d}_s + \frac{1}{2}\mathbf{d}_s^\top \nabla^2_{\mathbf{zz}}\mathcal{L}_p \mathbf{d}_s \tag{3.28a}$$

$$\text{s.t.:} \quad \mathbf{h}(\mathbf{z}_p) + \nabla\mathbf{h}(\mathbf{z}_p)^T \mathbf{d}_z = \mathbf{r}_{h,p}, \tag{3.28b}$$

$$\mathbf{g}(\mathbf{z}_p) + \mathbf{s}_p + \nabla\mathbf{g}(\mathbf{z}_p)^T \mathbf{d}_z + \mathbf{d}_s = \mathbf{r}_{g,p}, \tag{3.28c}$$

$$(\mathbf{d}_z, \mathbf{d}_s) \in T_p. \tag{3.28d}$$

Ideally, we would like that the trust region step satisfies constraints (3.28b)-(3.28c) with $\mathbf{r}_{g,p} = \mathbf{0}$ and $\mathbf{r}_{h,p} = \mathbf{0}$. However, the feasible set may be empty if the trust region T_p does not intersect the linearized constraints. These reasons motivate the introduction of the residual vector $\mathbf{r}_{g,p}$ and $\mathbf{r}_{h,p}$ ensuring that the feasible set is non-empty [136].

The issue about the specific choice of $\mathbf{r}_{g,p}$ and $\mathbf{r}_{h,p}$ remains. This can be carried out by two-dimensional subspace minimization, for which local and global convergence properties guarantee to make progress towards optimality and feasibility [137, 138]. The main idea is to replace the original problem by two trust region subproblems of smaller dimension. The total step $\mathbf{d}_z$ is decomposed into a normal step $\mathbf{d}_{z,n}$ and a tangential step $\mathbf{d}_{z,t}$ such as $\mathbf{d}_z = \mathbf{d}_{z,n} + \mathbf{d}_{z,t}$. The normal step aims to find a value of the residual vector that first makes problem (3.28) feasible. Then, the tangential step focuses on optimality as long as the point remains feasible. This step can be solved by conjugate gradient iterations. The preconditioning will ensure efficient solutions for ill-conditioned problems and the Steihaug's stopping test [139] allows to deal with indefinite Hessian. An efficient implementation can be found in [140].

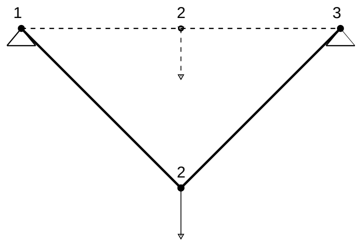

Figure 3.1: The two-bar truss example with the initial ground structure in dashed line and the optimum in solid line

3.6.3 Verification test

Hereafter, we compare solutions of barrier problem (3.24) for Newton's method with line search and for sequential quadratic programming with trust region. The gradient of the objective function and the constraint Jacobian are provided analytically. Regarding the Hessian of the Lagrangian, different options are examined in contrast. An efficient implementation of these algorithms can be found in general-purpose software like Knitro [141] or fmincon toolbox in Matlab [142].

Two-bar truss

Consider a simple two-bar truss example for which the design space can be visualized (Fig. 3.1). The ground structure is composed of three nodes interconnected by two members. The structure is subject to a downward load of magnitude 1 applied to the central node. The minimum volume problem is investigated with limiting stresses $\overline{\sigma}_e{}^+ = 1$ and $\overline{\sigma}_e{}^- = 1$. The central node is allowed to move downwardly. For this problem, we use the set of optimization variables is $\left(q_{t,1}^+, q_{t,2}^+, q_{t,1}^-, q_{t,2}^-, x_4\right)$ for the reduced formulation under single loading:

$$\min_{\substack{\mathbf{q}_t^+ \in \mathbb{R}_+^2 \\ \mathbf{q}_t^- \in \mathbb{R}_+^2 \\ \mathbf{x} \in \mathbb{R}^6}} \left\{ \sum_{e=1}^{2} \left(q_{t,e}^+ + q_{t,e}^-\right) \mathbf{x}^\top \mathbf{C}_e \mathbf{x} \;\middle|\; \sum_{e=1}^{2} \left(q_{t,e}^+ - q_{t,e}^-\right) \mathbf{P}\mathbf{C}_e \mathbf{x} = \mathbf{f},\ \mathbf{x} \in X \right\}. \tag{3.29}$$

The Lagrangian function of (3.29) is

$$\mathcal{L}\left(q_{t,1}^+, q_{t,2}^+, q_{t,1}^-, q_{t,2}^-, x_4, \boldsymbol{\lambda}_h\right) = \sum_{e=1}^{2} \left(q_{t,e}^+ + q_{t,e}^-\right) \mathbf{x}^\top \mathbf{C}_e \mathbf{x} + \boldsymbol{\lambda}_h^\top \left[\sum_{e=1}^{2} \left(q_{t,e}^+ - q_{t,e}^-\right) \mathbf{P}\mathbf{C}_e \mathbf{x} - \mathbf{f}\right]. \tag{3.30}$$

where $(\lambda_{h,1}, \lambda_{h,2})$ are Lagrange multipliers associated to equilibrium constraints. To test the algorithm under difficult condition, the initial point is set at zero for all variables. At this point, the design space is flat and the analytical Hessian is given by

$$\nabla^2 \mathcal{L}\Bigg|_{\substack{q_{t,1}^+ = 0 \\ q_{t,2}^+ = 0 \\ q_{t,1}^- = 0 \\ q_{t,2}^- = 0 \\ x_4 = 0}} = \begin{bmatrix} 0 & 0 & 0 & 0 & \lambda_{h,1} + \lambda_{h,2} \\ 0 & 0 & 0 & 0 & \lambda_{h,1} + \lambda_{h,2} \\ 0 & 0 & 0 & 0 & -\lambda_{h,1} - \lambda_{h,2} \\ 0 & 0 & 0 & 0 & -\lambda_{h,1} - \lambda_{h,2} \\ \lambda_{h,1} + \lambda_{h,2} & \lambda_{h,1} + \lambda_{h,2} & -\lambda_{h,1} - \lambda_{h,2} & -\lambda_{h,1} - \lambda_{h,2} & 0 \end{bmatrix}. \tag{3.31}$$

The indefiniteness of the Hessian is confirmed by the presence of both positive and negative components in the vector of eigenvalues $(\lambda_{h,1} + \lambda_{h,2}) \begin{bmatrix} -2 & 0 & 0 & 0 & 2 \end{bmatrix}$. In order to visualize the design space, we represent $q_{t,1}^+$ and x_4 because compressive force densities $q_{t,1}^-$ and $q_{t,2}^-$ tend to zero at the solution, and by symmetry $q_{t,1}^+ = q_{t,2}^+$. The global optimum for this problem is $q_{t,1}^+ = 0.5$ and $x_4 = -1$.

Given the starting point and the optimum, the trajectories of iterates are systematically drawn in Figure 3.2 for both line search and trust region procedures and different Hessian options. For the

BFGS method (Fig. 3.2(a)), the trust region step succeeds in finding the optimal solution whereas the line search converges to an incorrect point away from the optimum. The SR1 method (Fig. 3.2(b)) forthwith fails at the outset with the line search procedure because of the negative curvature. Once again, the trust region method reaches the optimal point quite efficiently. Then, the finite-difference approximation of the Hessian (actually, the Hessian-vector product) (Fig. 3.2(c)) and the exact evaluation (Fig. 3.2(d)) exhibits a similar behaviour for the trust region step. The difference between both arises in the number of gradient evaluations which are twice higher with the finite-difference technique.[1]

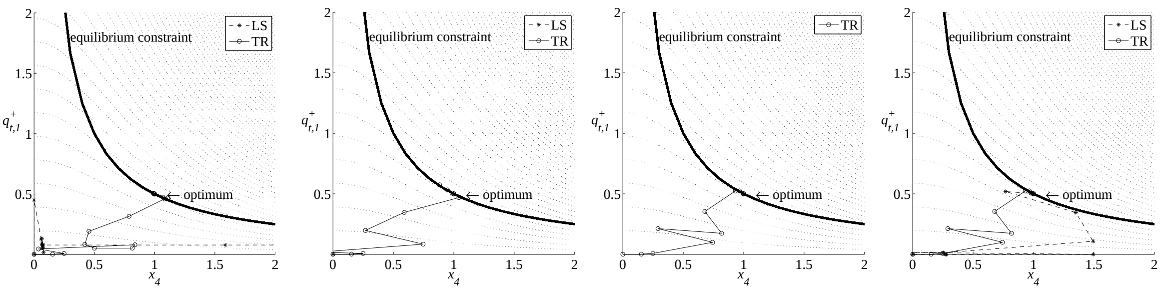

(a) Quasi-Newton BFGS (b) Quasi-Newton SR1 (c) Finite-difference Hessian-vector product (d) Exact Hessian

Figure 3.2: Design space of the two-bar truss for different Hessian options. The line search (LS) iteration path is represented with a dashed line and the trust region (TR) path is represented with a solid line.

Cantilever truss

To further investigate sequential quadratic programming with trust regions on problem of moderate size, consider the cantilever of Fig. 3.3(a) [90]. The design domain is a rectangular 4×3 grid regularly spaced with unit square modules, and supported by the three leftmost nodes $(1, 2, 3)$. The 27-bar structure is subjected to a downward load of magnitude 1 applied on node 11. Except for the supports, all nodes are allowed to move in all spatial directions. The sparsity pattern of the constraints Jacobian and the Hessian matrix for this small problem is depicted in Figs. 3.3(b) and 3.3(c), respectively.

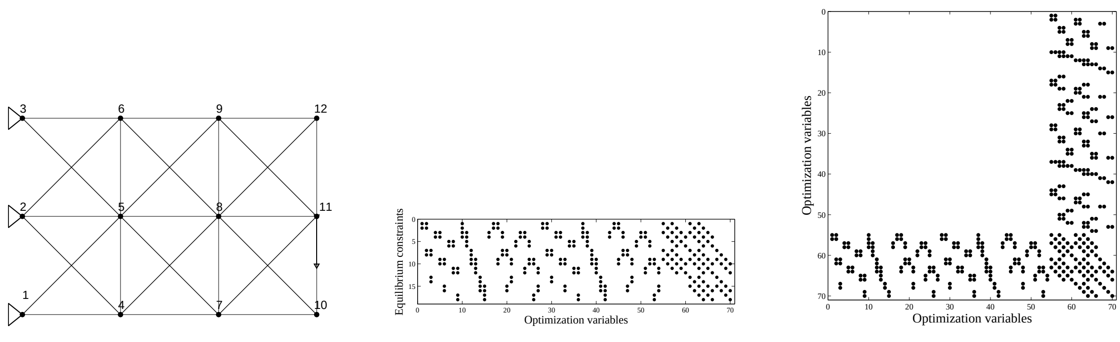

(a) Initial ground structure (b) Jacobian (c) Hessian

Figure 3.3: Cantilever truss. The initial ground structure is given in (a). The sparisty pattern of the Jacobian of constraints is depicted in (b) and the Hessian of the Lagrangian function is depicted in (c), where the empty square corresponds to topological variables. Note that, unlike this small example, the filling density on larger problem sizes are usually less than 1%.

The optimization is performed with different Hessian options, as depicted in Fig. 3.4. Unlike the SR1 method (Fig. 3.4(b)), the limited-memory BFGS method (Fig. 3.4(a)) provides a satisfactory

[1] Line search with finite-difference is not allowed in Knitro, and for the exact case a switch to the trust region step has been necessary for some iterates.

optimal value. However, those solutions significantly differ from the finite-difference (Fig. 3.4(c)) and the exact Hessian (Fig. 3.4(d)), which have very close values of the objective function.

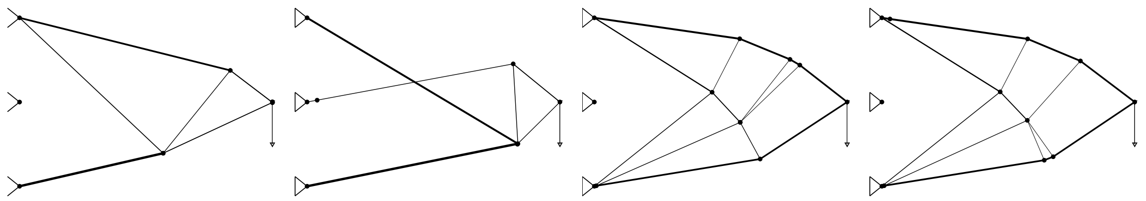

(a) TR–lBFGS, $V^* = 8.844$ (b) TR–SR1, $V^* = 13.685$ (c) TR–Diff., $V^* = 8.259$ (d) TR–Exact, $V^* = 8.256$

Figure 3.4: Different solutions and their objective function of the cantilever truss

From results of the two-bar truss and the cantilever examples, one can conclude that sequential quadratic programming with trust region exhibits a more robust behavior compared to Newton's method with line search procedure. Regarding the Hessian option, both finite-difference vector product and analytical Hessian provide very good results. Hence, if the analytical Hessian cannot be calculated, it generally suffices to work with finite-difference vector products.

3.7 Design settings

In this section an academic benchmark (see e.g. [90,119]) is used to illustrate several design settings and to discuss differences among formulations along with some theoretical considerations. These results extend certain statements on topology optimization to the case of geometry optimization. Although they do not provide a rigorous proof, some preliminary comments could initiate further prospects in the field.

The example consists in the optimization of a two-dimensional bridge. The initial ground structure is a rectangular grid of 6×1 unit modules (Fig. 3.5). The neighboring nodes are connected by 31 truss members. The supports block the displacements of the leftmost node in both main directions whereas the rightmost node is only blocked vertically. Five downward unit loads are applied on the lower nodes. While the single loading case will consider all the loads simultaneously, the multiple loading case will successively apply the five loads individually. When the geometry is optimized, the upper nodes are allowed to move in all directions. To allow an easy comparison of results, Young's moduli $E_e = 1$ for all $e = 1, \ldots, N_b$. Unless explicitly mentioned, the self-weight of structural members is neglected.

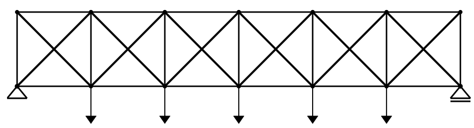

Figure 3.5: Initial ground structure of the two-dimensional truss bridge

For the optimization process, the interior-point method with sequential quadratic programming and trust regions is performed using Knitro [141]. The analytical first derivatives are provided and the Hessian of the Lagrangian function is approximated by finite-difference vector-product. All the solutions that are presented above are claimed to be local optima. They were obtained in less than one minute CPU on a personal desktop, quad-core processor 2.67GHz and 8GiB RAM. We also check the optimality using a multi-start procedure with 100 initial trial points but the technique was generally unable to improve the results.

Thus, consider the numerical solutions depicted in Figs. 3.6-3.12. The optimal values of the objective function are denoted V^* for volume and C^* for compliance. The figure captions indicate

Figure	Setting	Formulation	Loading	Self-weight	Stress	Displacement
Fig. 3.6	Geometry optimization	(3.22)	Single	–	✓	–
Fig. 3.7	Member self-weight	(3.10)	Single	✓	✓	–
Fig. 3.8	Compatibility condition	(3.9-3.10)	Multiple	–	✓	–
Fig. 3.9	Displacement constraints	(3.9)	Single & Mult.	–	✓	✓
Fig. 3.10	Unequal limiting stresses	(3.10)	Single & Mult.	–	✓	–
Fig. 3.11	Volume constraint	(3.17)	Multiple	–	–	–
Fig. 3.12	Volume constraint	(3.20)	Multiple	–	–	–

Table 3.1: Design settings and formulations used in the optimization of the simple bridge structure

the formulations used to obtain the solution as well as the design settings. A summary is reported in Table 3.1. Based on these results, the following comments are drawn:

- *Geometry optimization* (Fig. 3.6). In comparison to the solution obtained by pure topology optimization, the consideration of geometrical variables leads to significant gains in terms of structural performance. It is not surprising because the solution of geometry and topology optimization is statically determinate, unlike the case of pure topology optimization.
- *Member self-weight* (Fig. 3.7). If the self-weight of structural members is considered, the optimal geometry is modified to comply with the shape-dependent loading. Some upper nodes move towards supports. We also verify that the truss members are not fully stressed, as noticed in [47] for topology optimization.
- *Compatibility condition* (Fig. 3.8). According to [55, 68], the removal of the compatibility condition from the minimum volume problem introduces a relatively small error on the optimal solution. This example supports this assertion by showing that the lower-bound solution is only 2.23% lower than for the elastic design. However, the geometry is clearly different.
- *Displacement constraints* (Fig. 3.9). To exhibit the impact of displacement constraints on the minimum volume problem, the displacement variables are tightly bounded so that the design is mainly driven by those constraints. The volumes obtained in solutions for both single and multiple loading cases drastically increase. Yet, while the optimal geometry is independent of displacement constraints for a statically determinate solution, it actually differs when the solution is redundant as for the multiple loading case.
- *Unequal limiting stresses* (Fig. 3.10). The imposition of different values for tensile and compressive stress limits demonstrates that, for the single loading case, the solution is fully stressed and hence justifies the use of the reduced formulation (3.22) to solve the problem, as shown in [53] for topology optimization. Moreover, the geometry does not change compared to the basic solution in plastic design under single loading. This statement does not hold for the multiple loading case where the arch is truly heightened compared to the plastic design of Fig. 3.8. Again, the statical determinacy of the solution is determinant.
- *Volume constraint* (Fig. 3.11 and Fig. 3.12). The effect of volume constraints on compliance optimization is investigated for the weighted-average and the worst-case compliance. Both results confirm that the optimal geometries and topologies are not affected by the volume constraint. By contrast, the sections are uniformly scaled by 10 times, hence decreasing the optimal compliance by a factor 1/10, as shown in [58] for topology optimization.

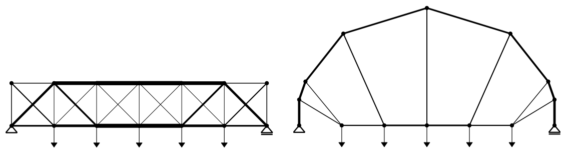

(a) $V^* = 56.000$ (b) $V^* = 34.977$

Figure 3.6: Geometry optimization. Optimal designs under single loading by topology optimization (a) and including geometry optimization of upper nodes in every spatial directions (b). Both solutions are generated using the reduced formulation (3.22) with $\kappa = 1$.

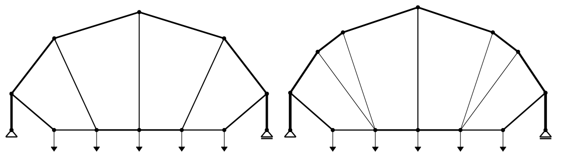

(a) $V^* = 35.564$ (b) $V^* = 38.389$

Figure 3.7: Member self-weight. For the single loading case, the gravitational magnitudes for the vector $\mathbf{g}_e$ in the plastic design formulation (3.10) are set at 0.001 (a) and 0.01 (b). Limiting stresses are set at $\overline{\sigma}^{+}_{e,k} = 1$ and $\overline{\sigma}^{-}_{e,k} = 1$.

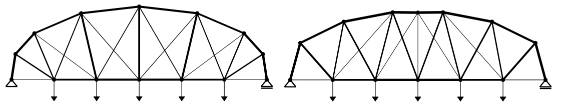

(a) $V^* = 17.702$ (b) $V^* = 18.096$

Figure 3.8: Compatibility condition. Five individual loadings are successively applied. The structure is first optimized using the formulation (3.10) in plastic design (a) and using the formulation (3.9) in elastic design with unbounded displacement variables (b). Limiting stresses are set at $\overline{\sigma}^{+}_{e,k} = 1$ and $\overline{\sigma}^{-}_{e,k} = 1$.

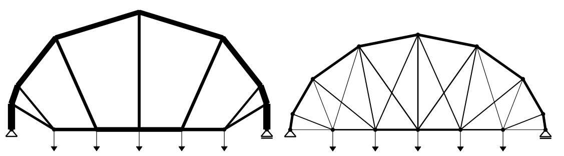

(a) $V^* = 244.674$ (b) $V^* = 137.137$

Figure 3.9: Displacement constraints. The displacement variables are unit bounded, i.e. $\overline{u}^{+}_{i,k} = 1$ and $\overline{u}^{-}_{i,k} = 1$. The formulation (3.9) of the minimum volume problem in elastic design is solved either for the single loading case (a) and the five individual loading cases (b). Limiting stresses are set at $\overline{\sigma}^{+}_{e,k} = 1$ and $\overline{\sigma}^{-}_{e,k} = 1$.

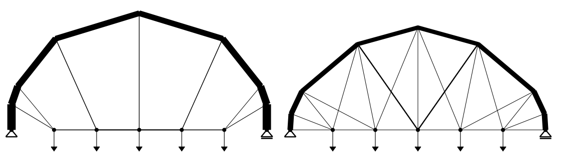

(a) $V^* = 192.372$ (b) $V^* = 80.501$

Figure 3.10: Unequal limiting stresses. For the minimum volume problem in plastic design (3.10), we set different limiting stresses in tension and compression, $\overline{\sigma}^{+}_{e,k} = 1$ and $\overline{\sigma}^{+}_{e,k} = 1/10$. The optimization is performed for the single loading case (a) and the five individual loading cases (b).

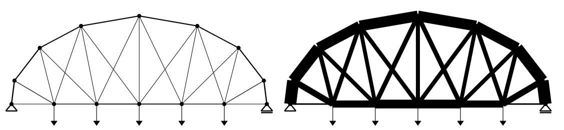

(a) $C^* = 126.430$ (b) $C^* = 12.643$

Figure 3.11: Volume constraint. For the weighted-average minimum compliance problem (3.17) under the five individual loading cases with $w_k = 0.2$ for all $k = 1, \ldots, 5$, the quantity of available material is set at $\overline{V} = 1$ (a) and $\overline{V} = 10$ (b).

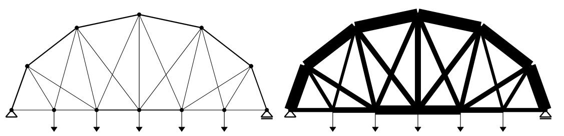

(a) $C^* = 139.289$ (b) $C^* = 13.929$

Figure 3.12: Volume constraint. For the worst-case compliance (3.20) under the five individual loading cases, the quantity of available material is set at $\overline{V} = 1$ (a) and $\overline{V} = 10$ (b).

3.8 Concluding remarks

This chapter proposed a novel formulation for truss geometry and topology optimization. Our approach to overcome numerical singularities disaggregates the equilibrium equations and reformulate the problem by simultaneous analysis and design. It results in several formulations based on a unique set of parameters that are general enough to cover minimum volume and compliance problems including self-weight and multiple loading, as well as stress and displacement constraints. The impact of the optimization algorithm and of different design settings on the solution is also studied.

With the proposed formulation, the stability of lightweight structures is not addressed yet. Given the importance of such considerations on the optimal design, Chapter 4 will present a method to ensure stability.

4 Stability considerations

This chapter presents a computationally efficient method for truss layout optimization with stability constraints. Previously proposed approaches that ensures stability of optimal frameworks are first reviewed in Section 4.1, showing that existing studies are almost all restricted to topology optimization. The present contribution generalizes the approach to simultaneous geometry and topology optimization. In Section 4.2, the lower-bound plastic design formulation under multiple loading will serve as basis for this purpose. The numerical difficulties associated with geometrical variations are identified and the parametrization is adapted accordingly. To avoid nodal instability, the nominal force method introduces artificial loading cases which simulate the effect of geometric imperfections (Section 4.3). Hence, the truss systems with unstable nodes are eliminated from the set of optimal solutions. At the same time, the local stability of structural members is ensured via a consistent local buckling criterion (Section 4.4). As shown in Section 4.5, this novel formulation leads to optimal configurations that can be practically used for the preliminary design of structural frameworks. Three applications illustrate the impact of stability constraints on the solution. The importance of geometry optimization is also pointed out by comparing with optimal solutions that are unachievable by topology optimization only.

4.1 Literature review

Designing lightweight structures using truss layout optimization constitutes an excellent starting point to obtain cost-effective solutions. This process naturally drives design towards light and slender structures, therefore making them sensitive to instabilities. Traditionally, structural engineering deals with these undesirable effects later in the design process: the hinges present in the optimal solution are often replaced by (semi) rigid connections to avoid mechanisms, and structural members are resized to comply with standard codes. These post-processes may, however, considerably deteriorate structural performance if stability issues have been neglected in early design stages.

The consideration of stability issues is thus meaningful for practical design and has aroused interest among researchers [143]. Structural stability theory is a vast field of engineering covering static and dynamic response, creep, fracture and damage-induced instability, to mention a few [144]. Here, we are particularly concerned with those applying for truss layout optimization, in view of generalization to geometry optimization. Although the instability of structural frameworks can be viewed as a combination of local and global buckling, Tyas and co-authors [145] have put forward a more precise classification in this context:

- *Local instability* of a member occurs when the compression force exceeds its critical buckling load. Frequently Euler's formula is considered, although it may overestimate the actual buckling strength (Fig. 4.1(a));
- *Nodal instability* is basically related to the presence of mechanisms in compression chain due to the lack of bracing members (Fig. 4.1(b)). By extension, nodal instability occurs when a static equilibrium state cannot be found due to some perturbation in the loads applied on compression nodes, as in the common case of inverted hanging chains in optimal geometries;

- *Global instability* occurs when a braced structure buckles as a whole due to insufficient elastic stiffness (Fig. 4.1(c)). Note that the global stability implies the nodal stability. The inverse is not necessarily true.

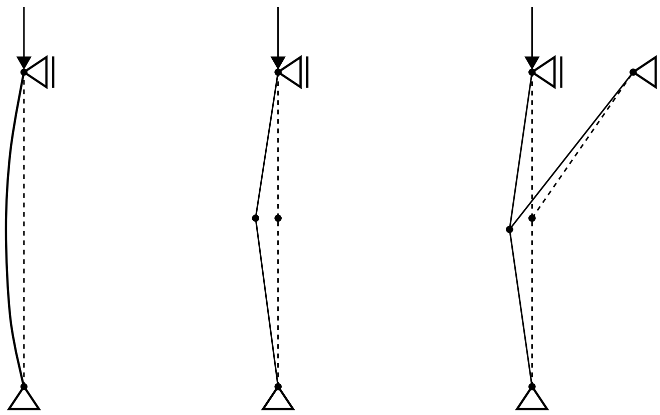

(a) (b) (c)

Figure 4.1: Classifications of instabilities in trusses: (a) local instability, (b) nodal instability, (c) global instability

These issues can be addressed in different ways but some problem statements are irrelevant. Indeed, the sole consideration of stress and local buckling constraints is meaningless for the ground structure approach because the optimal topology may include compression chains in unstable equilibrium for which the calculation of the local buckling strength is misled [80, 146]. Furthermore, replacing the compression chain by a full-length element at the end of the optimization process leads to non-optimal solutions. To solve this problem, Achtziger [147, 148] has integrated a node cancellation procedure in the optimization process via an equivalent formulation affordable by mathematical programming.

A more general approach, capable of identifying nodal instability in any kinds of truss system, has been reported in [149, 150]. In this method, linearized global stability constraints are included in the minimum compliance formulation so that the external loading remains below the critical buckling capacity of the entire structure. A similar method has been applied to the stress-constrained minimum volume problem with overlapping bars [151]. For the multiple loading case, [152] has shown that numerical singularities arise and a relaxation method has been proposed accordingly. Note that these constraints can be formulated via semi-definite programming to reduce the computational effort.

Alternatively, structural optimization under uncertainty attempts to closely resemble realistic engineering design problems. Two main approaches are available: robust design optimization seeks to minimize the influence of stochastic variability on the mean design [153], whereas reliability-based design optimization are problems subject to a constraint on the probability of failure [154]. Regarding the uncertainty, it can be applied to various design parameters, for instance in the magnitude and location of applied loads to ensure nodal stability [155, 156]. Other methods, e.g. those accounting for manufacturing defects such as geometric imperfection [157, 158] and material variability [159], produce stable structures as well. At the time of this writing, despite recent advances in model reduction for stochastic processes (e.g. [160]), the high computational expense associated to these methods suggest that applications are still limited to structures of moderate size.

The nominal force method essentially shares similar goals with robust design optimization methods, except that deterministic loads are considered instead: the method adds to the primary loading cases some small occasional perturbation loadings. One relevant setting is that only nodes under compression are stabilized. The underlying principle comes from Winter's method [161] whose aim was to assess the magnitude of horizontal forces required to stabilize the rigid bar model of multi-level columns subject to geometric imperfection. The magnitude of these lateral forces is scaled by the compression force in the column. This approach can be found in most current design codes [162]

and has been successfully adapted to truss topology optimization in order to stabilize compression chains [145]. Although without absolute guarantee, the optimal solution may also result in a globally stable system as a welcome side effect. This conceptually simple, yet powerful approach clearly stands as the best alternative to comply with geometry optimization.
Despite the considerable importance of combining geometry and topology optimization [99], most studies on ensuring stability of optimal frameworks focus on truss topology optimization. The non-linearity induced by geometrical variations certainly complicates the implementation. The optimal solution may also include melting nodes and local buckling singularities, causing serious convergence difficulties when dealing with nonlinear programming algorithms [91]. Hence, classical elastic design formulations must be recast to cover all numerical deficiencies. The lower-bound plastic design formulation, as described in [119], will be used to incorporate the nominal force method together with the local buckling criterion.

4.2 Lower-bound plastic design formulation

The development of a suitable strategy for ensuring local and nodal stability must be achieved in accordance with the optimization formulation and the design context. It should be reminded that, in practical use, geometry and topology optimization should be used at early design stages. Subsequently, the solution will be checked and member sizes verified using a conventional analysis process. Hence, more computationally efficient optimization approach would be of more benefit in practice. These reasons motivates the consideration of lower-bound plastic design formulations as a sound framework to incorporate stability constraints.
The primary advantage with plastic design is that local buckling singularities are eliminated together with the removal of compatibility condition. Moreover, to permit a specific treatment of compression members, we express the stress components in terms of non-negative tension $\sigma^+_{e,k}$ and compression $\sigma^-_{e,k}$ parts such as $\sigma_{e,k} = \sigma^+_{e,k} - \sigma^+_{e,k}$. The precise relations are

$$\sigma^+_{e,k} := \frac{q^+_{t,e,k}}{q_{a,e}} \in \mathbb{R}_+,\ \forall e = 1, \ldots, N_b,\ \forall k = 1, \ldots, N_c, \tag{4.1a}$$

$$\sigma^-_{e,k} := \frac{q^-_{t,e,k}}{q_{a,e}} \in \mathbb{R}_+,\ \forall e = 1, \ldots, N_b,\ \forall k = 1, \ldots, N_c, \tag{4.1b}$$

which are linearly bounded by the set of admissible stresses for tension and compression:

$$S := \big\{ \boldsymbol{\sigma}^+_k \in \mathbb{R}^{N_b}_+ \ \big|\ 0 \le \sigma^+_{e,k} \le \overline{\sigma}^+_{e,k},\ e = 1, \ldots, N_b,\ k = 1, \ldots, N_c, \tag{4.2a}$$

$$\boldsymbol{\sigma}^-_k \in \mathbb{R}^{N_b}_+ \ \big|\ 0 \le \sigma^-_{e,k} \le \overline{\sigma}^-_{e,k},\ e = 1, \ldots, N_b,\ k = 1, \ldots, N_c \big\}. \tag{4.2b}$$

Thus, the alternative lower-bound plastic design formulation under multiple loading (3.10) can be written in terms of $\left\{\mathbf{q}_a, \boldsymbol{\sigma}^+_k, \boldsymbol{\sigma}^-_k, \mathbf{x}\right\}$ as follows

$$\min_{\mathbf{q}_a, \boldsymbol{\sigma}^+_k, \boldsymbol{\sigma}^-_k, \mathbf{x}} \ \sum_{e=1}^{N_b} v_e\left(\mathbf{q}_a, \mathbf{x}\right) \tag{4.3a}$$

$$\text{s.t.:}\ \sum_{e=1}^{N_b} q_{a,e}\left(\sigma^+_{e,k} - \sigma^-_{e,k}\right)\mathbf{P}\mathbf{C}_e\mathbf{x} = \mathbf{f}_k + \sum_{e=1}^{N_b} v_e\left(\mathbf{q}_a, \mathbf{x}\right)\mathbf{g}_e,\ \forall k = 1, \ldots, N_c, \tag{4.3b}$$

$$\mathbf{q}_a \in \mathbb{R}^{N_b}_+, \left\{\boldsymbol{\sigma}^+_k, \boldsymbol{\sigma}^-_k\right\} \in S, \mathbf{x} \in X. \tag{4.3c}$$

Solution of problem (4.3) leads to an optimal behaviour of the truss structure under the specified loads but stability issues are not yet addressed. An intuitive way to generate stable optimal designs is to consider additional loading cases that should increase the redundancy of the truss system. Obviously, the reliability of this strategy depends on the designer's ability to correctly guess the envelope of every possible loading scenarios. Furthermore, the difficulty of estimating a suitable magnitude for perturbation loads remains. Hereafter, these issues will be addressed in a systematic way. Nodal instabilities are eliminated by implementing a nominal force method, afterwards a consistent Euler buckling criterion for geometry and topology optimization will be derived and finally incorporated in problem (4.3).

4.3 Nominal force method for local stability

The nominal force method has its origins in Winter's method [161] for the design of steel frameworks. The principle behind the nominal force method is to determine the restraining forces required to stabilize compression chains (Fig. 4.2(a)). The bracing elements must be sized to resist these lateral forces. Their magnitude is proportional to the compressive loads in the chain, to the degree of geometrical imperfection, and to the stiffness of structural members. Numerical experiments showed that the two first factors are predominant over the latter [163]. Hence, the magnitude of the lateral force is taken as a small percentage α_s of the compressive load in the column that depends on the degree of out-of-straightness. Typically, a value $\alpha_s = 0.02$ is taken.

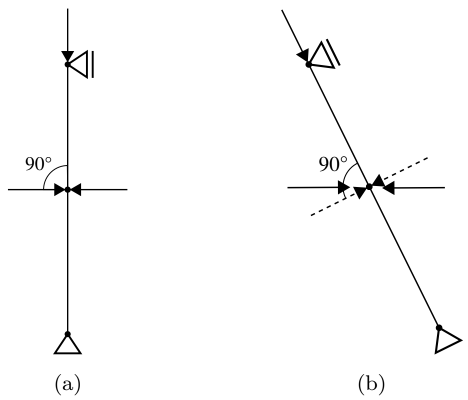

Figure 4.2: The nominal lateral forces when (a) the Cartesian global axes coincide with the main axes of the collinear chain or (b) in any direction

Tyas and co-authors [145] had adapted the concept to topology optimization using the ground structure approach. They proposed to consider the orientation of strut forces, which are projected in Cartesian axes to generate the nominal forces. One of the major concern was how to interpret these nominal forces for a space truss in which the orientation of truss members does not necessarily coincide with Cartesian axes. Ideally, an infinite number of loading cases would be considered in all directions to capture the worst case. As an approximation, Tyas and co-authors [145] introduce six nominal loading cases projected in either direction to the three Cartesian axes. They correctly emphasized that when the compression chain is not parallel to one of the Cartesian axes (Fig. 4.2(b)), taking the orientation into account may decrease the magnitude of nominal forces in a range from 0.5 to 1, i.e. it can vary up to 50%.

This aspect is especially important when the problem is extended to geometry optimization. In that case, the optimal shapes often comprise inverted hanging chains for which the variable orientation is beyond the scope of straight compression chains. Since the magnitude of the nominal forces is rather subjective and differs among standard codes, a conservative approach is chosen: every contribution of compression force acting on a specified node is considered regardless the orientation of adjacent bars. Then, the method proposed hereafter lets the possibility to the designer to prescribe the orientations of nominal forces according to the structural design problem. Defining the most critical orientations for the nominal forces is not particularly difficult, as illustrated in the numerical examples.

Mathematically, the problem can be stated as follows. Let $\mathcal{E}_i$ be the set of elements $e_i \in \{1,\dots,N_b\}$ connecting the i-th degree of freedom, the magnitude of the nominal force is taken to be proportional to the sum of compressive forces over $\mathcal{E}_i$. For each nominal loading case $k_s \in \{1,\dots,N_s\}$, the calculated force is then applied on the i-th degree of freedom in a direction specified by the designer whose values are collected in a matrix of direction cosines $\theta_{i,k_s} \in [-1,1]$. For instance, consider that the i-th degree of freedom corresponds to the X-axis. If the nominal force of the k_s-th loading case is applied in this direction, $\theta_{i,k_s} = 1$; in the opposite direction, $\theta_{i,k_s} = -1$; in the perpendicular case, $\theta_{i,k_s} = 0$. Gathering all these parts in a function vector of the nominal forces $\mathbf{f}_{k_s}$ leads to the new definition:

$$\begin{aligned}&\mathbf{f}_{k_s} : \mathbb{R}_+^{N_b} \mapsto \mathbb{R}^{N_d}, \quad \mathbf{t}^- \mapsto f_{i,k_s}\left(\mathbf{t}^-\right) := \alpha_s \theta_{i,k_s} \sum_{e_i \in \mathcal{E}_i} t_{e_i}^-, \\ &\forall i = 1,\dots,N_d,\ \forall k_s = 1,\dots,N_s.\end{aligned} \tag{4.4}$$

where $\mathbf{t}^- \in \mathbb{R}_+^{N_b}$ denotes the compression force in every elements. Using (4.4), these stability loading cases are introduced by means of N_s additional systems of static equilibrium constraints:

$$\sum_{e=1}^{N_b} q_{a,e} \left(\sigma_{e,k_s}^+ - \sigma_{e,k_s}^-\right) \mathbf{P}\mathbf{C}_e \mathbf{x} = \mathbf{f}_{k_s}\left(\mathbf{t}^-\right),\ \forall k_s = 1,\dots,N_s. \tag{4.5}$$

In order to maintain the regularity of the formulation in presence of melting nodes, it is necessary to deal with the vector of compression forces $\mathbf{t}^- \in \mathbb{R}_+^{N_b}$. Expressing this vector as $t_e^- = q_{a,e}\sigma_e^- l_e$ would reintroduce the undesirable length function in the formulation. To circumvent these problems, the internal force vector $\mathbf{t}^-$ is set as auxiliary variables (whose main purpose is to remove the length function of the formulation). The internal force should be taken as the maximum of internal forces over all primary loading cases $k = 1,\dots,N_c$:

$$t_e^- = \max_{k=1,\dots,N_c} q_{a,e}\sigma_{e,k}^- l_e\left(\mathbf{x}\right),\ \forall e = 1,\dots,N_b. \tag{4.6}$$

This can be done in a smooth way by introducing inequality constraints obtained from squaring (4.6):

$$\left(t_e^-\right)^2 \geq q_{a,e}^2 \left(\sigma_{e,k}^-\right)^2 \mathbf{x}^\top \mathbf{C}_e \mathbf{x},\ \forall e = 1,\dots,N_b,\ \forall k = 1,\dots,N_c. \tag{4.7}$$

In a simultaneous analysis and design context, the advantage of this method is that a solution to the problem which includes disturbing forces can be found without the need for an iterative procedure. The introduction of constraints (4.5) and (4.7) into problem (4.3) would ensure that the optimal solution is in static equilibrium with respect to the primary loading cases while maintaining the nodal stability for small perturbations on compression members. Preserving solutions from local instability of structural members only remains.

4.4 Local buckling criterion

The effect of local buckling considerably affects the optimal truss design by discarding long and slender elements in compression for the benefit of short and tensile members. The local stability of structural members can be ensured by applying the following inequality constraints for primary and nominal loading cases:

$$t_{e,k}^- \leq t_{cr,e},\ \forall e = 1,\dots,N_b,\ \forall k = 1,\dots,N_c, \tag{4.8a}$$

$$t_{e,k_s}^- \leq t_{cr,e},\ \forall e = 1,\dots,N_b,\ \forall k_s = 1,\dots,N_s. \tag{4.8b}$$

For instance, the critical load $t_{cr,e}$ can be calculated by Euler's formula

$$t_{cr,e} := \frac{\pi^2 E_e I_e}{l_{\text{eff},e}^2} \in \mathbb{R}_+,\ \forall e = 1, \ldots, N_b, \tag{4.9}$$

where $I_e \in \mathbb{R}_+$ is the second moment of inertia, $E_e \in \mathbb{R}_+$ the Young's modulus of the material, and $l_{\text{eff},e} \in \mathbb{R}_+$ is the effective buckling length of the e-th member (taken equal to the actual length of the truss element for convenience). Although we consider an elastic modulus, we do work in plastic design since the (elastic) compatibility condition is neglected. In the single load case with a statically determinate optimum, the solution is the same as in elastic design [64]. For the multiple loading case, the plastic optimum is a lower-bound solution which differs by a few percent to the elastic design solution [145].

In order to express the critical buckling load in terms of the design variable $a_e \in \mathbb{R}_+$, I_e can be written as $I_e = \beta_e a_e^2$ with the invariant factor $\beta_e \in \mathbb{R}_+$ whose value depends on the shape of the cross-section [147]. By putting

$$s_e := \pi^2 E_e \beta_e \in \mathbb{R}_+,\ \forall e = 1, \ldots, N_b, \tag{4.10}$$

the local buckling constraints are rewritten as follows

$$t_{e,k}^{-} \mathbf{x}^\top \mathbf{C}_e \mathbf{x} \leq s_e a_e^2,\ \forall e = 1, \ldots, N_b,\ \forall k = 1, \ldots, N_c, \tag{4.11a}$$

$$t_{e,k_s}^{-} \mathbf{x}^\top \mathbf{C}_e \mathbf{x} \leq s_e a_e^2,\ \forall e = 1, \ldots, N_b,\ \forall k_s = 1, \ldots, N_s. \tag{4.11b}$$

For information, $s_e = \pi E_e/4$ for a circular cross-section and $s_e = \pi^2 E_e/12$ for a square cross-section. Although constraints (4.11) are regular with respect to $(\mathbf{a}, \mathbf{x}, \mathbf{t}^-)$, the parametrization must be changed in order to be integrated into formulation (4.3). By working with $\left\{\mathbf{q}_a, \mathbf{x}, \boldsymbol{\sigma}_k^-, \boldsymbol{\sigma}_{k_s}^-\right\}$ and squaring both sides of the inequality, the local buckling constraints are written in a continuous form:

$$\left(\sigma_{e,k}^-\right)^2 \mathbf{x}^\top \mathbf{C}_e \mathbf{x} \leq s_e^2 q_{a,e}^2,\ \forall e = 1, \ldots, N_b,\ \forall k = 1, \ldots, N_c, \tag{4.12a}$$

$$\left(\sigma_{e,k_s}^-\right)^2 \mathbf{x}^\top \mathbf{C}_e \mathbf{x} \leq s_e^2 q_{a,e}^2,\ \forall e = 1, \ldots, N_b,\ \forall k_s = 1, \ldots, N_s. \tag{4.12b}$$

As already mentioned in Section 2.4.5, these constraints do not suffer from the local buckling singularity phenomenon arising in elastic design formulations since the compatibility condition has been removed.

4.5 Formulation including stability constraints

Introducing constraints (4.5), (4.7), and (4.12) in problem (4.3) yields the novel formulation for truss geometry and topology optimization incorporating local and nodal stability considerations:

$$\min_{\substack{\mathbf{q}_a, \boldsymbol{\sigma}_k^+, \boldsymbol{\sigma}_k^-, \mathbf{x} \\ \mathbf{t}^-, \boldsymbol{\sigma}_{k_s}^+, \boldsymbol{\sigma}_{k_s}^-}} \quad \sum_{e=1}^{N_b} v_e\left(\mathbf{q}_a, \mathbf{x}\right), \tag{4.13a}$$

$$\text{s.t.:} \quad \sum_{e=1}^{N_b} q_{a,e}\left(\sigma_{e,k}^+ - \sigma_{e,k}^-\right)\mathbf{P}\mathbf{C}_e\mathbf{x} = \mathbf{f}_k + \sum_{e=1}^{N_b} v_e\left(\mathbf{q}_a, \mathbf{x}\right)\mathbf{g}_e, \ \forall k = 1, \ldots, N_c, \tag{4.13b}$$

$$\sum_{e=1}^{N_b} q_{a,e}\left(\sigma_{e,k_s}^+ - \sigma_{e,k_s}^-\right)\mathbf{P}\mathbf{C}_e\mathbf{x} = \mathbf{f}_{k_s}\left(\mathbf{t}^-\right), \ \forall k_s = 1, \ldots, N_s, \tag{4.13c}$$

$$\left(\sigma_{e,k}^-\right)^2 \mathbf{x}^\top \mathbf{C}_e \mathbf{x} \leq s_e^2 q_{a,e}^2, \ \forall e = 1, \ldots, N_b, \ \forall k = 1, \ldots, N_c, \tag{4.13d}$$

$$\left(\sigma_{e,k_s}^-\right)^2 \mathbf{x}^\top \mathbf{C}_e \mathbf{x} \leq s_e^2 q_{a,e}^2, \ \forall e = 1, \ldots, N_b, \ \forall k_s = 1, \ldots, N_s, \tag{4.13e}$$

$$\left(t_e^-\right)^2 \geq q_{a,e}^2 \left(\sigma_{e,k}^-\right)^2 \mathbf{x}^\top \mathbf{C}_e \mathbf{x}, \ \forall e = 1, \ldots, N_b, \ \forall k = 1, \ldots, N_c, \tag{4.13f}$$

$$\mathbf{q}_a \in \mathbb{R}_+^{N_b}, \left\{\boldsymbol{\sigma}_k^+, \boldsymbol{\sigma}_k^-\right\} \in S, \mathbf{x} \in X, \mathbf{t}^- \in \mathbb{R}_+^{N_b}, \left\{\boldsymbol{\sigma}_{k_s}^+, \boldsymbol{\sigma}_{k_s}^-\right\} \in S. \tag{4.13g}$$

Similarly to the previous chapter, formulation (4.13) is able to converge to KKT optimal solutions including melting nodes using nonlinear programming algorithms. Although the proposed formulation includes a large number of constraints, the computational process is surprisingly efficient. Indeed, the simple mathematical structure greatly simplifies the calculation of derivatives and avoids having to use adjoint methods [164]. The constraint Jacobian and the Hessian matrices are extremely sparse. Thus, features that make sparse algorithms of Section 3.3 very efficient are, here, best exploited.

4.6 Numerical examples

The following numerical examples illustrate the effects of local and nodal stability considerations on the design of simple structural frameworks. In every case, limiting tensile and compressive stresses are taken as unit. The shape of cross-sections is circular ($s_e = \pi/4$ with a unit Young's modulus). Here also, the optimization problem is performed using the interior-point method with sequential quadratic programming and trust regions in Knitro [141]. Analytical derivatives are provided and the Hessian of the Lagrangian function is computed via finite-difference at each iteration. All solutions obtained in the remainder are claimed to be locally (but not necessarily globally) optimal.

4.6.1 Three-hinged arch

The first example consists in the optimization of a two-dimensional arch. The initial ground structure is a rectangular grid of 6×1 unit modules (Fig. 4.3(a)). The neighboring nodes are connected by 31 truss members. The whole structure is pin-supported at both extremities and is subjected to downward unit loads, which are applied on the top. The position of upper nodes are optimized along the vertical direction whereas the lower free nodes could shift in both spatial directions within a bounding box of ± 2 units around their initial position.

In Fig. 4.3(b), the optimal solution without stability considerations generates an inverted hanging model in unstable equilibrium. To strengthen the arch, stability considerations are introduced. A parametric study is performed to produce the range of results depicted in Fig. 4.4. The magnitude factor α_s and the number of nominal loading cases are progressively increased. All solutions resemble a same structural typology of three-hinged arch.

The first row of results (Figs. 4.4(a)-4.4(c)) for a low intensity of nominal forces $\alpha_s = 0.02$ exhibits slender arches with weak transversal strength. Evidently, second and third rows show thicker configurations due to the higher magnitude of nominal forces. One can also observe that these truss systems are more redundant when the number of nominal loading cases increases. Nevertheless, the differences among optimal volumes – for a given α_s – are not significant, hence showing that the use of some nominal loading cases is generally sufficient to obtain satisfying results. Still, these additional loading cases must be suitably chosen for best results. Note that all results include vanishing bars with melting nodes and are obtained in less than one minute of computational time.

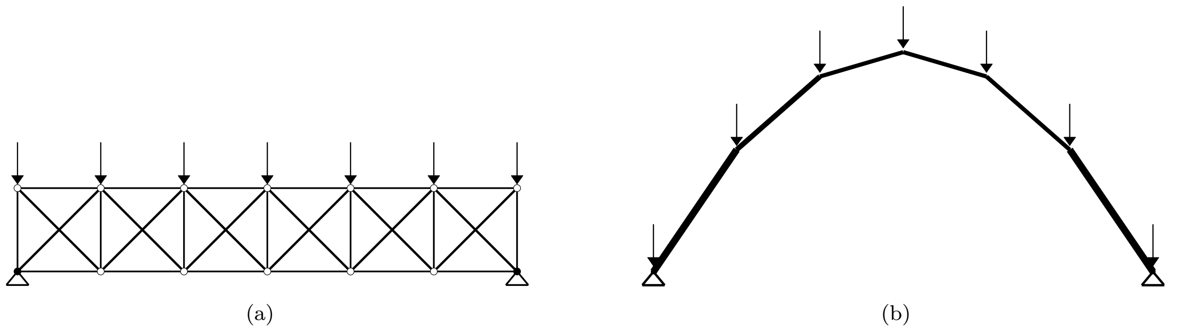

Figure 4.3: Simple arch example: (a) initial ground structure and (b) optimal solution without stability considerations, $V^* = 20.533$

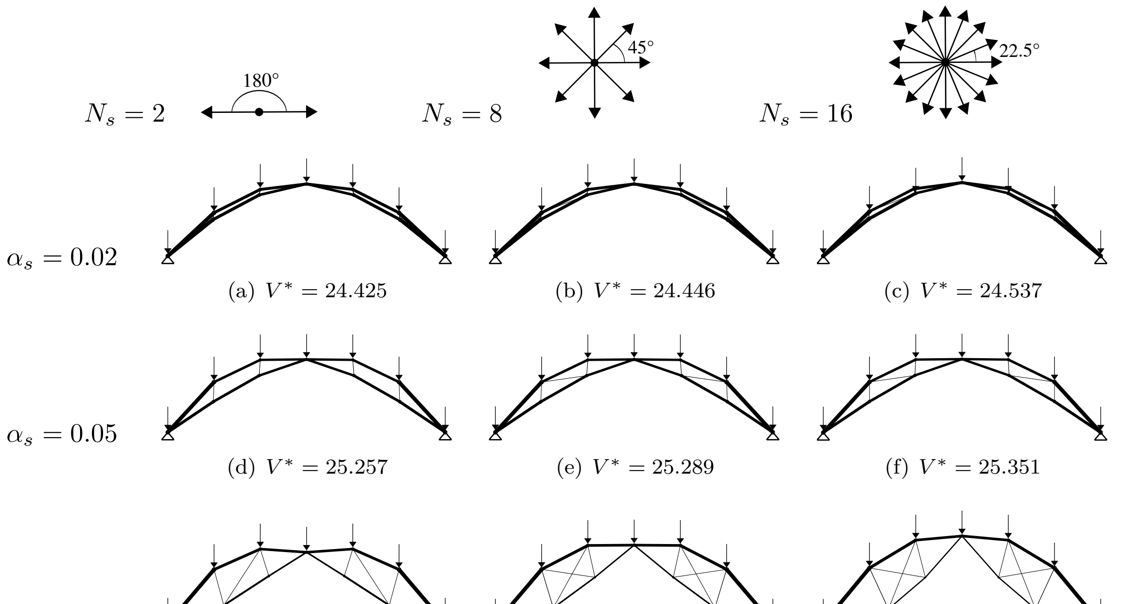

Figure 4.4: Simple arch example. The pattern of solutions obtained by increasing the magnitude of the nominal forces via the coefficient α_s (solutions from the top to the bottom) and by increasing the number of nominal loading cases N_s (solutions from the left to the right). For $N_s = 2$, the nominal loading cases are oriented every 180°. For $N_s = 8$, the nominal loading cases are oriented every 45°. For $N_s = 16$, the nominal loading cases are oriented every 22.5°.

4.6.2 L-shaped frame

The second example has been previously addressed in [145, 150] using topology optimization. The L-shaped design domain is discretized by 28 connected nodes, as shown in Fig. 4.5(a). The four upper nodes are pin-supported. Two unit loads are applied on the upper tip of the structure. Six nominal loading cases are oriented in either directions parallel to the three Cartesian axes, and $\alpha_s = 0.02$.

For comparison purpose, topology optimization with nodal stability constraints is performed. The results are depicted in Fig. 4.5(b). In this particular case, it is possible to reformulate the problem by linear programming that ensures the finding of the global minimizer, as proposed in [145]. The optimal volume $V^* = 71.510$ is slightly higher than the value $V^* = 70.398$ reported in [145]. The difference is explained by the conservative definition for the magnitude of nominal lateral forces, as discussed in Section 4.3.

Then, geometry and topology optimization is performed. The rightmost and lower nodes are defined as active nodes. The bounding box is set at $1 \times 1 \times 1$ units around each nodal position. The optimization converges to a fully stressed solution without stability consideration (Fig. 4.5(c)). The structure is a combination of two optimum trusses included in their respective plane, each one possessing a limited number of structural components. In Fig. 4.5(d), the inclusion of local and nodal stability constraints increases the optimal volume by 25.42%. The configuration is no longer a combination of two independent systems. Instead, both movable frames melt their nodes.

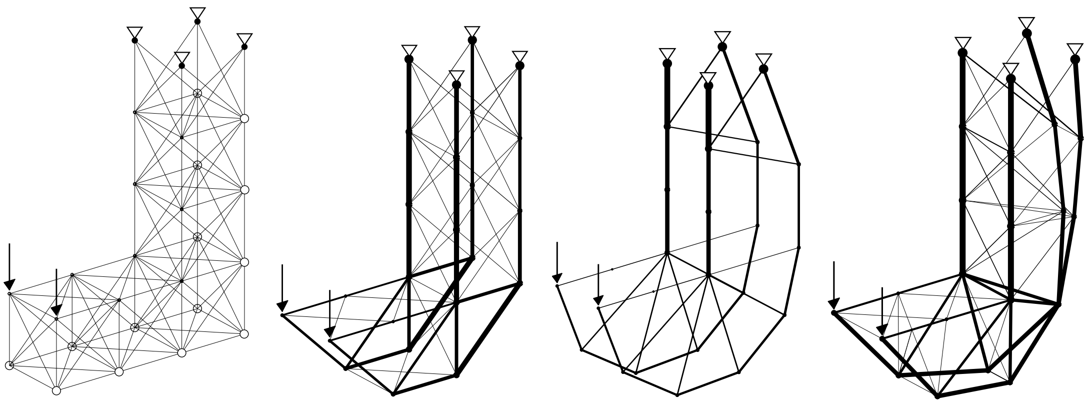

(a) (b) $V^* = 71.510$ (c) $V^* = 54.098$ (d) $V^* = 67.849$

Figure 4.5: L-shaped truss frame. The initial ground structure is given in (a) where the bold dots are the pin supports. Then, the process is performed for (b) topology optimization with nodal stability, (c) geometry and topology optimization without stability consideration, and (d) geometry and topology optimization with local and nodal stability.

4.7 Concluding remarks

In this chapter, we developed an efficient method for ensuring local and nodal stability in truss geometry and topology optimization. The novel formulation of Chapter 3 is used as basis to incorporate stability considerations. Our approach combines the nominal lateral force method with local buckling constraints. The resulting formulation permits the inclusion of compression-only members, overcomes local buckling singularity, and admits optimal geometries with melting nodes. Two simple examples exhibits the good behaviour of the method.

It turns out that the computional effort depends more on the problem complexity (i.e. the number of local optima) rather than the size of the problem. The relative influence of the intensity and the orientation of nominal forces has been illustrated. In most cases, a few number of nominal loading cases suffices to generate robust designs against nodal instability but the designer's choice about their orientation is a key issue.

The next chapter will demonstrate the applicability of the different methods developed in this thesis on several large-scale applications.

5 Structural design applications

The following series of structural design examples aims at illustrating the scope of the proposed method on realistic applications. The first problem of Section 5.1 is the design of a reticulated dome under multiple loading conditions and different constraint types. In Section 5.2, we investigate the design of a three-dimensional stabilizing system to reduce the slenderness of a column. Then, Sections 5.3 and 5.4 address the design of two different typologies of lightweight bridges, namely arch and suspension systems. Finally, Section 5.5 focuses on the design of reticulated glass dome covering the Dutch Maritime Museum. The optimization is performed by the Knitro package [141]. The interior-point algorithm is based on a sequential quadratic programming model with trust regions. The inivial value for the barrier parameter is set by default to 0.1. Analytical derivatives are provided via a sparse indexing and the Hessian-vector product of the Lagrangian function is computed via finite-difference at each iteration. Assuming a linear-elastic material, units are omitted for convenience and the solutions could be scaled after the optimization process if necessary.

5.1 Reticulated dome

The first example is the design of a reticulated dome. The initial layout is included in a circular plate and contains 912 members and 241 nodes, as shown in Fig. 5.1. The angle between two radial frames is 15° whereas a unit shift between two circles is done for a total radius of 10 units. The nodes at the outer perimeter are blocked in every spatial direction. The remaining nodes are allowed to move upwards with no restriction on the height. The structure is subject to three loading cases applied on every node: the first includes downward unit forces whereas the others have a lower magnitude of 0.2 units and are projected in the horizontal plane, in either direction of the Cartesian axes.

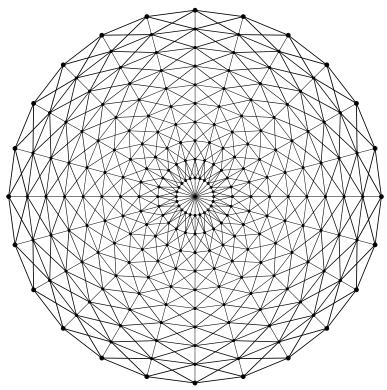

Figure 5.1: Top view of the initial ground structure for the reticulated dome

Formulations (3.9) and (3.17) are compared via a parametric study. This reveals a similar evolution of the global shape, from a dome to a cone. Although the minimum volume and weighted-average compliance problems are generally not equivalent for the multiple loading case [58], the present example suggests that some correlations might still exist, which would require further studies.

For the minimum volume problem, limiting stresses are varied with respect to the loading cases via the ratio defined as the stress limits of the first loading case over the two others, i.e. $\overline{\sigma}^{+,-}_{e,k=1}/\overline{\sigma}^{+,-}_{e,k=2,3}$ for all $e = 1, \ldots, N_b$. Low values of this ratio generate an optimal structure mainly driven by the first loading, and vice-versa (Fig. 5.2(a)-5.2(c)).
For the weighted-average compliance, the allowable volume of material is set at $\overline{V} = 1$. The weights assigned to each individual compliance are varied with respect to the loading cases. The measure is defined as the ratio of the weights corresponding to the first loading over the two others, i.e. $w_{k=1}/w_{k=2,3}$, hence giving a similar behavior to the minimum volume problem when the ratio is changed (Fig. 5.2(d)-5.2(f)).

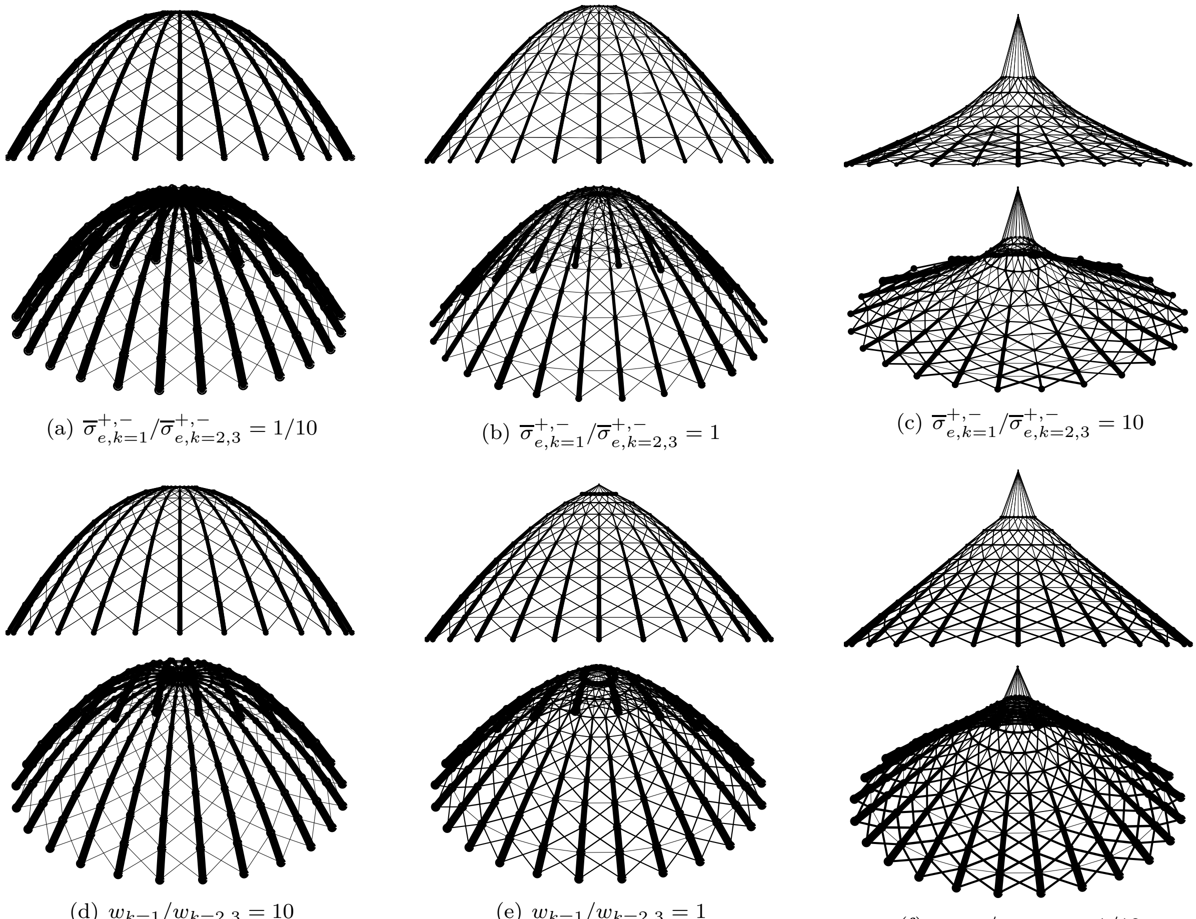

(a) $\overline{\sigma}^{+,-}_{e,k=1}/\overline{\sigma}^{+,-}_{e,k=2,3} = 1/10$ (b) $\overline{\sigma}^{+,-}_{e,k=1}/\overline{\sigma}^{+,-}_{e,k=2,3} = 1$ (c) $\overline{\sigma}^{+,-}_{e,k=1}/\overline{\sigma}^{+,-}_{e,k=2,3} = 10$

(d) $w_{k=1}/w_{k=2,3} = 10$ (e) $w_{k=1}/w_{k=2,3} = 1$ (f) $w_{k=1}/w_{k=2,3} = 1/10$

Figure 5.2: Comparison of solutions under multiple loading. In the upper row (a-c), the minimum volume problem formulation (3.9) is solved for different stress constraints with respect to the multiple loading cases. In the lower row (d-f), the minimum compliance problem formulation (3.17) is solved for different weights of individual compliance with respect to the multiple loading cases.

5.2 Lateral bracing of Winter's type column

The second example is the design of a column under compression. The goal is to reduce the buckling length by bracing the system. Using Winter's rigid bar model, the chain is subdivided in 9 elements of unit length connecting 10 nodes. The node at the bottom is pin-supported and the node on the top is restrained in the horizontal plane only.

Obviously, the structure is stable for a unit force pulling on the top. Inversely, the chain under compression is unstable and must be encompassed in a three-dimensional framework. Therefore, the ground structure is made of 30 adjacently connected nodes based on an equilateral triangle of unit side, Fig. 5.3(a). These encompassing nodes are allowed to move in the set X defined as ± 1 unit around their respective initial position. Using formulation (4.13), the nodal stability is considered through six nominal loading cases; their nominal lateral forces being oriented in either direction parallel to the three bisections of the triangle, and $\alpha_s = 0.02$.

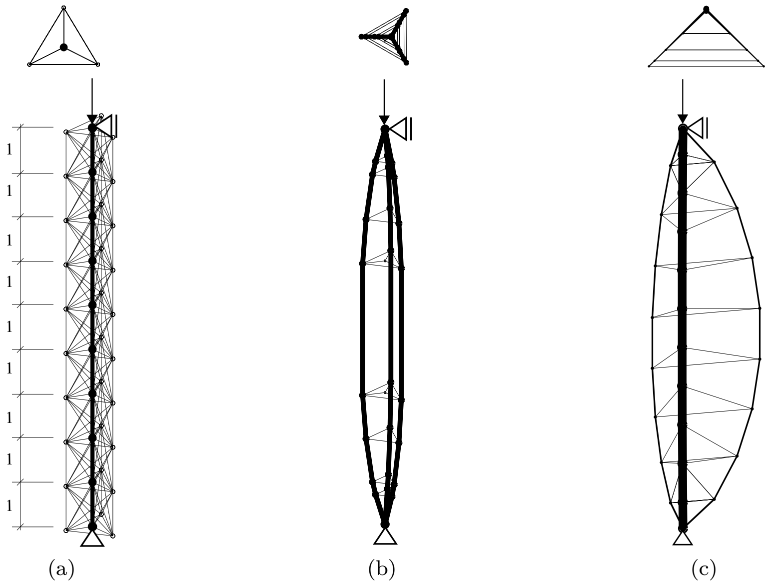

Figure 5.3: Column simply loaded on the top: (a) initial ground structure; (b) structural optimization with nodal stability, $V^* = 9.372$; (c) structural optimization with local and nodal stability, $V^* = 13.165$

In Fig. 5.3(b), the structure is first optimized without local stability constraint. Since the tensile and compressive stress constraints are the same, the number of loading cases could be reduced to three in order to save computational effort. The optimal solution is symmetrical with respect to each bisection. It is rather surprising to observe that the central chain vanishes at the benefit of the bracing-only members which actually serves a load-carrying purpose. The phenomenon is explained by the fact that the structure must resist transversally to the nominal load cases, hence generating these bracing members. Furthermore, the theoretical optimum without geometrical restrictions is one single load-bearing member of volume $V^* = 9$. To approach this optimum while enforcing constraints, the optimization algorithm would spread nodes with nominal forces towards supports since the nodes belonging to the column are fixed by the problem definition.

If the local instabilities are also considered, the optimum design significantly changes, Fig. 5.3(c). The solution is obtained in 1,032 s of process time. The structure is neither symmetric with respect to each bisection nor evolving towards a single bar anymore. The load-bearing column becomes straight due to the higher cost of structural members with active buckling constraints. Since stresses are constant along the chain, the nominal lateral loading is uniformly distributed. The addition of local buckling constraints has increased the optimal volume about 40.47%. It results in an efficient structure which is nodally stable but globally unstable, although rigid connections would ensure global stability in detailed design phases.

5.3 Arch bridge

The preliminary design of an arch bridge constitutes the third application (Fig. 5.5). The design domain is a rectangular box consisting of 60 nodes adjacently connected by 258 potential truss members (Fig. 5.5(a)). The supports are blocked in the three spatial directions and located at both extremities. The 258-bar structure is subject to downward loads of magnitude 1 applied to the lower nodes of the deck as well as a horizontal load of 0.2 perpendicular to the main axis of the bridge. All the upper nodes are allowed to move in the three spatial directions within a bounding box of size $2 \times 2 \times 10$ units around its initial position for each one.

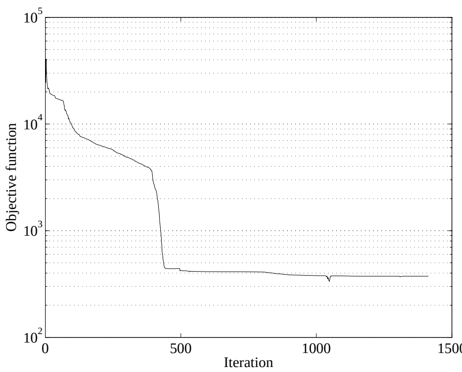

(a) Convergence history with an optimal volume $V^* = 408.807$

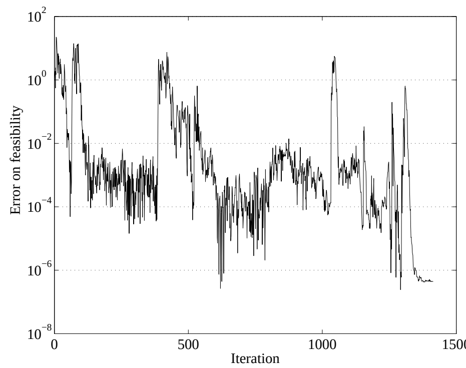

(b) The error on feasibility at the solution is 4.431e-7

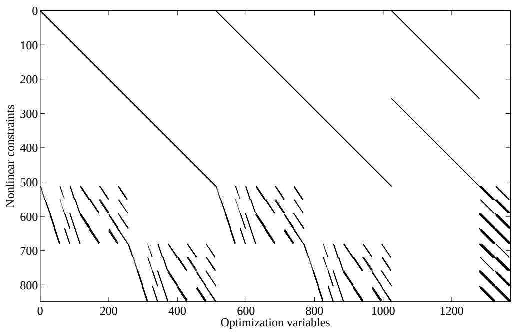

(c) Sparsity pattern of the constraint Jacobian: the number of nonzeros is 3,232 and the density is 2.787%

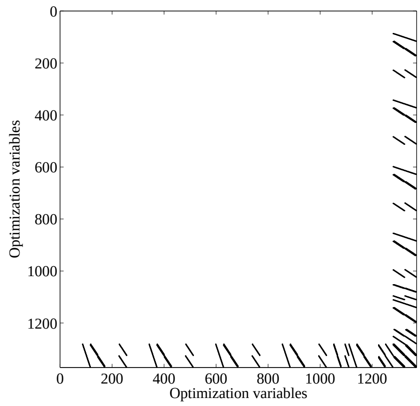

(d) Sparsity pattern of the Hessian: the number of nonzeros is 3,568 and the density is 0.978%

Figure 5.4: Information on the numerical optimization process with the convergence history (a), the feasibility history (b), the sparsity pattern for the constraint Jacobian (c) and the Hessian of the Lagrangian (d)

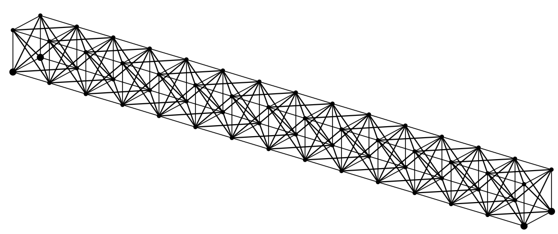

(a) Initial ground structure with supports indicated by bold dots

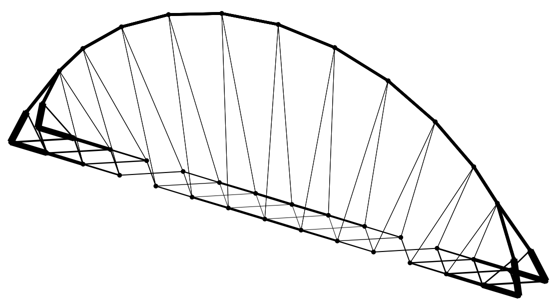

(b) Optimal structure

Figure 5.5: Geometry and topology optimization of the three-dimensional bridge structure subjected to two load cases

The optimization process is performed independently for formulations in plastic (3.10) and elastic design (3.9). Since the optimal configuration is statically determinate, the optimal solution is similar. In Fig. 5.5(b), one can observe that the geometry and topology optimization for the two load cases nicely shapes as an arch bridge. The global shape is dominated by the first load case whereas the bracing system of the deck is determined by the second one. Both upper frames merge into a single one.

The noteworthy fact is that such an optimal solution can only be obtained, without any convergence difficulty, by properly covering the melting node effect.

The overall process is relatively fast since the optimal solution is obtained in 18 min in Matlab (with a personal desktop, quad-core processor 2.67GHz and 8GiB RAM). A local minimizer satisfying the Karush-Kuhn-Tucker conditions is found after 1,414 iterations (Fig. 5.4(a)). The equilibrium constraints are enforced at the optimum with a high level of accuracy (see Fig. 5.4(b)). Obviously, these performance values are purely illustrative as the convergence speed and the solution found depends on the initial guess and the variable bounds, so that the solution might be improved.

Finally, for the plastic design formulation, note that the constraint Jacobian (Fig. 5.4(c)) and the Hessian of the Lagrangian function (Fig. 5.4(d)) are very sparse, as indicated by the very low filling density. This leads to significant memory savings.

5.4 Suspension bridge

This example addresses the preliminary shape design of a suspension bridge. This type of structural system suspends the deck to a hanging cable. An important design concern is how to determine the funicular of loads to provide a maximal overall stiffness. For straight bridges, the stiffness of the deck might be neglected at early design stages. By contrast, the interaction between the deck and the suspension system is crucial for curved bridges [13].

Let us assume a S-shaped deck inspired by the College footbridge designed by Ney&Partners (Fig. 5.6) [165]. From the top view (Fig. 5.6(c)), the deck consisted of two curved segments having a radius of 14 units connected by a straight part with a length of 22 units. The cross-section of the deck is a triangular framework made of truss members. The width and the height are set at 1.5 and 0.5 units, respectively. The deck is supported at both extremities in every spatial direction. The initial shape for the suspension system is shown in Fig. 5.6(a) (the height of the upper cable is 4 units). Two pin-supported columns are used to bear the suspension cables. A single loading condition is considered, consisting of downward unit loads acting on the upper nodes of the deck.

The plastic design formulation (3.22) is used to analyse and optimize the model. Whereas the structural members of the deck are classical truss elements, slack cables are introduced by means of a zero strength in compression ($\overline{\sigma}_e^- = 0$ for elements belonging the suspension system). The nodes lying along the suspension cable are defined as geometrical variables to achieve a funicular shape. In addition, the nodal positions of the frame under the deck are also optimized to enhance the interaction between the suspension cable, the tie-rods and the deck. Finally, the positions of the supports at the bottom of columns are also optimized in order to find an inclination able to balance the tension in the suspension system.

The resulting lightness and slenderness of the structure enhance the architectural aspect. The lower frame of the deck is smoothly curved to best comply with the equilibrium shape of the funicular cable. The supports at the bottom of columns are also modified. Given the complexity of the design problem, the computational efficiency is noteworthy since the optimal solution is obtained in less than 11 minutes CPU.

5.5 Dutch Maritime Museum

In this last example we revisit the renovation project of the Dutch Maritime Museum in Amsterdam. Built in the 17$^{\text{th}}$ century, the current historic museum is based on a square building surrounding a central courtyard. As part of the renovation project, the circulation of the building was no longer adequate to welcome visitors and has been renovated accordingly. The project's program requires to expand the circulation via the courtyard. This necessitates a minimal intervention to enclose the wide space. The winners of the competition – structural engineers and architects Ney&Partners – proposed

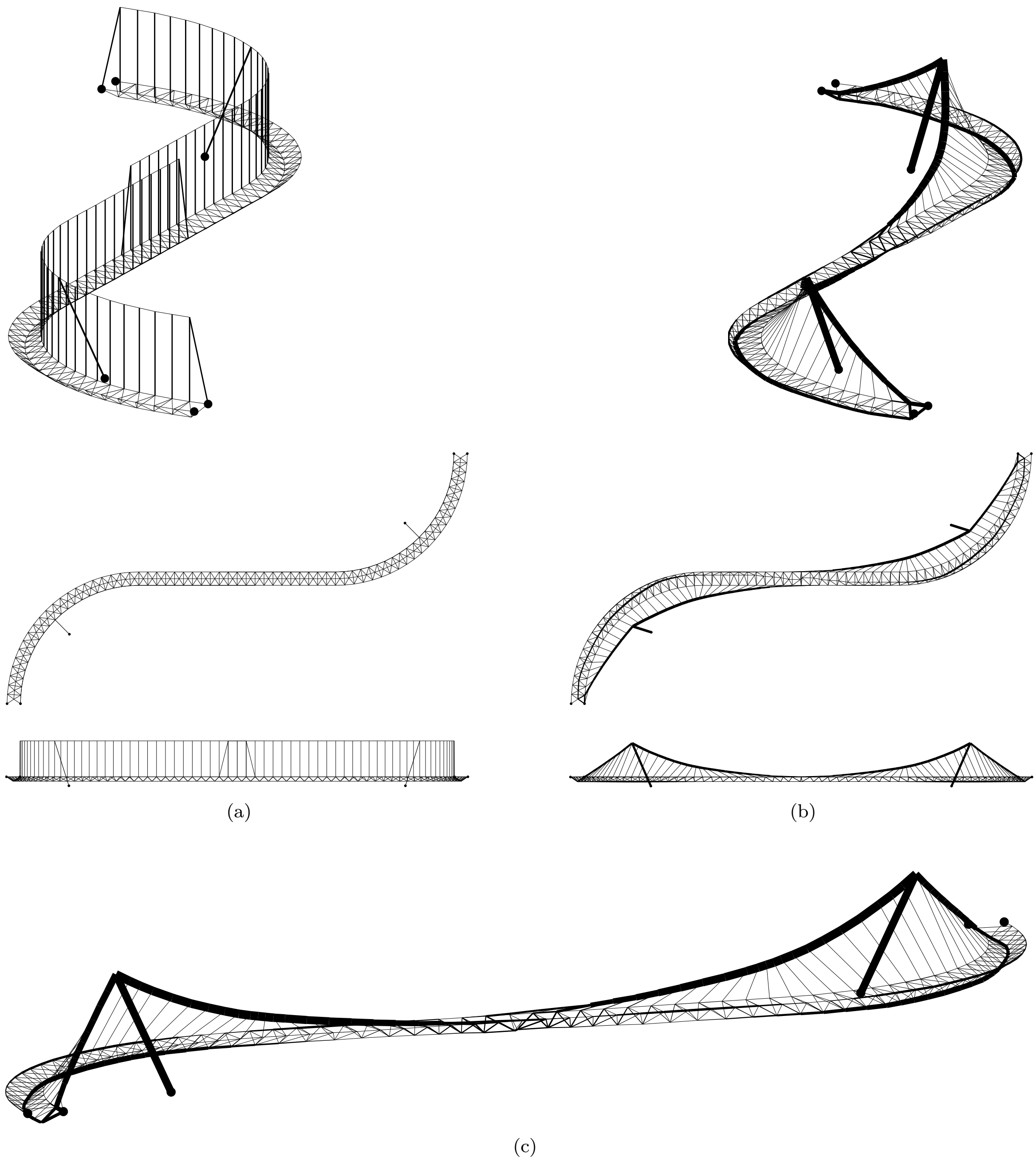

Figure 5.6: Design of a suspension footbridge. Different views of the initial configuration are given in (a). The optimal design is given in (b). An additional figure emphasizes the slenderness of the designed structure (c).

a steel glass cover. The appealing idea behind the proposal was to define the planar geometry of the steel structural mesh using a maritime map with 16 wind roses. Due to the wide span (34 m) of the courtyard, the structure is curved to behave like a dome and achieve lightness and stiffness. The boundary conditions and the technological constraints were the following [165]:

- the dome cannot appear above the historic building, thus restricting the dome's height to 4.5 m;
- except at the four corners, the façades can only carry additional vertical loads;
- the planarity of nontriangular glass elements must be enforced.

An original design satisfying these constraints has been made possible by sequentially applying dynamic relaxation for the form finding, afterwards a geometrical optimization was performed for ensuring planarity of glass elements [166, 167]. The purpose of the present investigation is to show how our formulation handles the different design issues in an integrated way, and suggests further extensions for improving the range of applications.

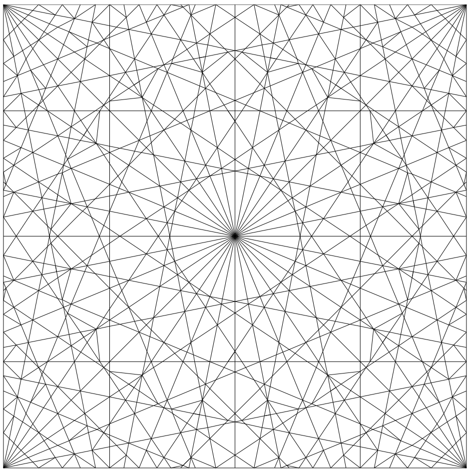

(a) Geometry of the mesh

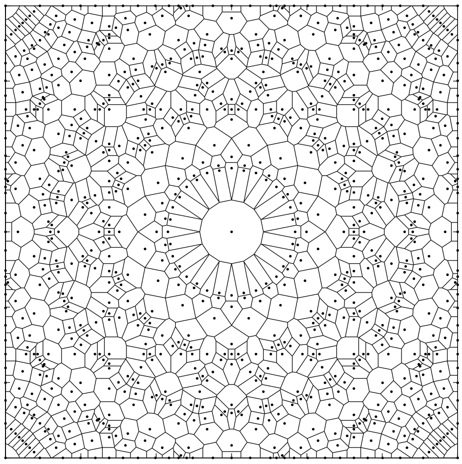

(b) Voronoi diagram

Figure 5.7: The Dutch Maritime Museum. Top view of the geometric mesh (a) and the Voronoi diagram used for distributing loads on nodes (b).

The initial ground structure is depicted in Fig. 5.7(a). The structure is subjected to a continuous loading of downward unit forces, which are distributed on nodes proportionally to the area of Voronoi's diagram depicted in Fig. 5.7(b). Given the boundary conditions imposed by the existing situation, the structure is simply supported vertically at the whole perimeter while the four corners are pin-supported.

Regarding the geometrical constraints, the imposition of a maximal height is simply carried out by bounding the geometrical variables to 4.5 units. In order to ensure the planarity of glass panels, Adriaenssens et al. [168] proposed to associate a plane $p = 1, \ldots, N_p$ to each nontriangular facet. Based on this idea, we define three plane coefficients $(\alpha_{p,1}, \alpha_{p,2}, \alpha_{p,3})$ and the set J_p of the j_p-th nodes associated to the p-th plane. The planarity and maximal height constraints are defined via the set:

$$X := \{\mathbf{x} \in \mathbb{R}^{d.N_n} \;\big|\; z_{j_p} = \alpha_{p,1} x_{j_p} + \alpha_{p,2} y_{j_p} + \alpha_{p,3},\ 0 \leq x_i \leq 4.5, \tag{5.1a}$$

$$j_p \in J_p,\ p = 1, \ldots, N_p,\ \forall i = 1, \ldots, N_d\}. \tag{5.1b}$$

To solve the design problem, we first incorporate Eq. (5.1b) into the reduced formulation for single loading case (3.22). It turns out, however, that the problem is infeasible: both planarity and equilibrium constraints are not accurately satisfied (Fig. 5.9(a)). The underlying reason of this failure is an incorrect problem statement: due to the kinematic indeterminacy of the truss model, the determination of the load-dependent shape is conflicting with the imposition of planarity constraints. Hence, a feasible solution does not exist in general. This problem motivates the development of a novel element incorporating out-of-straight forces.
Consider the original static equilibrium equations of a truss element in the expanded form (Fig. 5.8(a)):

$$\begin{bmatrix} q_{t,e,x} & 0 & 0 & -q_{t,e,x} & 0 & 0 \\ 0 & q_{t,e,x} & 0 & 0 & -q_{t,e,x} & 0 \\ 0 & 0 & q_{t,e,x} & 0 & 0 & -q_{t,e,x} \\ -q_{t,e,x} & 0 & 0 & q_{t,e,x} & 0 & 0 \\ 0 & -q_{t,e,x} & 0 & 0 & q_{t,e,x} & 0 \\ 0 & 0 & -q_{t,e,x} & 0 & 0 & q_{t,e,x} \end{bmatrix} \begin{bmatrix} x_1 \\ y_1 \\ z_1 \\ x_2 \\ y_2 \\ z_2 \end{bmatrix} = \begin{bmatrix} f_{x,1} \\ f_{y,1} \\ f_{z,1} \\ f_{x,2} \\ f_{y,2} \\ f_{z,2} \end{bmatrix}. \tag{5.2}$$

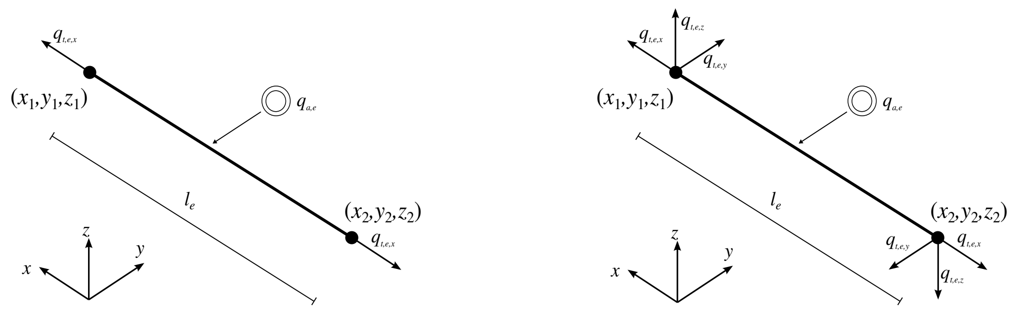

(a) Axial force density (b) Axial and shear force density

Figure 5.8: Representation of the classical truss element with axial force densities only (a) and with the addition of shear force densities (b)

As described in Section 3.3, axial force densities $q_{t,e,x} \in \mathbb{R}$ are defined as the ratio of the axial forces on the length. Now, extending the concept of force densities to shear forces gives the novel static equilibrium equations (Fig. 5.8(b)):

$$\begin{bmatrix} q_{t,e,x} & q_{t,e,y} & q_{t,e,z} & -q_{t,e,x} & -q_{t,e,y} & q_{t,e,z} \\ q_{t,e,z} & q_{t,e,x} & q_{t,e,y} & -q_{t,e,z} & -q_{t,e,x} & -q_{t,e,y} \\ q_{t,e,y} & q_{t,e,z} & q_{t,e,x} & -q_{t,e,y} & -q_{t,e,z} & -q_{t,e,x} \\ -q_{t,e,x} & -q_{t,e,y} & -q_{t,e,z} & q_{t,e,x} & q_{t,e,y} & q_{t,e,z} \\ -q_{t,e,z} & -q_{t,e,x} & -q_{t,e,y} & q_{t,e,z} & q_{t,e,x} & q_{t,e,y} \\ -q_{t,e,y} & -q_{t,e,z} & -q_{t,e,x} & q_{t,e,y} & q_{t,e,z} & q_{t,e,x} \end{bmatrix} \begin{bmatrix} x_1 \\ y_1 \\ z_1 \\ x_2 \\ y_2 \\ z_2 \end{bmatrix} = \begin{bmatrix} f_{x,1} \\ f_{y,1} \\ f_{z,1} \\ f_{x,2} \\ f_{y,2} \\ f_{z,2} \end{bmatrix}, \tag{5.3}$$

where the *shear force densities* $q_{t,e,y} \in \mathbb{R}$ and $q_{t,e,z} \in \mathbb{R}$ are defined as the ratio of shear forces on the length. This parametrization preserves the linearity of static equilibrium equations with respect to the force density variables. In a form-finding context, one could directly prescribe the force densities and solve the static equilibrium equations to obtain an equilibrium shape. In an optimization context, Eqs. (5.3) are incorporated into formulation (3.22) with the non-negative force densities for tension $q^+_{t,e,\alpha} \in \mathbb{R}_+$ and compression $q^-_{t,e,\alpha} \in \mathbb{R}_+$ for all $\alpha = 1, \ldots, d$ and $e = 1, \ldots, N_b$. The objective function is defined as a weighted sum of the form

$$\min_{\substack{\mathbf{q}^+_{t,\alpha} \in \mathbb{R}^{N_b} \\ \mathbf{q}^-_{t,\alpha} \in \mathbb{R}^{N_b} \\ \mathbf{x} \in \mathbb{R}^{d.N_n}}} \quad \sum_{\alpha=1}^{d} \sum_{e=1}^{N_b} w_\alpha \left(q^+_{t,e,\alpha} + q^-_{t,e,\alpha}\right) \mathbf{x}^\top \mathbf{C}_{e,\alpha} \mathbf{x} \tag{5.4a}$$

$$\text{s.t.:} \quad \sum_{\alpha=1}^{d} \sum_{e=1}^{N_b} \left(q^+_{t,e,\alpha} - q^-_{t,e,\alpha}\right) \mathbf{P} \mathbf{C}_{e,\alpha} \mathbf{x} = \mathbf{f}, \;\; \alpha = 1, \ldots, d, \tag{5.4b}$$

$$q^+_{t,e,\alpha} \geq 0, \;\; q^-_{t,e,\alpha} \geq 0, \;\; \mathbf{x} \in X, \;\; \forall e = 1, \ldots, N_b, \;\; \alpha = 1, \ldots, d. \tag{5.4c}$$

where $\mathbf{C}_{e,\alpha} \in \mathbb{R}^{d.N_n \times d.N_n}$ is a symmetric, positive-semidefinite assembly matrix containing exactly d^3 non-zero entries of ± 1. The imposition of different weights $w_\alpha \in [0, 1]$ for axial and shear components determines the cost associated to each force direction to design the structure: a very low value for $q_{t,e,x}$ generates a structure mainly subjected to traction/compression forces, and vice-versa.

Applying formulation (5.4) for the design of the Dutch Maritime Museum is found to be successful. The overall problem includes 15,345 variables and 4,043 equality constraints. Despite its large size, a local optimum is reached in less than an hour. Both planarity and equilibrium constraints are satisfied within a given tolerance of 10^{-5}, thus clearly below fabrication tolerances (Fig. 5.9(b)). The optimal design is depicted in Fig. 5.10(b). The important beams on the perimeter balance the buttresses of the dome-like structure.

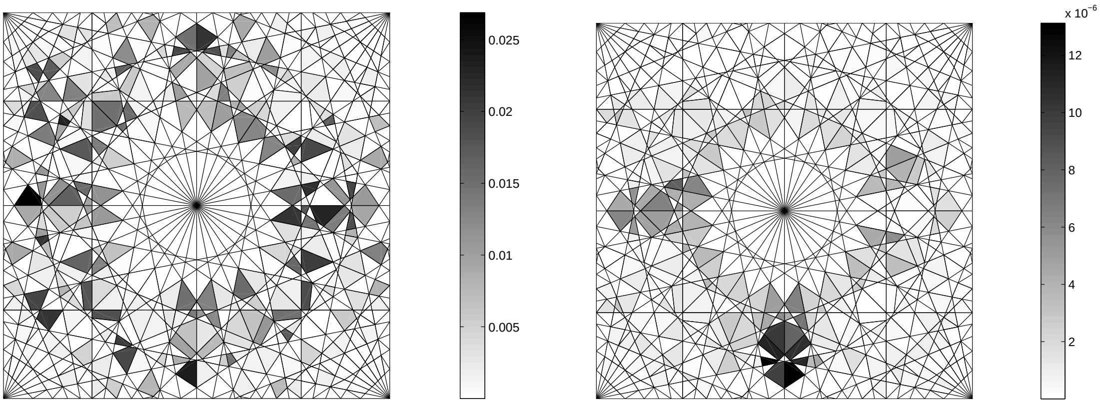

(a) Using formulation (3.22)

(b) Using formulation (5.4)

Figure 5.9: Planarity error for the optimal structure with two different formulations

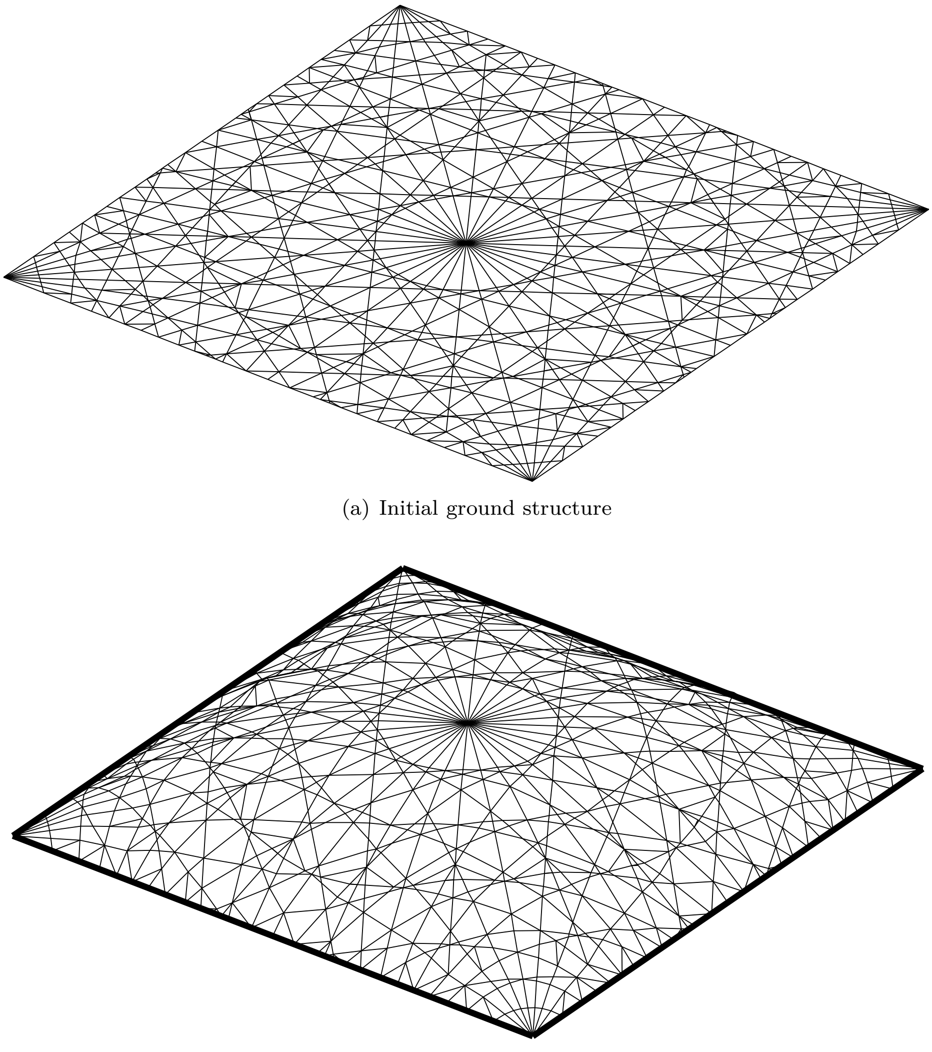

(a) Initial ground structure

(b) Optimal design

Figure 5.10: Perspective view of the steel glass dome covering the Dutch Maritime Museum

6 Conclusions and future prospects

The aim of the research is the development of a computational method for the preliminary shape design of lightweight structures made of discrete components. Our investigations led to the conceptual framework of truss layout optimization. Although previously proposed methods mostly focused on topology optimization, the shaping process of lightweight structures requires the optimization of geometrical variables as well. Furthermore, the treatment of equilibrium is of prominent issue for these structures. As such, the method developed in this dissertation stands at midway between form finding and structural optimization.

To enable large-scale applications, we investigate the mathematical programming framework. Still, *truss geometry and topology optimization* is prone to numerical difficulties for the following reasons: the possibility of finding an equilibrium state highly depends on the structural shape (which may contain mechanisms), and the structural layout is modified during the design process (due to vanishing bars, melting nodes, etc.). Consequently, standard constraint qualifications of mathematical programming – which are required for the convergence of nonlinear programming algorithms – are often violated. The present work collects and identifies the different singularities to enables a global understanding of the computational challenges:

- *Stress singularity* occurs in topology optimization of redundant systems. For some vanishing members, there are situations in which stress constraints and compatibility condition might not be satisfied simultaneously. Such an optimum is located in a degenerate subregion of the feasible design space.

- *Local buckling singularity* closely resembles stress singularity, although the problem is actually worse since the degenerate subspace is disconnected from the feasible region and thus unattainable by an interior path.

- *Melting node effect* occurs when the length of some members vanishes due to the melting of their truss end nodes. The geometrical configurations are frequently optimal but correspond to non-differentiable points in the design space.

Commonly accepted approaches to alleviate these singularities use either regularization techniques or work-around constraints of the critical region, although often resulting in non-optimal solutions. By contrast, our strategy recasts the conventional nested formulations via a simultaneous analysis and design approach. Since the displacement formulation is not flexible enough, the system has been disaggregated into static equilibrium, compatibility, and constitutive equations. This operation enables to reformulate the problem through a novel set of parameters.

Inspired by the parametrization of form-finding methods – in particular, the force density method – we develop a unified formulation for truss geometry and topology optimization that incorporates stress and displacement constraints, as well as member self-weight and multiple loading. For the minimum volume, the proposed formulation in elastic design provides a general basis which can reduce to plastic design for computational efficiency. For the minimum compliance problem, the principle of minimum complementary energy allows us to find the actual stress state without the compatibility

Formulation	Eq.	Compatibility	Multiload	Self-weight	Stress	Displ.	Stability
Elastic volume	(3.9)	✓	✓	✓	✓	✓	–
Plastic volume	(3.10)	–	✓	✓	✓	–	–
Weighted compliance	(3.17)	✓	✓	✓	✓	–	–
Worst compliance	(3.20)	✓	✓	✓	✓	–	–
Reduced formulation	(3.22)	✓	–	–	✓	–	–
Nominal lateral force	(4.13)	–	✓	✓	✓	–	✓

Table 6.1: Design features of formulations that have been developed in the thesis

condition. Hence, the weighted-average and the worst-case compliance problem formations have a simple mathematical structure. Finally, volume and compliance problems are merged into a compact formulation for the single loading case. A thorough study of nonlinear programming algorithms demonstrates that combining the interior-point method with sequential quadratic programming and trust regions performs best. The application to several numerical examples also emphasizes similarities and differences among the proposed formulations and design settings.

Stability issues considerably impacts the design of lightweight structures. Thus, the second part of this work considers the incorporation of local and nodal stability constraints. A brief review of the literature shows that a convenient approach to state the basic problem of truss geometry and topology optimization is based on plastic design. To ensure nodal stability, the nominal force method is adapted for incorporating geometrical variations. The local buckling criterion is in turn reformulated to include geometrical variables. The resulting strategy to ensure stability (a) braces the nodes connecting compression members, (b) permits the presence of bracing-only members, (c) allows the incorporation of local buckling constraints, (d) is computationally efficient. Although global elastic stability is not considered, one can reasonably assume that the optimal solutions are excellent candidates for the preliminary design. Numerical examples demonstrate the efficiency and the design possibilities of the proposed method for the preliminary design of lightweight structures.

Finally, the practical applicability of the present method is demonstrated on several realistic applications. They also show how geometry and topology issues can be merged into an elegant and versatile design approach. We emphasize on the capability of the present method to incorporate additional project constraints such as the planarity constraints of the quadrangular glass panels covering the Dutch Maritime Museum courtyard. For this latter project, an extension of the method to out-of-plane force elements is suggested.

A summary of proposed formulations is reported in Table 6.1. From the designer's point of view, the present method allows for stating the design problem in terms of objective and constraints. Compared to form finding methods, the imposition of values for tricky variables like the force densities is no longer necessary. Instead, bounds on optimization variables are prescribed and the optimization algorithm does the job. In general, large bounds can be arbitrarily prescribed without affecting the convergence, except for permissible nodal positions which greatly influence the optimal solution. The most demanding task when dealing with our method is a strong knowledge about structural design: if the problem statement (including the building of an initial design) is infeasible, no matter efficient the optimization algorithm is, no solution can be found.

Although our method provides a strong basis for truss geometry and topology optimization, there are still room for improvements and future works:

- One of the most promising axis of research is probably the development of *out-of-plane* force elements to enhance the feasibility of design projects with complex geometrical constraints. As demonstrated in the Maritime Museum application, the presence of specific boundary conditions together with geometrical constraints may require a slight bending stiffness of structural members to ensure the existence of a solution [168]. Our approach suggests that a suitable formulation can be achieved by defining a "shear density" variable as the ratio of the shear force on the length.

- The *natural force density* method proposed by Pauletti and Pimenta [169] for the form finding of lightweight structures unifies both truss and membrane element formulations. The mathematical structure of the equilibrium equations is extremely useful in view of combining with the present optimization method. Preliminary works on the topic are promising. At the present time, the remaining issue is the study of optimality conditions to devise an efficient implementation. Applications range shape and thickness optimization of metal sheet and thin-shell structures.

- Regarding *stability* issues, truss geometry and topology optimization can be extended to ensure global elastic stability of structural framework [150]. A consistent approach would be to consider the linear buckling model, but the singularities associated with those inequality constraints remain unsolved at the present time [152]. To solve this problem, we recommend to disaggregate the global stability constraints as for equilibrium equations. Alternatively, robust design optimization can be investigated within the framework of simultaneous analysis and design.

- The *dynamic* behavior of lightweight structures is another important concern. Although a structure designed for maximal stiffness and stability is supposed to be less sensitive to low frequencies encountered in construction, the self-weight repartition may strongly influence the dynamic response of the structural system. Hence, the imposition of eigenfrequency constraints certainly constitutes a contribution for truss geometry and topology optimization [143], although the necessity of assessing the dynamic behavior at early design stages is an open debate.

- Our numerical experiments also give rise to several theoretical considerations about the different design settings. In the literature, the relation between volume and compliance optimization for the multiple loading case is currently investigated in a topology optimization context [58, 62]. Without formal proof, we have demonstrated that a certain correlation might be established. This work should be pursued to extract properties which can be further used to improve computational procedures.

- Finally, the proposed method essentially works with continuous variables. To use a finite number of standard section profiles for structural components, the elastic and plastic design formulations can also be used for devising formulations with discrete variables using branch-and-bounds [170, 171]. The lower and upper-bounds solutions of the present work provide the necessary tools in that regard.

A Appendices

A.1 Structural form-finding methods

In 1760, Joseph-Louis Lagrange studied one of the most famous shape optimization problem: Plateau's problem. Named after the soap film experimented later by Joseph Plateau, the differential geometry problem of minimizing the surface area within boundaries is mechanically equivalent to finding an equilibrium surface with an isotropic stress field. This methodological idea may support the development of structural *form finding* for lightweight systems.

In general, structural form-finding methods relies on the prescription of the internal stress state to obtain an equilibrium shape by solving the equilibrium equations. However, Haber and Abel [172,173] pointed out that a stress field cannot be imposed in any situation, and thus prefer the term *initial equilibrium problem*. The literature covering structural form finding by computational methods traces back to the early 1970's. Due to the large number of publications, this section is limited to the most important methods (more details can be found in the comprehensive overview [174]).

Originally applied to cable-net structures, the *force density* method has been first proposed by Linkwitz and Scheck [117, 175, 176]. This material-free method is based on the definition of a force-to-length ratio called force density. By doing so, the system of static equilibrium equation becomes linear with respect to the force densities and can be directly solved by linear algebra routines to obtain the equilibrium geometry. The method has been extended to the case of membrane elements with the surface stress density method [177]. However, the method becomes iterative. Later, Pauletti and Pimenta [169] succeeds in recovering a linear expression with the natural force density method, which unifies both truss and membrane formulations. Derived from continuum mechanics, the update reference strategy can be viewed as a general case of the force density method [178–180]. Several variants also applies to the form finding of tensegrity systems [181, 182]. Self-weight loads are considered in [183]. It has been shown that all these methods share common geometric functional [184, 185].

In parallel, Day [186] first proposed another explicit method for form finding called *dynamic relaxation*. Unlike Newton-based iterative procedures, the form-finding process solves an equivalent dynamic equilibrium problem by means of step-by-step time increments to arrive at a steady-state solution. The numerical process has been improved several times (also in nonlinear analysis), e.g. [187–193]. Besides, dynamic relaxation has been extended to accommodate membrane, bending, and torsion elements [194, 195]. This method is thus ideal for designing bending-active structures like gridshell.

One should also mention the thrust network analysis which is a graphical method for finding equilibrium solution in compression-only systems [23]. This intuitive method allows to visualize the polygon of forces for three-dimensional systems through reciprocal relation between primal and dual grids. Finally, the particle-spring system closely resembles hanging-chain models by introducing masses on the nodes that are connected by elastic springs [184].

A.2 Metaheuristics for truss design

Metaheuristics are general-purpose optimization algorithms. With very limited a priori knowledge, they apply stochastic rules to iteratively converge toward an optimal solution. In theory, they would be able to reach the global optimum; yet, there is no guarantee of finding it. But their robustness on a broad range of problems substitutes for the high performance of gradient-based algorithms. Albeit computationally demanding, they have shown their effectiveness in countless structural design problems. Their two major characteristics are intensification and diversification: while the former means concentrating efforts in the neighborhood of the current solution, the latter tends to widely explore the design space. In the sequel, we briefly describe some of their applications in truss design. Due to their widespread availability, the enumeration is by no means comprehensive and mainly focuses on recent investigations.

The class of trajectory-based metaheuristics assigns a single agent to run through the design space. Starting from an arbitrary initial location, these intensification techniques evaluate several directions at each iteration; a downhill solution is always accepted, while uphill solutions are considered with a certain probability in order to avoid getting stuck in local optima. Independently proposed by Kirkpatrick et al. [196] and Černỳ [197], the most popular and powerful is probably the simulated annealing: it relies on the analogy between the cooling process toward a minimal state energy and the convergence toward the global optimum. The method is originally developed for combinatorial problems, but recent investigations in truss design have demonstrated its applicability to sizing optimization problems with discrete [198] and continuous variables [199], as well as in mixed sizing, shape, and topology optimization [200]. Nevertheless, driving parameters must be set carefully. The tabu search [201, 202] is another interesting algorithm that looks at a better solution around the current point while keeping track (using a taboo list) of visited regions in the design space. The algorithm is best suited for local search in combinatorial problems, thus preferably hybridized with more exploratory algorithms in structural design problems [203].

Using several agents rather than a single one, population-based metaheuristics serve for exploration purposes. By observation of natural systems, the process suggests improving a group by promoting interaction between agents. According to the famous holistic expression "the whole is better than the sum of its parts" , natural systems are viewed as a unit. Hence, treating them solely in terms of individuals is meaningless. Some nature-inspired methods mimic the social behavior of living species. They postulate that better solutions can be found using swarm intelligence rather than those from a single agent. The particle swarm optimization algorithm imitates the social behavior of birds in a flock. The algorithm shows good performance for large truss optimization problems [204, 205]. Similarly, [206] first proposed the ant colony optimization that simulates the search for the shortest path to food by ant colonies. Due to the discrete nature of the algorithm, sizing optimization with discrete sections has been investigated [207, 208]. Similarly, the bee algorithm is a metaphor of the foraging of bees and has been applied to sizing optimization with continuous design variables [209]. Also, more recent developments in the field are concerned with bat algorithms [210], firefly algorithms [211], and cuckoo search algorithms [212,213], all of which have successfully been applied to numerous analytical structural optimization cases. Further investigations would be concerned with large-scale truss design.

The family of evolutionary algorithms – which encompasses genetic algorithms, genetic programming, evolution strategy, and evolutionary programming – is inspired by the natural evolution of biological species. For a good overview, the interested reader is referred to [214, 215]. These algorithms are the most popular class of metaheuristics up to now and have been used in many research fields. In particular, genetic algorithms have been widely applied to truss optimization with respect to sizing, geometry, and topology, including mixed variables [216]. A few publications have been reported regarding evolutionary strategies for truss design because of the continuous nature of the algorithm [217].

Finally, a worthwhile reading would be [218]. It compares several well-known algorithms in the case of continuous sizing optimization of truss structures. It follows from this study that simulated annealing and evolutionary strategy work best. However, it is well known that the efficiency of metaheuristics is highly related to the implementation issues. Because metaheuristics disregards the mathematical properties of the problem to be optimized, their performances are limited to applications of moderate size (typically 50-100 design variables).

A.3 Example of implementation

In the following, we give an example of implementation for the lower-bound formulation (3.10) of the minimum volume problem in plastic design. For conveniency, we apply the variable change $q_{t,e,k} = q^+_{t,e,k} - q^-_{t,e,k}$. From that, formulation (3.10) becomes (neglecting self-weight):

$$\min_{\substack{\mathbf{q}_a \in \mathbb{R}^{N_b} \\ \mathbf{q}^+_{t,k} \in \mathbb{R}^{N_b} \\ \mathbf{q}^-_{t,k} \in \mathbb{R}^{N_b} \\ \mathbf{x} \in \mathbb{R}^{d.N_n}}} \quad \sum_{e=1}^{N_b} v_e\left(\mathbf{q}_a, \mathbf{x}\right) \tag{A.1a}$$

$$\text{s.t.:} \quad \sum_{e=1}^{N_b} \left(q^+_{t,e,k} - q^-_{t,e,k}\right) \mathbf{P}\mathbf{C}_e\mathbf{x} = \mathbf{f}_k,\ \forall k = 1,\ldots,N_c, \tag{A.1b}$$

$$\frac{q^+_{t,e,k}}{\overline{\sigma}^+_{e,k}} + \frac{q^-_{t,e,k}}{\overline{\sigma}^-_{e,k}} \leq q_{a,e},\ \forall e = 1,\ldots,N_b,\ \forall k = 1,\ldots,N_c, \tag{A.1c}$$

$$q_{a,e} \geq 0,\ q^+_{t,e,k} \geq 0,\ q^-_{t,e,k} \geq 0,\ \mathbf{x} \in X,\ \forall e = 1,\ldots,N_b,\ \forall k = 1,\ldots,N_c. \tag{A.1d}$$

Now let $\mathbf{z} \in \mathbb{R}^{N_z}$ be the vector collecting the optimization variables. The first derivatives of the total volume $V \in \mathbb{R}_+$ with respect to $\mathbf{z}$ are given by

$$\nabla_{\mathbf{z}} V = \left[\nabla_{q_{a,e}} V \quad \nabla_{q^+_{t,e,k}} V \quad \nabla_{q^-_{t,e,k}} V \quad \nabla_{x_i} V\right]^T \tag{A.2}$$

where the non-zero terms are

$$\nabla_{q^+_{a,e}} V = \mathbf{x}^T \mathbf{C}_e \mathbf{x},\ \forall e = 1,\ldots,N_b, \tag{A.3a}$$

$$\nabla_{x_i} V = 2\sum_{e=1}^{N_b} q_{a,e}\mathbf{x}^T \mathbf{C}_e \nabla_{x_i}\mathbf{x},\ \forall i = 1,\ldots,d.N_n. \tag{A.3b}$$

The Jacobian matrix of the equilibrium constraints $\mathbf{h}_k \in \mathbb{R}^{N_h}$ is given by

$$\nabla_{\mathbf{z}} \mathbf{h}_k = \left[\nabla_{q_{a,e}} \mathbf{h}_k \quad \nabla_{q^+_{t,e,k}} \mathbf{h}_k \quad \nabla_{q^-_{t,e,k}} \mathbf{h}_k \quad \nabla_{x_i} \mathbf{h}_k\right]^T \tag{A.4}$$

where the non-zero terms are

$$\nabla_{q^+_{t,e,k}} \mathbf{h}_k = \mathbf{P}\mathbf{C}_e\mathbf{x},\ \forall e = 1,\ldots,N_b,\ \forall k = 1,\ldots,N_c, \tag{A.5a}$$

$$\nabla_{q^-_{t,e,k}} \mathbf{h}_k = -\mathbf{P}\mathbf{C}_e\mathbf{x},\ \forall e = 1,\ldots,N_b,\ \forall k = 1,\ldots,N_c, \tag{A.5b}$$

$$\nabla_{x_i} \mathbf{h}_k = \sum_{e=1}^{N_b} \left(q^+_{t,e,k} - q^-_{t,e,k}\right) \mathbf{P}\mathbf{C}_e \nabla_{x_i}\mathbf{x},\ \forall i = 1,\ldots,d.N_n,\ \forall k = 1,\ldots,N_c. \tag{A.5c}$$

The Jacobian matrix of the stress constraints $\mathbf{g}_k \in \mathbb{R}^{N_g}$ is given by

$$\nabla_{\mathbf{z}}\mathbf{g}_k = \begin{bmatrix} \nabla_{q_{a,e}}\mathbf{g}_k & \nabla_{q^+_{t,e,k}}\mathbf{g}_k & \nabla_{q^-_{t,e,k}}\mathbf{g}_k & \nabla_{x_i}\mathbf{g}_k \end{bmatrix}^T \tag{A.6a}$$

where the non-zero terms are

$$\nabla_{q_{a,e}} g_{e,k} = -1,\ \forall e = 1, \ldots, N_b,\ \forall k = 1, \ldots, N_c, \tag{A.7}$$

$$\nabla_{q^+_{t,e,k}} g_{e,k} = \frac{1}{\overline{\sigma}^+_{e,k}},\ \forall e = 1, \ldots, N_b,\ \forall k = 1, \ldots, N_c, \tag{A.8}$$

$$\nabla_{q^-_{t,e,k}} g_{e,k} = \frac{1}{\overline{\sigma}^-_{e,k}},\ \forall e = 1, \ldots, N_b,\ \forall k = 1, \ldots, N_c. \tag{A.9}$$

The Hessian of the Lagrangian function (3.25) is given by

$$\nabla^2_{\mathbf{zz}}\mathcal{L}(\mathbf{z}) = \begin{bmatrix} \nabla^2_{\mathbf{q}_a\mathbf{q}_a}\mathcal{L} & \nabla^2_{\mathbf{q}_a\mathbf{q}^+_t}\mathcal{L} & \nabla^2_{\mathbf{q}_a\mathbf{q}^-_t}\mathcal{L} & \nabla^2_{\mathbf{q}_a\mathbf{x}}\mathcal{L} \\ & \nabla^2_{\mathbf{q}^+_t\mathbf{q}^+_t}\mathcal{L} & \nabla^2_{\mathbf{q}^+_t\mathbf{q}^-_t}\mathcal{L} & \nabla^2_{\mathbf{q}^+_t\mathbf{x}}\mathcal{L} \\ & & \nabla^2_{\mathbf{q}^-_t\mathbf{q}^-_t}\mathcal{L} & \nabla^2_{\mathbf{q}^-_t\mathbf{x}}\mathcal{L} \\ \text{sym.} & & & \nabla^2_{\mathbf{xx}}\mathcal{L} \end{bmatrix} \tag{A.10}$$

where the non-zero terms of the second-order derivatives of the volume function are

$$\nabla^2_{q_{a,e}x_i} V = 2\mathbf{x}^T\mathbf{C}_e\nabla_{x_i}\mathbf{x},\ \forall e = 1, \ldots, N_b,\ \forall i = 1, \ldots, d.N_n, \tag{A.11a}$$

$$\nabla^2_{x_ix_j} V = 2\sum_{e=1}^{N_b} q_{a,e}\nabla_{x_i}\mathbf{x}^T\mathbf{C}_e\nabla_{x_j}\mathbf{x},\ \forall i = 1, \ldots, d.N_n,\ \forall j = 1, \ldots, d.N_n, \tag{A.11b}$$

and the non-zero terms of the second-order derivatives of the equilibrium constraints are

$$\nabla^2_{q^+_{t,e,k}x_i}\mathbf{h}_k = \mathbf{P}\mathbf{C}_e\nabla_{x_i}\mathbf{x},\ \forall e = 1, \ldots, N_b,\ \forall i = 1, \ldots, d.N_n,\ \forall k = 1, \ldots, N_c, \tag{A.12a}$$

$$\nabla^2_{q^-_{t,e,k}x_i}\mathbf{h}_k = -\mathbf{P}\mathbf{C}_e\nabla_{x_i}\mathbf{x},\ \forall e = 1, \ldots, N_b,\ \forall i = 1, \ldots, d.N_n,\ \forall k = 1, \ldots, N_c. \tag{A.12b}$$

Related publications

Chapter in books

B. Descamps and R. Filomeno Coelho, *Graph theory in evolutionary truss design optimization*, pp. 241–268. Metaheuristic Applications in Structures and Infrastructures, Elsevier B.V., 2013.

Articles in international journals

B. Descamps and R. Filomeno Coelho, "The nominal force method for truss geometry and topology optimization incorporating stability considerations," *International Journal of Solids and Structures*, 2013, *submitted*.

B. Descamps and R. Filomeno Coelho, "A unified formulation for truss geometry and topology optimization covering elastic and plastic design," *Structural and Multidisciplinary Optimization*, 2013, *submitted*.

B. Descamps and R. Filomeno Coelho, "A lower-bound formulation for the geometry and topology optimization of truss structures under multiple loading," *Structural and Multidisciplinary Optimization*, vol. 48, pp. 49–58, 2013.

B. Descamps, R. Filomeno Coelho, L. Ney, and Ph. Bouillard, "Multicriteria optimization of lightweight bridge structures with a constrained force density method," *Computers and Structures*, vol. 89, pp. 277–284, 2011.

Conferences with proceedings

B. Descamps and R. Filomeno Coelho, "Shape and topology optimization for the stress-based truss design under multiple loading," in *3rd International Conference on Engineering Optimization (EngOpt 2012)*, (Rio de Janeiro, Brazil), 2012.

B. Descamps and R. Filomeno Coelho, "A simultaneous analysis and design formulation for the shape and topology optimization of large-scale trusses," in *10th World Congress on Computational Mechanics (WCCM X)*, (São Paulo, Brazil), 2012.

B. Descamps, Ph. Bouillard, L. Ney, and R. Filomeno Coelho, "The principia design method for the form finding and optimization of truss grids," in *Proceedings of the IABSE-IASS symposium*, (London, UK), 2011.

B. Descamps, Ph. Bouillard, and R. Filomeno Coelho, "Recherche d'équilibre et d'optimalité au travers d'un process de conception intégrée," in *Entretiens avec Jürg Conzett*, (Louvain-La-Neuve, Belgium), 2011.

B. Descamps, Ph. Bouillard, L. Ney, and R. Filomeno Coelho, "Shape and topology optimization of space structures by the force density method and hybrid genetic algorithms," in *Proceedings of the IASS symposium*, (Shanghai, China), 2010.

Bibliography

[1] G. S. Kang and A. Kren, "Structural Engineering Strategies Towards Sustainable Design," tech. rep., SEAONC Sustainable Design Committee, 2007.

[2] A. Eriksson and A. Gunnar Tibert, "Redundant and force-differentiated systems in engineering and nature," *Computer Methods in Applied Mechanics and Engineering*, vol. 195, pp. 5437–5453, 2006.

[3] W. J. Lewis, *Tension Structures*. London: Thomas Telford, 2003.

[4] M. Kawaguchi, "The Lighter, the Better?," in *Proceedings of the IABSE-IASS Symposium*, (London, UK), pp. 18–25, 2011.

[5] E. Hines and D. P. Billington, "Anton Tedesko and the Introduction of Thin Shell Concrete Roofs in the United States," *Journal of Structural Engineering (ASCE)*, vol. 130, pp. 1639–1650, 2004.

[6] M. E. Moreira Garlock and D. P. Billington, *Static and Dynamic Analysis of Structures*. Princeton: Yale University Press, 2008.

[7] M. E. M. Garlock and D. P. Billington, *The Art of Structural Design: A Swiss Legacy*. New Haven: Yale University Press, 2003.

[8] B. Espion and P. Halleux, "Contributions of André Paduart to the art of thin concrete shell vaulting," in *First International Congress on Construction History, Madrid*, pp. 829–838, 2003.

[9] F. Otto and B. Rasch, *Finding Form: Towards an Architecture of the Minimal*. Berlin: Axel Menges, 1996.

[10] B. Descamps, Ph. Bouillard, and R. Filomeno Coelho, "Recherche d'équilibre et d'optimalité au travers d'un process de conception intégrée," in *Entretiens avec Jürg Conzett*, (Louvain-La-Neuve, Belgium), 2011.

[11] J. Y. Zhang, M. Ohsaki, and Y. Kanno, "A direct approach to design of geometry and forces of tensegrity systems," *International Journal of Solids and Structures*, vol. 43, pp. 2260–2278, 2006.

[12] B. Descamps, Ph. Bouillard, L. Ney, and R. Filomeno Coelho, "Shape and topology optimization of space structures by the force density method and hybrid genetic algorithms," in *Proceedings of the IASS symposium, Shanghai, China*, 2010.

[13] B. Descamps, R. Filomeno Coelho, L. Ney, and Ph. Bouillard, "Multicriteria optimization of lightweight bridge structures with a constrained force density method," *Computers and Structures*, vol. 89, pp. 277–284, 2011.

[14] J. N. Richardson, S. Adriaenssens, R. Filomeno Coelho, and Ph. Bouillard, "Coupled form finding and grid optimization approach for single layer grid shells," *Engineering Structures*, vol. 52, pp. 230–239, 2013.

[15] M. Quagliaroli and P. G. Malerba, "Flexible bridge decks suspended by cable nets. A constrained form finding approach," *International Journal of Solids and Structures*, vol. 50, pp. 2340–2352, 2013.

[16] J. N. Richardson, S. Adriaenssens, Ph. Bouillard, and R. Filomeno Coelho, "Multiobjective topology optimization of truss structures with kinematic stability repair," *Structural and Multidisciplinary Optimization*, vol. 46, pp. 513–532, 2012.

[17] B. Descamps and R. Filomeno Coelho, *Graph theory in evolutionary truss design optimization*, pp. 241–268. Metaheuristic Applications in Structures and Infrastructures, Elsevier B.V., 2013.

[18] K.-E. Kurrer, *The History of the Theory of Structure, from Arch Analysis to Computational Mechanics*. Berlin: Ernst & Sohn Verlag, 2008.

[19] R. Hooke, *A Description of Helioscope, and some other Instruments*. London: John Martyn, 1675.

[20] D. Gregory, "Catenaria," *Philosophical Transactions of the Royal Society*, vol. 19, pp. 637–652, 1697.

[21] H. Moseley, "On the equilibrium of the arch," *Cambridge Philosophical Transactions*, vol. 5, pp. 293–313, 1835.

[22] E. Méry, "Mémoire sur l'équilibre des voûtes en berceau," *Annales des Ponts et Chaussées*, pp. 50–70, 1840.

[23] P. Block and J. Ochsendorf, "Thrust network analysis: A new methodology for three-dimensional equilibrium," *Journal of the International Association for Shell and Spatial Structures*, vol. 48, pp. 1–7, 2007.

[24] T. Van Mele, L. Lachauer, M. Rippmann, and P. Block, "Geometry-based Understanding of Structures," *Journal of the International Association for Shell and Spatial Structures*, vol. 53, pp. 285–295, 2012.

[25] S. Huerta, "Structural Design inthe Work of Gaudí," *Architectural Science Review*, vol. 49, pp. 324–339, 2006.

[26] J. Heyman, "Navier's straitjacket," *Architectural Science Review*, vol. 42, pp. 91–95, 1999.

[27] E. Wilson, *Static and Dynamic Analysis of Structures*. Berkely: Computers and Structures, Inc., 1998.

[28] M. R. Horne, "Fundamental Propositions in the Plastic Theory of Structures," *Journal of the ICE*, vol. 34, pp. 174–177, 1950.

[29] C. Burgoyne, "Are structures being repaired unnecessarily?," *The Structural Engineer*, vol. 82, pp. 22–26, 2004.

[30] A. G. M. Michell, "The limits of economy of material in frame-structures," *Philosophical Magazine*, vol. 8, pp. 589–597, 1904.

[31] A. V. Pichugin, A. Tyas, and M. Gilbert, "Michell structure for a uniform load over multiple spans," in *9th World Congress of Structural Multidisciplinary Optimization*, (Shizuoka, Japan), 2011.

[32] K. Zhou and J. Li, "The exact weight of discretized michell trusses for a central point load," *Structural and Multidisciplinary Optimization*, vol. 28, pp. 69–72, 2004.

[33] P. Dewhurst, N. Fang, and S. Srithongchai, "A general boundary approach to the construction of michell truss structure," *Structural and Multidisciplinary Optimization*, vol. 39, pp. 373–384, 2009.

[34] T. Sokól and T. Lewiński, "On the solution of the three forces problem and its application to optimally designing a class of symmetric frameworks of least weight," *Structural and Multidisciplinary Optimization*, vol. 42, pp. 835–853, 2010.

[35] G. I. N. Rozvany and T. Sokól, "Exact truss topology optimization: allowance for support costs and different permissible stresses in tension and compression – extensions of a classical solution by Michell," *Structural and Multidisciplinary Optimization*, vol. 45, pp. 367–376, 2012.

[36] G. I. N. Rozvany, *Shape and layout optimization of structural systems and optimality criteria methods*. New-York: Springer-Verlag, 1992.

[37] T. J. Pritchard, M. Gilbert, and A. Tyas, "Plastic Layout Optimization of Large-scale Frameworks Subject to Multiple Load Cases, Member Self-Weight and with Joint Length Penalties," in *6th World Congress of Structural Multidisciplinary Optimization, Rio de Janeiro, Brazil*, 2005.

[38] W. Baker, "Taller," in *Proceedings of the IABSE-IASS Symposium*, (London, UK), pp. 1–6, 2011.

[39] A. Mordecai, *Nonlinear Programming: Analysis and Methods*. New York: Dover Publications, 2003.

[40] D. W. Peterson, "A review of constraint qualifications in finite-dimensional spaces," *SIAM Review*, vol. 15, pp. 639–654, 1973.

[41] D. Alevras and M. W. Padberg, *Linear Optimization and Extensions: Problems and Solutions*. Berlin,Germany: Springer-Verlag, 2001.

[42] J. Petersson, "On continuity of the design-to-state mappings for trusses with variables topology," *International Journal of Engineering Science*, vol. 39, pp. 1119–1141, 2001.

[43] S. Pellegrino and C. R. Calladine, "Matrix analysis of statically and kinematically indeterminate frameworks," *International Journal of Solids and Structures*, vol. 22, pp. 409–428, 1986.

[44] S. Pellegrino, "Structural computations with singular value decomposition of the equilibrium matrix," *International Journal of Solids and Structures*, vol. 30, pp. 3025–3035, 1993.

[45] Lewiński, T and Zhou, M and Rozvany G I N, "Extended exact solutions for least-weight truss layouts. Part I: Cantilever with a horizontal axis of symmetry," *International Journal of Mechanical Sciences*, vol. 36, pp. 375–398, 1994.

[46] W. Dorn, R. Gomory, and H. Greenberg, "Automatic design of optimal structures," *Journal de Mécanique*, vol. 3, pp. 25–52, 1964.

[47] M. Bendsøe and O. Sigmund, *Topology Optimization: Theory, Methods and Applications*. Berlin: Springer, 2003.

[48] M. Bendsøe, A. Ben-Tal, and J. Zowe, "Optimization methods for truss geometry and topology design," *Structural Optimization*, vol. 7, pp. 141–159, 1994.

[49] W. Achtziger, M. Bendsøe, A. Ben-Tal, and J. Zowe, "Equivalent Displacement Based Formulations for Maximum Strength Truss Topology Design," *Impact of Computing in Science and Engineering*, vol. 4, pp. 315–345, 1992.

[50] Y. Kanno and M. Ohsaki, "Minimum Principle of Complementary Energy for Nonlinear Elastic Cable Networks with Geometrical Nonlinearities," *Journal of Optimization Theory and Applications*, vol. 126, pp. 617–641, 2005.

[51] P. Pedersen, "On the minimum mass layout of trusses," in *AGARD Conference Proceedings No. 36, Symposium on Structural Optimization*, pp. 189–192, 1970.

[52] W. S. Hemp, *Optimum Structures*. New York: Clarendon Press, 1973.

[53] W. Achtziger, “Truss topology optimization including bar properties different in tension and compression,” *Structural Optimization*, vol. 12, pp. 63–74, 1996.

[54] T. Sokól, “A 99 line code for discretized Michell truss optimization written in Mathematica,” *Structural and Multidisciplinary Optimization*, vol. 43, pp. 181–190, 2011.

[55] M. Gilbert and A. Tyas, “Layout optimization of large-scale pin-jointed frames,” *Engineering Computations*, vol. 20, pp. 1044–1064, 2003.

[56] T. Sokól and G. I. N. Rozvany, “On the adaptive ground structure approach for multi-load truss topology optimization,” in *10th World Congress of Structural Multidisciplinary Optimization, Orlando, USA*, 2013.

[57] O. da Silva Smith, “Topology optimization of trusses with local stability constraints and multiple loading conditions – a heuristic approach,” *Structural Optimization*, vol. 13, pp. 155–166, 1997.

[58] K. Mela and J. Koski, “On the equivalence of minimium compliance and stress-constraind minimum weight design of trusses under multiple loading conditions,” *Structural and Multidisciplinary Optimmization*, vol. 46, pp. 679–691, 2012.

[59] M. Kočvara and J. Outrata, “Effective Reformulations of the Truss Topology Design Problem,” *Optimization and Engineering*, vol. 7, pp. 201–219, 2006.

[60] A. Makrodimopoulos, A. Bhaskar, and A. J. Keane, “Second-order cone programming formulations for a class of problems in structural optimization,” *Structural and Multidisciplinary Optimization*, vol. 40, pp. 365–380, 2010.

[61] C. Le, J. Norato, T. Bruns, C. Ha, and D. Tortorelli, “Stress-based topology optimization for continua,” *Structural and Multidisciplinary Optimmization*, vol. 41, pp. 605–620, 2010.

[62] A. Makrodimopoulos, A. Bhaskar, and A. J. Keane, “A compliance based design problem of structures under multiple load cases,” *Structural and Multidisciplinary Optimization*, vol. 42, pp. 739–743, 2010.

[63] U. Kirsch, “The effect of compatibility conditions on optimal design of flexural structures,” *International Journal for Numerical Methods in Engineering*, vol. 24, pp. 1173–1185, 1989.

[64] P. Pedersen, “Topology optimization of three dimensional trusses,” in *Topology Design of Structures*, pp. 19–30, Kluwer Academic Publisher, 1993.

[65] M. Kočvara, “Topology optimization with displacement constraints,” *Structural Optimization*, vol. 14, pp. 256–263, 1997.

[66] Q. Wang and J. S. Arora, “Optimization of large-scale truss structures using sparse SAND formulations,” *International Journal for Numerical Methods in Engineering*, vol. 69, pp. 390–407, 2007.

[67] J. S. Arora and Q. Wang, “Review of formulations for structural and mechanical system optimization,” *Structural and Multidisciplinary Optimization*, vol. 30, pp. 251–272, 2005.

[68] U. Kirsch, “On singular topologies in optimum structural design,” *Structural Optimization*, vol. 2, pp. 133–142, 1990.

[69] G. Cheng and Z. Jiang, “Study on topology optimization with stress constraints,” *Structural Optimization*, vol. 20, pp. 129–148, 1992.

[70] T. E. Bruns, “Zero density lower bounds in topology optimization,” *Computer Methods in Applied Mechanics and Engineering*, vol. 196, pp. 566–578, 2006.

[71] G. Sved and Z. Ginos, “Structural optimization under multiple loading,” *International Journal of Mechanical Sciences*, vol. 10, pp. 803–805, 1968.

[72] P. Hajela, *Techniques in optimal structural synthesis for static and dynamic constraints*. Standford University: Ph.D. Thesis, 1982.

[73] U. Kirsch, “Optimal topologies of flexural systems,” *Engineering Optimization*, vol. 11, pp. 141–149, 1987.

[74] U. Kirsch, “Optimal topologies of structures,” *Applied Mechanics Reviews*, vol. 42, pp. 223–239, 1989.

[75] U. Kirsch, “Optimal topologies of truss structures,” *Computer Methods in Applied Mechanics and Engineering*, vol. 72, pp. 15–28, 1989.

[76] W. Achtziger and C. Kanzow, “Mathematical programs with vanishing constraints: Optimality conditions and constraint qualifications,” *Mathematical Programming*, vol. 114, pp. 69–99, 2008.

[77] T. Hoheisel, C. Kanzow, and A. Schwartz, “Mathematical programs with vanishing constraints: a new regularization approach with strong convergence properties,” *Optimization: A Journal of Mathematical Programming and Operations Research*, vol. 61, pp. 619–636, 2012.

[78] W. Achtziger, T. Hoheisel, and C. Kanzow, “A smoothing-regularization approach to mathematical programs with vanishing constraints,” *Computational Optimization and Applications*, vol. 55, pp. 733–767, 2013.

[79] G. Cheng, “Some aspects of truss topology optimization,” *Structural Optimization*, vol. 10, pp. 173–179, 1995.

[80] G. I. N. Rozvany, “Difficulties in truss topology optimization with stress, local buckling and system stability constraints,” *Structural Optimization*, vol. 17, pp. 235–246, 1996.

[81] G. Cheng and X. Guo, “Epsilon-relaxed approach in structural topology optimization,” *Structural Optimization*, vol. 13, pp. 258–266, 1997.

[82] M. Stolpe and K. Svanberg, “On the trajectories of the epsilon-relaxation approach for stress-constrained truss topology optimization,” *Structural and Multidisciplinary Optimization*, vol. 21, pp. 140–151, 2001.

[83] M. Stolpe and K. Svanberg, “A note on stress-constrained truss topology optimization,” *Structural and Multidisciplinary Optimization*, vol. 25, pp. 62–64, 2003.

[84] X. Guo, G. Cheng, and K. Yamazaki, “A new approach for the solution of singular optima in truss topology optimization with stress and local buckling constraints,” *Structural and Multidisciplinary Optimization*, vol. 22, pp. 364–372, 2001.

[85] M. Gilbert, W. Darwich, A. Tyas, and P. Sheperd, “Application of Large-scale Layout Optimization Techniques in Structural Engineering Practice,” in *6th World Congress of Structural Multidisciplinary Optimization, Rio de Janeiro, Brazil*, 2005.

[86] U. Kirsch, “On the relationship between optimum structural topologies and geometries,” *Structural Optimization*, vol. 2, pp. 39–45, 1990.

[87] M. Kegl and B. Brank, “Shape optimization of truss-stiffened shell structures with variable thickness,” *Computer Methods in Applied Mechanics and Engineering*, vol. 195, pp. 2611–2634, 2006.

[88] K.-U. Bletzinger, M. Firl, J. Linhard, and R. Wüchner, “Computational morphogenesis of free form shells: Filter methods to create alternative solutions,” in *Proceedings of the IASS symposium, Valencia*, 2009.

[89] C. Le, T. Bruns, and D. Tortorelli, “A gradient-based parameter-free approach to shape optimization,” *Computer Methods in Applied Mechanics and Engineering*, vol. 200, pp. 985–996, 2011.

[90] W. Achtziger, “On simultaneous optimization of truss geometry and topology,” *Structural and Multidisciplinary Optimization*, vol. 33, pp. 285–304, 2007.

[91] W. Achtziger, “Simultaneous Optimization of Truss Topology and Geometry, Revisited,” in *IUTAM Symposium on Topological Design Optimization of Structures, Machine and Materials: Status and Perspectives*, pp. 413–423, 2006.

[92] Q. Xia, M. Y. Wang, and T. Shi, “A method for shape and topology optimization of truss-like structure,” *Structural and Multidisciplinary Optimization*, vol. 47, pp. 687–697, 2013.

[93] A. Ben-Tal, M. Kočvara, and J. Zowe, “Two nonsmooth approaches to simultaneous geometry and topology design of trusses,” in *Bendsoe, M P and Soares, C M (eds), Topology optimization of structures*, (Dordrecht, The Netherlands), pp. 31–42, Kluwer Academic Publishers, 1993.

[94] H. Rahami, A. Kaveh, and Y. Gholipour, “Sizing, geometry and topology optimization of trusses via force method and genetic algorithm,” *Engineering Structures*, vol. 30, pp. 2360–2369, 2008.

[95] M. W. Dobbs and L. P. Felton, “Optimization of truss geometry,” *Journal of Structural Division*, vol. 95, pp. 2105–2118, 1969.

[96] L. Gil and A. Andreu, “Shape and cross-section optimisation of a truss structure,” *Computers and Structures*, vol. 79, pp. 681–689, 2001.

[97] A. J. Torii and F. Biondini, “A simple geometry optimization method for statically indeterminate trusses,” in *8th World Congress on Structural and Multidisciplinary Optimization*, 2009.

[98] P. Pedersen, “On the minimum mass layout of trusses,” in *Symposium on Structural Optimization, Istanbule, Turkey*, pp. 1–17, 1969.

[99] P. Pedersen, “On the optimal layout of multi-purpose trusses,” *Computers and Structures*, vol. 2, pp. 695–712, 1972.

[100] P. Pedersen, “Optimal joint positions for space trusses,” *ASCE Journal of the Structural Division*, vol. 99, pp. 2459–2476, 1973.

[101] K. Svanberg, “Optimization of geometry in truss design,” *Computer Methods in Applied Mechanics and Engineering*, vol. 28, pp. 63–80, 1981.

[102] W. H. Zhang, M. Domaszewski, and C. Fleury, “A new mixed convex approximation method with applications for truss configuration optimization,” *Structural Optimization*, vol. 15, pp. 237–241, 1998.

[103] G. I. N. Rozvany, M. Bendsøe, and U. Kirsch, “Layout optimization of structures,” *Applied Mechanics Reviews*, vol. 48, pp. 41–119, 1995.

[104] G. N. Vanderplaats and F. Moses, “Automated Design of Trusses for Optimum Geometry,” *ASCE Journal of the Structural Division*, vol. 98, pp. 671–690, 1972.

[105] O. E. Lev, "Optimum Truss Geometry for Two Loading Conditions," *ASCE Journal of the Structural Division*, vol. 104, pp. 1203–1210, 1978.

[106] D. Wang, W. H. Zhang, and J. J. S, "Truss shape optimization with multiple displacement constraints," *Computer Methods in Applied Mechanics and Engineering*, vol. 191, pp. 3597–3612, 2002.

[107] M. Kočvara and J. Zowe, "How to optimize mechanical structures simultaneously with respect to geometry and topology," in *First World Congress of Structural and Multidisciplinary Optimization, Oxford, UK*, 1995.

[108] J. F. Bard, *Practical Bilevel Optimization: Algorithms and Applications*. Dordrecht Boston London: Kluwer Academic Publishers, 1998.

[109] B. Colson, P. Marcotte, and G. Savard, "Bilevel programming: A survey," *4OR: A Quaterly Journal of Operations Research*, vol. 3, pp. 87–107, 2005.

[110] P. Martínez, P. Martí, and O. M. Querin, "Growth method for size, topology, and geometry optimization of truss structures," *Structural and Multidisciplinary Optimization*, vol. 33, pp. 13–26, 2007.

[111] T. Hagishita and M. Ohsaki, "Topology optimization of trusses by growing ground structure method," *Structural and Multidisciplinary Optimization*, vol. 37, pp. 377–393, 2009.

[112] D. Bojczuk and A. Rębosz-Kurdek, "Topology and Configuration Optimization of Trusses Based on Virtual Bars Concept," in *10th World Congress of Structural Multidisciplinary Optimization, Orlando, USA*, 2013.

[113] B. Descamps, Ph. Bouillard, L. Ney, and R. Filomeno Coelho, "The principia design method for the form finding and optimization of truss grids," in *Proceedings of the IABSE-IASS symposium, London, UK*, 2011.

[114] L. A. Schmit and R. L. Fox, "An integrated approach to structural synthesis and analysis," *American Institute of Aeronautics and Astronautics Journal*, vol. 3, pp. 1104–1112, 1965.

[115] R. L. Fox and L. A. Schmit, "Advances in the integrated approach to structural synthesis," *Journal of Spacecraft and Rockets*, vol. 3, pp. 858–866, 1966.

[116] P. Breitkopf and R. Filomeno Coelho, *Multidisciplinary Design Optimization in Computational Mechanics*. Chippenham, UK: ISTE/John Wiley & Sons, 2010.

[117] K. Linkwitz, "About formfinding of double-curved structures," *Engineering Structures*, vol. 21, pp. 709–718, 1999.

[118] B. Descamps and R. Filomeno Coelho, "A simultaneous analysis and design formulation for the shape and topology optimization of large-scale trusses," in *10th World Congress on Computational Mechanics (WCCM X)*, (São Paulo, Brazil), 2012.

[119] B. Descamps and R. Filomeno Coelho, "A lower-bound formulation for the geometry and topology optimization of truss structures under multiple loading," *Structural and Multidisciplinary Optimization*, vol. 48, pp. 49–58, 2013.

[120] B. Descamps and R. Filomeno Coelho, "Shape and topology optimization for the stress-based truss design under multiple loading," in *3rd International Conference on Engineering Optimization (EngOpt 2012)*, (Rio de Janeiro, Brazil), 2012.

[121] J.-F. Bonnans, J. C. Gilbert, C. Lemarechal, and C. A. Sagastizábal, *Numerical Optimization: Theoretical and Practical Aspects*. Berlin: Springer-Verlag, 2006.

[122] K. Schittkowski, "A robust implementation of a sequential quadratic programming algorithm with successive error restoration," *Optimization Letters*, vol. 5, pp. 283–296, 2011.

[123] M. Burger and R. Stainko, "PhaseâĂŘ-Field Relaxation of Topology Optimization with Local Stress Constraints," *SIAM Journal on Control and Optimization*, vol. 45, pp. 1447–1466, 2006.

[124] V. E. Sonzogni and A. Queizan, "Simultaneous analysis and design of large structures by domain decomposition," in *6th World Congress of Structural Multidisciplinary Optimization, Rio de Janeiro*, 2005.

[125] A. Canelas, J. Herskovits, and J. C. F. Telles, "Shape optimization using the boundary element method and a SAND interior point algorithm for constrained optimization," *Computers and Structures*, vol. 86, pp. 1517–1526, 2008.

[126] R. H. Byrd, M. E. Hribar, and J. Nocedal, "An interior point algorithm for large scale nonlinear programming," *SIAM Journal on Optimization*, vol. 9, pp. 877–900, 1999.

[127] J. Nocedal and S. J. Wright, *Numerical Optimization*. New York: Springer series in Operations Research, Springer-Verlag, 1999.

[128] R. H. Byrd, M. Marazzi, and J. Nocedal, "On the convergence of Newton iterations to non-stationary points," *Mathematical Programming, Series A*, vol. 99, pp. 127–148, 2004.

[129] P. E. Gill, W. Murray, and M. S. Saunders, "SNOPT: An SQP Algorithm for Large-Scale Constrained Optimization," *SIAM Review*, vol. 47, pp. 99–131, 2005.

[130] D. M. Gay, M. L. Overton, and M. H. Wright, "A primal-dual interior point method for non-convex nonlinearly constrained optimization," in *Advances in Nonlinear Programming,Kluwer Academic Publishers, Dordrecht*, pp. 31–56, 1998.

[131] R. J. Vanderbei and D. F. Shanno, "An interior point algorithm for nonconvex nonlinear programming," *Computational Optimization and Applications*, vol. 13, pp. 231–252, 1999.

[132] J. T. Betts and P. D. Frank, "A Sparse Nonlinear Optimization Algorithm," *Journal of Optimization Theory and Applications*, vol. 82, pp. 519–541, 1994.

[133] W. Murray, "Sequential Quadratic Programming Methods for Large-Scale Problems," *Computational Optimization and Applications*, vol. 7, pp. 127–142, 1997.

[134] R. A. Waltz, J. L. Morales, J. Nocedal, and D. Orban, "An interior algorithm for nonlinear optimization that combines line search and trust region steps," *Mathematical Programming A*, vol. 107, pp. 391–408, 2006.

[135] R. H. Byrd, J.-C. Gilbert, and J. Nocedal, "A trust region method based on interior point techniques for nonlinear programming," *Mathematical Programming*, vol. 89, pp. 149–185, 2000.

[136] A. Vardi, "A trust region algorithm for equality constrained minimization: convergence, properties and implementation," *SIAM Journal on Numerical Analysis*, vol. 22, pp. 575–591, 1985.

[137] R. H. Byrd, R. B. Schnabel, and G. A. Schultz, "Approximate solution of the trust regions problem by minimization over two-dimensional subspaces," *Mathematical Programming*, vol. 40, pp. 247–263, 1988.

[138] E. Omojokun, *Trust region algorithms for optimization with nonlinear equality and inequality constraints.* PhD thesis, University of Colorado, 1989.

[139] T. Steihaug, "The conjugate gradient method and trust regions in large scale optimization," *SIAM Journal on Numerical Analysis*, vol. 20, pp. 626–637, 1983.

[140] M. Lalee, J. Nocedal, and T. Plantenga, "On the implementation of an algorithm for large-scale equality constrained optimization," *SIAM Journal on Optimization*, vol. 8, pp. 682–706, 1998.

[141] R. A. Waltz and T. D. Plantenga, "Knitro User's Manual Version 7.0," *Ziena Optimization, Inc*, 2010.

[142] Matlab, "Matlab: Optimization Toolbox, User's Guide," tech. rep., 2013.

[143] N. L. Pedersen and A. K. Nielsen, "Optimization of practical trusses with constraints on eigenfrequencies, displacements, stresses and buckling," *Structural and Multidisciplinary Optimization*, vol. 25, pp. 436–445, 2003.

[144] Z. P. Bažant, "Structural Stability," *International Journal of Solids and Structures*, vol. 37, pp. 55–67, 2000.

[145] A. Tyas, M. Gilbert, and T. Pritchard, "Practical plastic layout optimization of trusses incorporating stability considerations," *Computers and Structures*, vol. 84, pp. 115–126, 2006.

[146] M. Zhou, "Difficulties in truss topology optimization with stress and local buckling constraints," *Structural and Multidisciplinary Optimization*, vol. 11, pp. 134–136, 1996.

[147] W. Achtziger, "Local stability in the context of topology optimization – Part I: Exact modelling," *Structural Optimization*, vol. 17, pp. 235–246, 1999.

[148] W. Achtziger, "Local stability in the context of topology optimization – Part II: Numerical approach," *Structural Optimization*, vol. 17, pp. 247–258, 1999.

[149] A. Ben-Tal, F. Jarre, M. Kočvara, A. Nemirovski, and J. Zowe, "Optimal Design of Trusses Under a Nonconvex Global Buckling Constraint," *Optimization and Engineering*, vol. 1, pp. 189–213, 2000.

[150] M. Kočvara, "On the modelling and solving of the truss design problem with global stability constraints," *Structural and Multidisciplinary Optimization*, vol. 23, pp. 189–203, 2002.

[151] X. Guo, G. Cheng, and N. Olhoff, "Optimum design of truss topology under buckling constraints," *Structural and Multidisciplinary Optimization*, vol. 30, pp. 169–180, 2005.

[152] A. Evgrafov, "On globally stable singular truss topologies," *Structural and Multidisciplinary Optimization*, vol. 29, pp. 170–177, 2005.

[153] J. N. Richardson, R. Filomeno Coelho, and S. Adriaenssens, "Robust topology optimization of 2D and 3D continuum and truss structures using a spectral stochastic finite element method," in *10th World Congress on Structural and Multidisciplinary Optimization (WCSMO 10)*, (Orlando, USA), 2010.

[154] R. Filomeno Coelho and Ph. Bouillard, "Multi-objective reliability-based optimization with stochastic metamodels," *Evolutionary Computation*, vol. 19, pp. 525–560, 2011.

[155] A. Ben-Tal and A. Nemirovski, "Robust truss topology design via semidefinite programming," *SIAM Journal on Optimization*, vol. 7, pp. 991–1016, 1997.

[156] G. C. Calafiore and F. Dabbene, "Optimization under uncertainty with applications to design of truss structures," *Structural and Multidisciplinary Optimization*, vol. 35, pp. 189–200, 2006.

[157] J. K. Guest and T. Igusa, “Structural optimization under uncertain loads and nodal locations,” *Computer Methods in Applied Mechanics and Engineering*, vol. 198, pp. 116–124, 2008.

[158] M. Jalapour, T. Igusa, and J. K. Guest, “Optimal design of trusses with geometric imperfections: Accounting for global stability,” *International Journal of Solids and Structures*, vol. 48, pp. 3011–3019, 2011.

[159] A. Asadpoure, M. Tootkaboni, and G. J. K, “Robust topology optimization of structures with uncertainties in stiffness – application to truss structures,” *Computers and Structures*, vol. 89, pp. 1131–1141, 2011.

[160] F. Chinesta, P. Ladevèze, and E. Cueto, “A short review on model order reduction based on Proper Generalized Decomposition,” *Archives for Numerical Methods in Engineering*, vol. 18, pp. 395–404, 2011.

[161] G. Winter, “Lateral Bracing Of Columns And Beams,” *Transactions of the American Society of Civil Engineers*, vol. 125, pp. 807–826, 1960.

[162] Eurocodes, “Eurocode 3: Part 1. Design of steel structures, general rules and rules for buildings,” tech. rep., 2005.

[163] J. Yura, “Winter’s bracing approach revisited,” *Engineering Structures*, vol. 18, pp. 821–825, 1996.

[164] K. K. Choi and N.-H. Kim, *Structural Sensitivity Analysis and Optimization 1*. New-York: Springer, 2005.

[165] S. Adriaenssens, S. De Voldere, and L. Ney, *Laurent Ney: Shaping forces*. Brussels,Belgium: A+ editions, CIAUD-ICASD, 2010.

[166] S. Adriaenssens, L. Ney, E. Bodarwé, and C. Williams, “Dutch Maritime Museum: Form-finding of an irregular faceted skeletal shell – Part a,” in *Proceedings of the IASS symposium, Valencia*, 2009.

[167] S. Adriaenssens, L. Ney, E. Bodarwé, and C. Williams, “Dutch Maritime Museum: Form-finding of an irregular faceted skeletal shell – Part b,” in *Proceedings of the IASS symposium, Valencia*, 2009.

[168] S. Adriaenssens, L. Ney, E. Bodarwé, and C. Williams, “Finfing the Form of an Irregular Meshed Steel and Glass Shell Based on Construction Constraints,” *Journal of Architectural Engineering*, vol. 18, pp. 206–213, 2012.

[169] R. M. O. Pauletti and P. M. Pimenta, “The natural force density method for the shape finding of taut structures,” *Computer Methods in Applied Mechanics and Engineering*, vol. 197, pp. 4419–4428, 2008.

[170] M. Beckers, “Dual methods for discrete structural optimization problems,” *International Journal for Numerical Methods in Engineering*, vol. 48, pp. 1761–1784, 2000.

[171] M. Ohsaki and N. Katoh, “Topology optimization of trusses with stress and local constraints on nodal stability and member intersection,” *Structural and Multidisciplinary Optimization*, vol. 29, pp. 190–197, 2005.

[172] R. B. Haber and J. F. Abel, “Initial equilibrium solution methods for cable reinforced membranes, Part 1: formulations,” *Computer Methods in Applied Mechanics and Engineering*, vol. 30, pp. 263–284, 1982.

[173] R. B. Haber and J. F. Abel, “Initial equilibrium solution methods for cable reinforced membranes, Part 2: implementation,” *Computer Methods in Applied Mechanics and Engineering*, vol. 30, pp. 285–306, 1982.

[174] D. Veenendaal and P. Block, “An overview and comparison of structural form finding methods for general networks,” *International Journal of Solids and Structures*, vol. 49, pp. 3741–3753, 2012.

[175] K. Linkwitz, “New methods for the determination of cutting pattern of prestress cable nets and their application to the olympic roofs Munich,” in *Proceedings of the IASS pacific symposium on tension structures and space frames, Tokyo*, 1971.

[176] H.-J. Scheck, “The force density method for the form-finding and computation of general networks,” *Computer Methods in Applied Mechanics and Engineering*, vol. 3, pp. 115–134, 1974.

[177] B. Maurin and R. Motro, “The surface stress density method as a form-finding tool for tensile membranes,” *Engineering Structures*, vol. 20, pp. 712–719, 1998.

[178] K.-U. Bletzinger and E. Ramm, “A General Finite Element Approach to the Form Finding of Tensile Structures by the Updated Reference Strategy,” *International Journal of Solids and Structures*, vol. 14, pp. 131–145, 1999.

[179] K.-U. Bletzinger and E. Ramm, “Structural optimization and form finding of lightweight structure,” *Computers and Structures*, vol. 79, pp. 2053–2062, 2001.

[180] K.-U. Bletzinger, R. Wüchner, F. Daoud, and N. Camprubi, “Computational methods for form finding and optimization of shells and membranes,” *Computer Methods in Applied Mechanics and Engineering*, vol. 194, pp. 3438–3452, 2005.

[181] A. G. Tibert and S. Pellegrino, “Review of form-finding methods for tensegrity structures,” *International Journal of Space Structures*, vol. 18, pp. 209–223, 2003.

[182] J. Y. Zhang and M. Ohsaki, “Adaptive Force Density Method for the Form Finding Problem of Tensegrity Structures,” *International Journal of Solids and Structures*, vol. 43, pp. 5658–5673, 2006.

[183] L. Greco and M. Cuomo, “On the force density method for slack cable nets,” *International Journal of Solids and Structures*, vol. 49, pp. 1526–1540, 2012.

[184] A. Kilian and J. Ochsendorf, "Particle-spring systems for structural form finding," *Journal of the International Association for Shell and Spatial Structures*, vol. 46, pp. 77–84, 2005.

[185] M. Miki and K. Kawaguchi, "Extended force denstiy method for form-finding of tension structures," *Journal of the International Association for Shell and Spatial Structures*, vol. 51, pp. 291–303, 2011.

[186] A. S. Day, "An introduction to dynamic relaxation," *The Engineer*, vol. 219, pp. 218–221, 1965.

[187] M. R. Barnes, *Form-finding and analysis of tension space structures by dynamic relaxation.* PhD thesis, City University, London, 1977.

[188] M. R. Barnes, "Form-finding and analysis of pre-stressed nets and membranes," *Computers and Structures*, vol. 30, pp. 685–695, 1988.

[189] M. R. Barnes, "Form Finding and Analysis of Tension Structures by Dynamic Relaxation," *International Journal of Space Structures*, vol. 14, pp. 89–104, 1999.

[190] P. D. Gosling and W. J. Lewis, "Optimal structural membranes–i. Formulation of a curved quadrilateral element for surface definition," *Computers and Structures*, vol. 61, pp. 871–883, 1996.

[191] P. D. Gosling and W. J. Lewis, "Optimal structural membranes–ii. Form-finding of prestressed membranes using a curved quadrilateral finite element for surface definition," *Computers and Structures*, vol. 61, pp. 885–895, 1996.

[192] R. Wood, "A simple technique for controlling element distortion in dynamic relaxation form-ïňĄnding of tension membranes," *Computers and Structures*, vol. 80, pp. 2115–2120, 2002.

[193] S. Han and K. Lee, "A study of the stabilizing process of unstable structures by dynamic relaxation method," *Computers and Structures*, vol. 81, pp. 1677–1688, 2003.

[194] S. Adriaenssens and M. R. Barnes, "Tensegrity spline beam and grid shell structures," *Engineering Structures*, vol. 23, pp. 29–36, 2001.

[195] M. R. Barnes, S. Adriaenssens, and M. Krupka, "A novel torsion/bending element for dynamic relaxation modeling," *Computers and Structures*, vol. 119, pp. 60–67, 2013.

[196] S. Kirkpatrick and C. D. Gelatt, "Optimization by simulated annealing," *Science*, vol. 220, pp. 671–680, 1985.

[197] V. Černỳ, "Thermodynamical approach to the traveling salesman problem: an efficient simulation algorithm," *Journal of Optimization Theory and Applications*, vol. 45, pp. 41–51, 1985.

[198] B.-W. Xiang, R.-Q. Chen, and T. Zhang, "Optimization of trusses using simulated annealing for discrete variables," in *International Conference on Image Analysis and Signal Processing (IASP)*, (Taizhou, China), 2009.

[199] L. Lamberti, "An efficient simulated annealing for design optimization of truss structures," *Computers and Structures*, vol. 86, pp. 1936–1953, 2008.

[200] O. Hasançebi and F. Erbatur, "Layout optimisation of trusses using simulated annealing," *Advances in Engineering Software*, vol. 33, pp. 681–696, 2002.

[201] F. Glover, "Tabu search – Part 1," *ORSA Journal on Computing*, vol. 1, pp. 190–206, 1989.

[202] F. Glover, "Tabu search – Part 2," *ORSA Journal on Computing*, vol. 2, pp. 4–32, 1990.

[203] S. O. Degertekin, M. P. Saka, and M. S. Hayalioglu, "Optimal load and resistance factor design of geometrically nonlinear steel space frames via tabu search and genetic algorithm," *Engineering Structures*, vol. 30, pp. 197–205, 2008.

[204] H. M. Gomes, "Truss optimization with dynamic constraints using particle swarm algorithm," *Expert Systems with Applications*, vol. 38, pp. 957–968, 2011.

[205] G.-C. Luh and C.-Y. Lin, "Optimal design of truss-structures using particle swarm optimization," *Computers and Structures*, vol. 89, pp. 2221–2232, 2008.

[206] M. Dorigo and T. Stützle, *Ant Colony Optimization.* Cambridge: MIT Press, 2004.

[207] A. Kaveh and S. Schojaee, "Optimal design of skeletal structures using ant colony optimization," *International Journal of Numerical Methods in Engineering*, vol. 70, pp. 563–581, 2007.

[208] G.-C. Luh and C.-Y. Lin, "Optimal design of truss-structures using ant colony optimization," *Structural and Multidisciplinary Optimization*, vol. 36, pp. 365–379, 2008.

[209] M. Sonmez, "Artificial Bee Colony algorithm for optimization of truss structures," *Applied Soft Computing*, vol. 11, pp. 2406–2418, 2011.

[210] X. Yang and A. H. Gandomi, "Bat algorithm: a novel approach for global engineering optimization," *Engineering Computations*, vol. 29, pp. 464–483, 2012.

[211] A. H. Gandomi, X. Yang, and A. H. Alavi, "Mixed variable structural optimization using firefly algorithm," *Computers and Structures*, vol. 89, pp. 2325–2336, 2011.

[212] X. Yang and A. H. Deb, "Engineering optimisation by cuckoo search," *International Journal of Mathematical Modelling and Numerical Optimisation*, vol. 1, pp. 330–343, 2010.

[213] A. H. Gandomi, X. Yang, and A. H. Alavi, "Cuckoo search algorithm: a metaheuristic approach to solve structural optimization problems," *Engineering with Computers*, vol. 29, pp. 17–35, 2013.

[214] T. Bäck, D. B. Fogel, and Z. Michalewicz, *Handbook of Evolutionary Computation*. Bristol: Oxford University Press and IOP Publishing Ltd., 1997.

[215] C. A. Coello Coello, D. A. Van Veldhuizen, and G. B. Lamont, *Evolutionary Algorithms for Solving Multi-Objective Problems*. New York: Kluwer Academic/Plenum Publishers, 2002.

[216] C. A. Coello Coello, M. Rudnick, and A. D. Christiansen, "Using genetic algorithms for optimal design of trusses," in *Sixth International Conference on Tools with Artificial Intelligence*, (Los Angeles, USA), 1994.

[217] O. Hasançebi, "Optimization of truss bridges within a specified design domain using evolution strategies," *Engineering Optimization*, vol. 39, pp. 737–756, 2007.

[218] O. Hasançebi, S. Çarbaş, E. Doğan, F. Erdal, and M. P. Saka, "Performance evaluation of metaheuristic search techniques in the optimum design of real size pin jointed structures," *Computers and Structures*, vol. 87, pp. 284–302, 2009.